Teoretyczne badanie trójpierścieniowych związków o charakterze leczniczym.

mgr inż. Małgorzata Szymańska

Promotor: Prof. dr hab. Irena Majerz

Spis treści

Streszczenie w języku polskim

Trójpierścieniowe związki o charakterze leczniczym mają szerokie zastosowanie w medycynie oraz ziołolecznictwie. Głównymi przedstawicielami tej grupy związków są fenotiazyny, dibenzoazepiny, antrony i antrachinony. Cechą charakterystyczną ich budowy są trzy pierścienie- dwa boczne aromatyczne i pierścień środkowy, który jest typowym alifatem. Na charakter środkowego pierścienia mają wpływ podstawniki, podwójne wiązania oraz obecność w nim heteroatomów. Brak doniesień literaturowych dotyczących wpływu powyższych czynników na struktury związków trójpierścieniowych wpłynęło na podjęcie pracy dotyczącej tego tematu.

Celem pracy była analiza zmian geometrii pochodnych fenotiazyn, dibenzoazepin, antronów i antrachinonów oraz 1,8-dihydroksy-9-antronu i 1,8-dihydroksy-9-antranolu. W tym celu wykorzystując program Gaussian przeprowadzono optymalizację pochodnych czterech serii związków. W każdej serii zbadano wpływ podstawników o charakterze elektronodonorowym i elektronoakceptorowym na geometrię pierścienia środkowego. Podstawiano pierścień środkowy oraz boczny pierścień aromatyczny. Istotne było zbadanie wpływu heteroatomów oraz wiązań podwójnych w centralnym pierścieniu. Parametrem geometrycznym, który w doskonały sposób opisuje wpływ powyższych czynników na analizowane struktury jest kąt pomiędzy płaszczyznami dwóch bocznych pierścieni aromatycznych. Im większa jest jego wartość, tym bardziej niepłaski jest związek. Warto zaznaczyć, że ze zmianami geometrii związana jest zmiana aromatyczności pierścieni a co za tym idzie również zmiany gęstości elektronowej oraz mobilność elektronów w wiązaniach. Do zbadania zmian aromatyczności wykorzystano geometryczne parametry aromatyczności HOMA i HOMED. Wykorzystując program generujący powierzchnie ACID zwizualizowano ruchliwość chmury elektronowej. Umożliwiło to omówienie wpływu podwójnych wiązań oraz obecności heteroatomów w środkowym pierścieniu na zmiany gęstości elektronowej. W celu potwierdzenia wiarygodności otrzymanych wyników w każdej serii związków porównywano je z geometrią związków krystalicznych z bazy CSD.

Głównym celem było poszukiwanie czynników, które w znaczący sposób zmieniają strukturę i tym samym wpływają także na właściwości fizykochemiczne. Z właściwościami fizykochemicznymi łączą się właściwości lecznicze oraz biodostępność związku. Znajomość wpływu różnych czynników na geometrię pomoże w projektowaniu nowych związków leczniczych, które będą charakteryzować się pożądanymi właściwościami.

The summary in English

Tricyclic compounds of a medicinal nature are widely used in medicine and herbal medicine. The main representatives of this group of compounds are phenothiazines, dibenzoazepines, anthrones and anthraquinones. A characteristic feature of their structure is three rings-two aromatic side rings and a middle ring, which is a typical aliphate. The character of the middle ring is influenced by substituents, double bonds and the presence of heteroatoms in it. The lack of literature reports on the influence of the above factors on the structures of tricyclic compounds influenced to undertake work on this topic.

The purpose of the work was to analyze the changes in the geometry of derivatives of phenothiazines, dibenzoazepines, anthrones and anthraquinones, as well as 1,8-dihydroxy-9-anthrone and 1,8-dihydroxy-9-anthranol. For this purpose, using the Gaussian program, optimization of the derivatives of four series of compounds was carried out. In each series, the effect of electron donor and electron acceptor substituents on the geometry of the middle ring was studied. Except the middle ring also the side aromatic ring was substituted. It was important to study the influence of heteroatoms and double bonds in the central ring. The geometrical parameter that perfectly describes the influence of the above factors on the analyzed structures is the angle between the planes of two side aromatic rings. A large value of the angle means that the compound is more non-flat. It is worth noting that associated with changes in geometry is a change in the aromaticity of the rings and, consequently, also changes in electron density and electron mobility in the bonds. The geometric aromaticity parameters HOMA and HOMED were used to study aromaticity changes. Using the ACID surface generation program, electron cloud mobility was visualized. This made it possible to discuss the influence of double bonds and heteroatoms in the middle ring on changes in electron density. In order to confirm the reliability of the obtained results in each series of compounds, they were compared with the geometry of crystalline compounds from the CSD database.

The main purpose was to search factors that significantly change the structure and thus also affect the physicochemical properties. Physicochemical properties are linked to therapeutic properties and bioavailability of the compounds. Knowledge of the influence of various factors on geometry will help in the design of new medicinal compounds that will be characterized by the desired properties.

Wstęp

Związki o właściwościach leczniczych nie stanowią jednorodnej grupy chemicznej lecz charakteryzują się różną budową oraz zawierają różne grupy funkcyjne. Również nie do końca oczywiste jest powiązanie konkretnych właściwości leczniczych z budową chemiczną leku. Dlatego też trudno jest na podstawie właściwości chemicznych przewidzieć właściwości biologiczne i farmaceutyczne. Niemniej jednak prowadzone są próby powiązania parametrów strukturalnych oraz właściwości chemicznych i fizycznych związku chemicznego z jego właściwościami biologicznymi i leczniczymi, przy czym ważny jest już etap wstępny polegający na wyborze odpowiednich parametrów fizykochemicznych w celu skorelowania ich z właściwościami biologicznymi i leczniczymi. Wśród parametrów fizykochemicznych powszechnie stosowanych na szczególną uwagę zasługują takie parametry jak moment dipolowy, polaryzowalność, różnica energii HOMO-LUMO, stałe opisujące właściwości podstawników jak stałe Hammeta czy Tafta, hydrofobowość, ilość protonodonorów i protonoakceptorów w cząsteczce oraz wiele innych parametrów opisujących zarówno właściwości dotyczące pojedynczych cząsteczek jak i związanych z właściwościami makroskopowymi związku.

Wszystkie parametry fizykochemiczne używane do opisu i przewidywania właściwości biologicznych i farmaceutycznych w sposób oczywisty wiążą się ze strukturą związku. Znajomość struktury jest więc niezbędna nie tylko ze względu na to, że niektóre parametry strukturalne są wprost powiązane z właściwościami biologicznymi, ale też dlatego, że ze struktury związku chemicznego wynikają parametry fizykochemiczne takie, jak na przykład moment dipolowy. Interpretacja właściwości leczniczych związku oraz projektowanie nowych leków wymaga więc znajomości zarówno struktury pojedynczej cząsteczki, jak i wzajemnego ułożenia cząsteczek w sieci krystalicznej.

Niektóre spośród wielu różnorodnych związków o charakterze leczniczym zbudowane są w taki sposób, iż dwa pierścienie aromatyczne połączone są ze sobą fragmentami alifatycznymi tworzącymi zamknięty cykl. Tak więc centralny pierścień alifatyczny skumulowany jest z dwoma pierścieniami aromatycznymi.

Związki trójpierścieniowe stanowią ważną grupę substancji o charakterze leczniczym. Do grupy leków trójpierścieniowych należą dibenzoazepiny o właściwościach przeciwdepresyjnych [1], fenotiazyny o właściwościach uspokajających [2] pochodne antronów stosowanych jako leki przeciwłuszczycowe [3] oraz antrachinony o właściwościach przeciwutleniających [4] (Rysunek 1). Warto zaznaczyć, że antrachinony są substancjami pochodzenia naturalnego dzięki czemu zainteresowanie nimi wciąż rośnie. Wspólną cechą wymienionych związków są trzy pierścienie z czego dwa boczne mają charakter aromatyczny a pierścień środkowy jest alifatem. Jedną z róż-

nic strukturalnych między wymienionymi grupami związków jest budowa środkowego pierścienia. Dibenzoazepiny charakteryzują się siedmioczłonowym środkowym pierścieniem, natomiast fenotiazyny i antrony posiadają pierścień sześcioczłonowy. Niektóre pochodne dibenzoazepin i fenotiazyn zawierają w pierścieniu środkowym heteroatom. Struktura środkowego pierścienia, obecność w nim heteroatomów oraz wiązań podwójnych mają znaczący wpływ na zmianę jego aromatyczności.
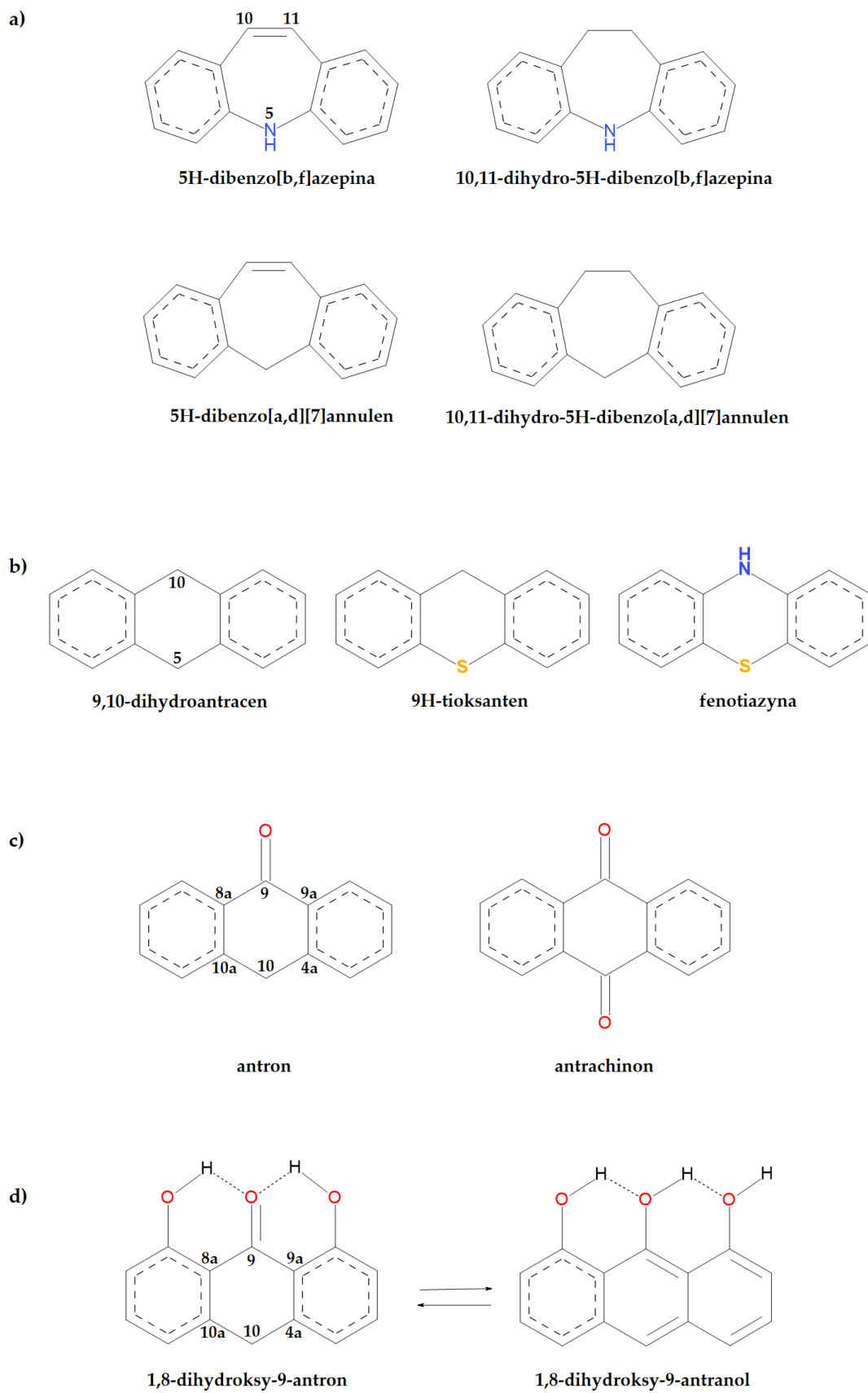
Celem pracy jest zbadanie wpływu podstawników w pierścieniu środkowym i w pierścieniach bocznych na geometrię całej cząsteczki trójpierścieniowych związków o charakterze leczniczym. Podczas doboru podstawników kierowano się ich wielkością oraz charakterem chemicznym. Wybrano podstawniki o charakterze elektronodonorowym i elektronoakceptorowym oraz o różnym rozmiarze aby zbadać wpływ przeszkód sterycznych. Najważniejszym etapem w badaniu wpływu podstawników na geometrię analizowanej cząsteczki jest znalezienie parametrów geometrycznych czułych na podstawienie. Jako charakterystyczny parametr strukturalny wybrano kąt pomiędzy dwoma bocznymi pierścieniami- tzw. kąt motylkowy. Zauważono, że jest on bardzo czuły na podstawienie, szczególnie na podstawienie w pierścieniu środkowym. Informuje on o niepłaskiej strukturze danego związku. Ze zmianą geometrii związane są zmiany aromatyczności. W związku z tym w opublikowanych pracach zbadano wpływ podstawników na zmianę parametru aromatyczności HOMA [5] pierścienia środkowego oraz pierścieni bocznych. Zmiany aromatyczności są związane ze zmianami gęstości elektronowej, zarówno w punktach krytycznych wiązań, jak i w pierścieniowych punktach krytycznych. Parametry opisujące zmiany gęstości elektronowej w punktach krytycznych wyznaczono dla każdej serii badanych związków.

Metodyka

W celu zbadania wpływu podstawników na geometrię cząsteczek dla każdej serii związków zoptymalizowano struktury z podstawnikami o różnej wielkości i różnym charakterze chemicznym, przede wszystkim biorąc pod uwagę ich właściwości elektronodonorowe i elektronoakceptorowe: NO_2, CHO, COOH, CH_3, CH_2CH_3, NH_2, OH, Cl, $C(CH_3)_3$. Dodatkowo przeanalizowano jak na geometrię badanych związków mogą wpływać wiązania podwójne, heteroatomy w środkowym pierścieniu oraz obecność wiązań wodorowych. Aby ocenić wpływ powyższych czynników na geometrię całej cząsteczki poszukano parametrów strukturalnych zmieniających się pod wpływem podstawienia. Wśród tych parametrów szczególnie ważny okazał się kąt pomiędzy dwoma bocznymi pierścieniami aromatycznymi.

W badaniach pochodnych dibenzoazepin analizowano cztery grupy związków: pochodne 5H-dibenzo[b,f]azepiny, 10,11-dihydro-5H-dibenzo[b,f]azepiny, 5H-dibenzo[a,d][7]annulenu, 10,11-dihydro-5H-dibenzo[a,d][7]annulenu (Rysunek 1-a). W przypadku drugiej serii związków analizowano pochodne fenotiazyn, 9,10-dihydriantracenu i 9H-tioksantenu (Rysunek 1-b). Kolejną serią związków były pochodne antronów i antrachinonów (Rysunek 1-c). Ze względu na równowagę keto-enolową jaka zachodzi pomiędzy 1,8-dihydroksy-9-antronem a 1,8-dihydroksy-9-antranolem (Rysunek 1-d) analizowano pochodne obu tych związków. Dodatkowo dla związków z tej serii badano wpływ wiązań wodorowych na geometrię cząsteczki. Ze względu na możliwy transfer protonu w przypadku serii dibenzoazepin i 1,8-dihydroksy-9-antronu zanalizowano również wszystkie możliwe tautomery. Na podstawie najniższej energii wybrano najbardziej prawdopodobne tautomery i właśnie dla nich zbadano wpływ podstawników.

Optymalizacja struktury została przeprowadzana w fazie gazowej przy użyciu programu Gaussian 16 [6] na poziomie DFT-D3 B3LYP/6-311++G** z uwzględnieniem dyspersji Grimma [7] w celu prawidłowego odtworzenia wiązań wodorowych. Dodatnie częstości otrzymane dla każdej optymalizowanej struktury potwierdzały osiągnięcie minimum energetycznego. Dla zoptymalizowanych cząsteczek, oprócz zanalizowania parametrów strukturalnych, wyznaczano parametry dotyczące gęstości elektronowej wykorzystując metodę QTAIM [8]. Do obliczeń związanych z ruchliwością chmury elektronowej wykorzystano program ACID (anisotropy of the current-induced density) [9]. Aby potwierdzić wyniki otrzymane metodami teoretycznymi porównywano je z wynikami otrzymanymi dla struktur krystalicznych pobranych z bazy CSD [10].

a)

5H-dibenzo[b,f]azepina

10,11-dihydro-5H-dibenzo[b,f]azepina

5H-dibenzo[a,d][7]annulen

10,11-dihydro-5H-dibenzo[a,d][7]annulen

b)

9,10-dihydroantracen

9H-tioksanten

fenotiazyna

c)

antron

antrachinon

d)

1,8-dihydroksy-9-antron

1,8-dihydroksy-9-antranol

Rysunek 1 Badane serie związków: a- dibenzoazepiny, b- fenotiazyny, c- antron i antrachinon, d- 1,8-dihydroksy-9-antron i 1,8-dihydroksy-9-anranol

Rezultaty

Geometria badanych związków

Najbardziej charakterystyczny parametr opisujący niepłaskość związków trójpierścieniowych to kąt α (Rysunek 2). Opisuje on kąt pomiędzy dwoma zewnętrznymi pierścieniami, które charakteryzują się wysoką aromatycznością. W każdej serii związków kąt α zmienia się w szerokim zakresie: seria dibeznzoazepin - 22-57° [11], fenotiazyn - 20-60° [12], antronów i antrachinonów - 0-41° [13], 1,8-dihydroxy-9-antronu i 1,8-dihydroxy-9-antranolu - 0-52° [14]. Na wartości kąta α ma wpływ nie tylko charakter chemiczny danego podstawnika, ale także jego wielkość i aksjalne lub ekwatorialne ułożenie w przestrzeni. Najmniejsze wartości kątów α uzyskano dla pochodnych antrachinonów ze względu na obecność dwóch grup karbonylowych w środkowym pierścieniu. Pochodne 1,8-dihydroxy-9-antranolu również charakteryzowały się niewielką wartością kąta α. Największe wartości kąta α w większości przypadków otrzymywano dla struktur podstawionych podstawnikiem tert-butylowym, co było spowodowane jego wielkością. Wyjątek stanowiła seria związków dibenzoazepin.
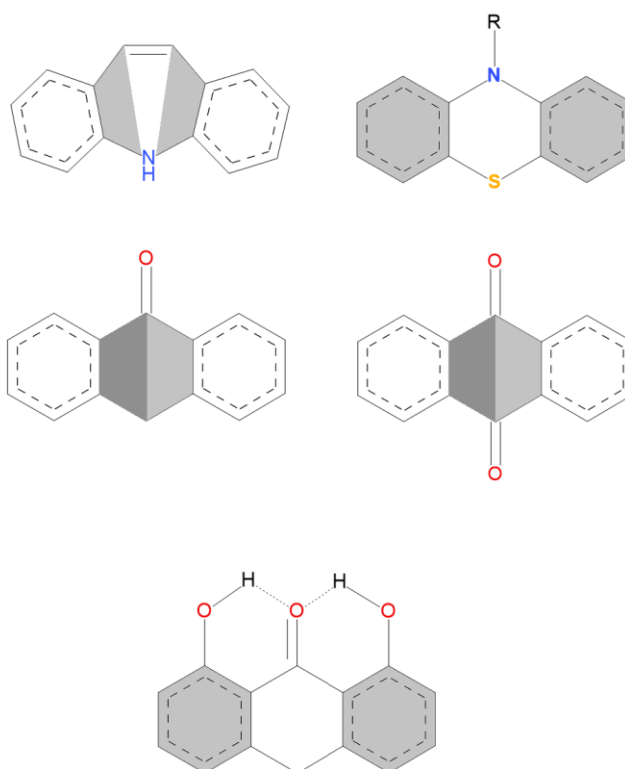
Rysunek 2 Kąt α wyznaczany dla analizowanych serii związków

W celu zbadania wpływu obecności heteroatomu w pierścieniu centralnym na geometrię 5H-dibenzo[b,f]azepiny, 10,11-dihydro-5H-dibenzo[b,f]azepiny, 5H-dibenzo[a,d][7]annulenu oraz 10,11-dihydro-5Hdibenzo[a,d][7]annulenu wyznaczono

odległość atomu azotu i węgla w pozycji 5 od płaszczyzny A (Rysunek 3). Jest to kolejny istotny parametr, który oprócz kąta α opisuje niepłaskość struktury. W tym celu zoptymalizowano serię pochodnych dibenzoazepin z podstawnikami NO_2, CHO, COOH, CH_3, CH_2CH_3, NH_2, OH, Cl, $C(CH_3)_3$. Wraz ze wzrostem odległości atomów C5 i N5 od płaszczyzny A wzrasta wartość kąta α co oznacza, że struktura analizowanych cząsteczek staje się mniej płaska. Skorelowano również odległości atomów węgla C10 i C11 od płaszczyzny A. Okazało się, że wraz ze wzrostem odległości jednego atomu od płaszczyzny wzrasta także odległość drugiego atomu.
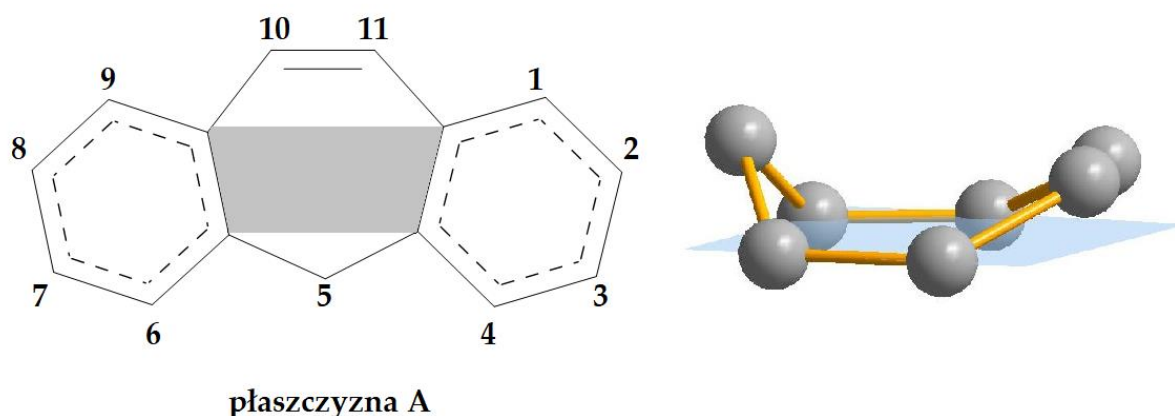
Rysunek 3. Odległość atomu azotu i węgla w pozycji 5 od płaszczyzny A.

Dla serii pochodnych antronów i antrachinonów zbadano również wpływ podstawników elektronodonorowych (NH_2) i elektronoakceptorowych (NO_2) w bocznym pierścieniu aromatycznym. Parametrem, który w jasny sposób opisywał ułożenie grup NH_2 i NO_2 względem podstawianego pierścienia był kąt β. Jest to kąt pomiędzy płaszczyzną podstawionego pierścienia a płaszczyzną wyznaczoną przez trzy atomy podstawnika. Im mniejsza była wartość kąta β, tym bardziej podstawnik układał się w pozycji równoległej do płaszczyzny podstawianego pierścienia. Grupa nitrowa wychyla się z płaszczyzny pierścienia benzenowego jeśli znajduje się w sąsiedztwie grupy ketonowej w środkowym pierścieniu. Wartość kąta α znacząco maleje, gdy w sąsiedztwie podstawnika nitrowego w pierścieniu aromatycznym nie ma grupy ketonowej lub innej grupy nitrowej Grupa nitrowa ma większy rozmiar niż grupa aminowa dlatego czterokrotne podstawienie tymi grupami powoduje utratę płaskiej struktury przez pierścień a kąt β w przypadku podstawienia grupami nitrowymi jest większy niż w przypadku grup aminowych. Dla pochodnych antronów i antrachinonów zbadano również wpływ wielokrotnego podstawienia bocznego pierścienia na

długość wiązania C-N łączącego podstawnik z pierścieniem. Wielokrotne podstawienie pierścienia aromatycznego podstawnikami NH_2 i NO_2 powoduje wydłużenie wiązania C-N. Sąsiedztwo grup aminowych i karbonylowych zmniejsza długość wiązania C-N w antronach i antrachinonach. Zauważono, że wiązanie C-N wydłuża się jeśli zwiększa się ilość podstawników.

Aby zbadać wpływ heteroatomów na geometrię analizowanych związków, zoptymalizowano pochodne dibenzoazepin i fenotiazyn z- i bez- heteroatomów w środkowym pierścieniu. Obecność heteroatomów wpływała na częściowo aromatyczny charakter środkowego pierścienia, co było to spowodowane obecnością wolnej pary elektronowej na heteroatomach.

Na geometrię związków trójpierścieniowych znaczący wpływ ma obecność wewnątrzcząsteczkowych wiązań wodorowych. Taką analizę przeprowadzono dla serii 1,8-dihydroxy-9-antronu i 1,8-dihydroxy-9-antranolu. Wraz ze wzrostem ilości wiązań wodorowych w pochodnych 1,8-dihydroxy-9-antronu i 1,8-dihydroxy-9-antranolu zmniejszała się wartość kąta α. Wyjątek stanowiły związki w formie ketonowej z podstawnikiem t-butylowym oraz karboksylowym i jednym wiązaniem wodorowym. Odstępstwa te są spowodowane różnicami w ułożeniu się podstawników w przestrzeni.

Aby potwierdzić wiarygodność przeprowadzonych obliczeń teoretycznych w przypadku każdej serii związków porównywano otrzymane wyniki z wynikami otrzymanymi dla struktur krystalicznych. Eksperymentalne dane strukturalne a w szczególności analizowane parametry geometryczne potwierdzają wpływ podstawników oraz obecność heteroatomów na strukturę środkowego pierścienia.

Aromatyczność pierścieni

Ze zmianami geometrii związane są zmiany aromatyczności pierścieni. Dla analizowanych struktur wykorzystywano geometryczny parametr aromatyczności HOMA (1) [5] oraz HOMED (2) [15], który uwzględnia siedmioczłonową budowę pierścienia oraz heteroatomy w pierścieniach.

$$HOMA = 1 - \frac{\alpha}{n}\sum\left(R_o - R_{ij}\right)^2 \qquad (1)$$

R_{opt}- zoptymalizowana długość wiązania CC w idealnie aromatycznym układzie równa 1.388 Å

R_{ij}- wyznaczona długość wiązania

α- stała standaryzacji

n- ilość wiązań

$$HOMED = 1 - \frac{\alpha}{n}\sum(R_o - R_{ij})^2 \qquad (2)$$

R_{opt}- zoptymalizowana długość wiązania CC w idealnie aromatycznym układzie równa 1.394 Å i zoptymalizowana długość wiązania CN równa 1.334 Å

R_{ij}- wyznaczona długość wiązania

α- stała standaryzacji: 5H-dibenzo[b,f]azepiny dla wiązania CN 84.52 i dla wiązania CC 80.90, 5H-dibenzo[a,d][7]annulenu dla wiązania CC 80.90, 10,11-dihydro-5H-dibenzo[b,f]azepiny dla wiązania CN 73.20 i dla wiązania CC 69.55, 10,11-dihydro-5H-dibenzo[a,d][7]annulenu dla wiązania CC 69.55

n- ilość wiązań

Zbadano wpływ wiązania podwójnego oraz heteroatomów w środkowym pierścieniu na aromatyczność pochodnych 5H-dibenzo[b,f]azepiny, 10,11-dihydro-5H-dibenzo[b,f]azepiny, 5H-dibenzo[a,d][7]annulenu,10,11-dihydro-5H-dibenzo[a,d][7]annulenu. Podwójne wiązanie w środkowym pierścieniu powodowało znaczącą delokalizację elektronów. Dodatkowo obecność atomu azotu z wolną parą elektronową w środkowym pierścieniu 5H-dibenzo[b,f]azepiny również wpływa na delokalizację elektronów co zwiększa parametr aromatyczności. W strukturze 10,11-dihydro-5H-dibenzo[a,d]annulenu, która nie zawiera w środkowym pierścieniu podwójnego wiązania i atomu azotu zaobserwowano najmniejszą wartość parametru HOMED. Na wartość parametru aromatyczności mogą także wpływać wiązania aromatyczne uwspólnione z bocznymi pierścieniami aromatycznymi.

Dla wszystkich serii analizowanych związków zaobserwowano, że na wartość parametru aromatyczności ma wpływ charakter elektronoakceptorowy lub elektronodonorowy podstawnika oraz jego wielkość. Aromatyczność pierścienia centralnego jest czuła nie tylko na podstawienie w pierścieniu środkowym, ale także w bocznym pierścieniu aromatycznym. Dodatkowo podstawienie środkowego pierścienia antronów, antrachinonów, 1,8-dihydroksy-9-antronu i 1,8-dihydroksy-9-antranolu za pomocą Cl, NO_2, CH_3, OH, NH_2 i t-but nie wpływa na rozkład gęstości elektronowej bocznych pierścieni aromatycznych a ich wartość parametru HOMA jest taka sama. Badając aromatyczność centralnego pierścienia w strukturach krystalicznych pochodnych dibenzoazepin zauważono, że może być ona łatwo modyfikowana nie tylko przez podstawnik, ale także otoczenie cząsteczki. Struktura z takim samym podstawnikiem

może być aromatyczna lub antyaromatyczna w zależności od upakowania w krysztale. Dlatego też HOMED środkowego pierścienia dla 5H-dibenzo[b,f]azepin mieścił się w szerokim zakresie (0.31-0.82), 5H-dibenzo[a,d][7]anulenu (0.28-0.94), 10,11-dihydro-5H-dibenzo[b,f]azepine (0.03-0.74), 10,11-dihydro-5H-dibenzo[a,d][7]anulen (-0.08-0.69).

Przeanalizowano również wpływ grup NH_2 i NO_2 podstawionych w pierścieniu bocznym na aromatyczność pierścienia centralnego. Najniższą wartość HOMA w pierścieniu centralnym zaobserwowano dla cząsteczki antronu, którą podstawiono czterema grupami nitrowymi w bocznym pierścieniu. Natomiast największy wzrost parametru HOMA dla pierścienia alifatycznego zaobserwowano w przypadku antrachinonu, który podstawiono dwoma grupami aminowymi w pozycji para w bocznym pierścieniu aromatycznym. Na gęstość elektronów w punkcie krytycznym centralnego pierścienia znacząco wpływa obecność grupy ketonowej. Jest to związane z tworzeniem się wiązań wodorowych między tlenem karbonylowym w środkowym pierścieniu a wodorem podstawnika aminowego w bocznym pierścieniu. Większą różnicę wartości HOMA w porównaniu ze strukturą niepodstawioną zaobserwowano dla struktur antrachinonów z podstawnikami w pierścieniu bocznym niż dla analogicznych antronów.
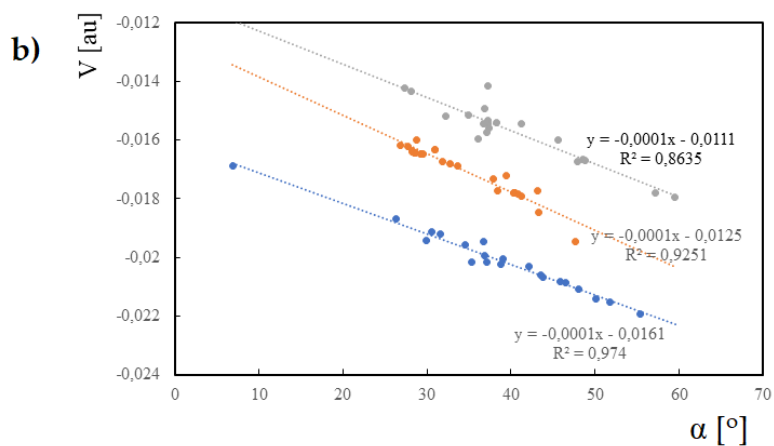
Gęstość elektronowa w punkcie krytycznym centralnego pierścienia

Wykorzystując metodę QTAIM (Quantum Theory of Atoms in Molecules) [8] wyznaczono gęstość elektronową w punkcie krytycznym pierścienia centralnego (RCP), energię kinetyczną i potencjalną elektronów w punkcie krytycznym centralnego pierścienia dla serii fenotiazyn oraz antronów i antrachinonów. Zauważono, że dla obu serii powyższe parametry są bardzo czułe na zmiany kąta pomiędzy dwoma bocznymi pierścieniami. Zwiększenie wartości kąta α wpływało na wzrost gęstości elektronowej i energii potencjalnej elektronów w punkcie krytycznym centralnego pierścienia. Odwrotna sytuacja miała miejsce dla energii kinetycznej elektronów- wraz ze wzrostem kąta α malała wartość energii kinetycznej elektronów w punkcie krytycznym środkowego pierścienia fenotiazyn oraz antronów i antrachinonów.

Skorelowano otrzymane wyniki gęstości elektronowej, energii potencjalnej i kinetycznej elektronów z kątem α dla pochodnych fenotiazyn (Rysunek 4) jak i 9,10-dihydriantracenu i 9H-tioksantenu. Pozwoliło to zbadać wpływ heteroatomów w pierścieniu alifatycznym na wyznaczane parametry gęstości elektronowej w punkcie krytycznym pierścienia. Zarówno dla pochodnych fenotiazyn jak i 9,10-dihydriantracenu i 9H-tioksantenu korelacje są różne i zależą od obecności heteroatomów w pierścieniu alifatycznym (Rysunek 4).
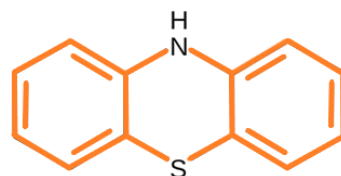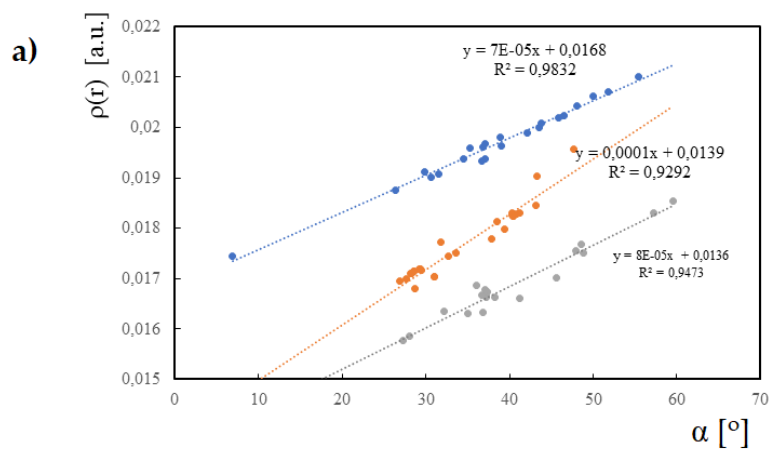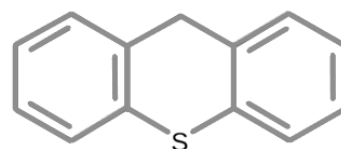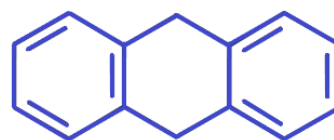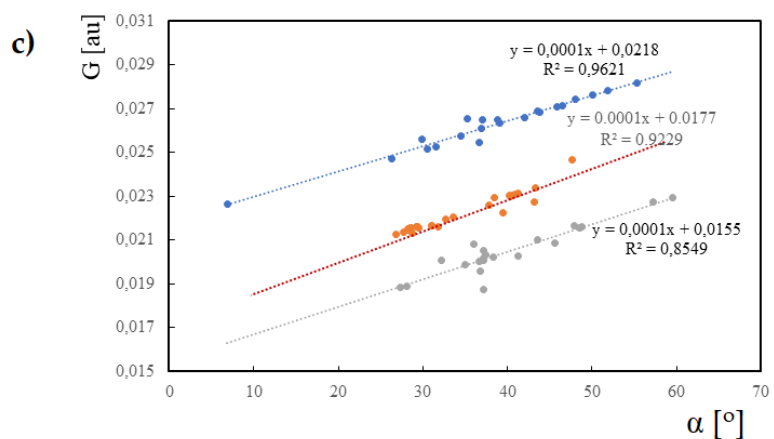
**Rysunek 4** Korelacja parametrów QTAIM w punkcie krytycznym pierścienia centralnego, gdzie a- gęstość elektronowa, b- energia kinetyczna, c- energia potencjalna gęstości elektronowej.

Eliptyczność wiązań w pierścieniu aromatycznym

Eliptyczność wiązania to parametr teorii QTAIM, który informuje o naturze wiązania a w szczególności o kształcie gęstości elektronowej wiązania łączącego dwa atomy. Jest ona zdefiniowana wzorem $\varepsilon = (\lambda_1/\lambda_2 - 1)$. Określa stopień preferencyjnego skupienia ładunku względem orientacji o najmniejszym λ. Dla wiązań cylindrycznie symetrycznych ε jest równe zeru a w przypadku wiązań podwójnych między atomami węgla ε wynosi około 0.74. Eliptyczność jest także miarą niestabilności strukturalnej. W przypadku wzrostu eliptyczności wiązanie staje się bardziej niestabilne. Warto zaznaczyć, że zmiana eliptyczności wiązań w pierścieniu aromatyczny może być powiązana ze zmianą aromatyczności. Oznacza to, że można wyznaczyć parametr aromatyczności wykorzystując nie tylko długości wiązań, ale także ich eliptyczność. Doskonałym przykładem parametru aromatyczności, w którym stosuje się eliptyczność wiązań jest EL [16].

Na eliptyczność i długość wiązań w środkowym pierścieniu wpływają podstawniki zarówno w środkowym, jak i w bocznym pierścieniu aromatycznym. Wyznaczono korelacje między eliptycznością wiązań a ich długościami. Dla serii antronów i antrachinonów oraz 1,8-dihydroksy-9-antronu i 1,8-dihydroksy-9-antranolu zaobserwowano spadek eliptyczności wraz ze wzrostem długości wiązania (Rysunek 5). W korelacjach 1,8-dihydroksy-9-antronu i 1,8-dihydroksy-9-antranolu dla wiązań C-C znajdujących się najbliżej grupy ketonowej wydzielono cztery grupy punktów: formę enolową, formę ketonową z dwoma wiązaniami wodorowymi, formę ketonową z jednym wiązaniem wodorowym i formę keto bez wiązań wodorowych. Zauważono, że największą eliptyczność i tym samym najkrótsze długości wiązań mają struktury w formie enolowej. Natomiast najniższe wartości eliptyczności i najdłuższe wiązania mają związki w formie ketonowej bez wiązań wodorowych. Daje to informację o tym, jak wiązania wodorowe wpływają na naturę wiązań w pierścieniu.

a)

$$y = 8.1013x^2 - 25.273x + 19.78$$
$$R^2 = 0.9915$$

b)

$$y = 7.9037x^2 - 24.763x + 19.457$$
$$R^2 = 0.9909$$
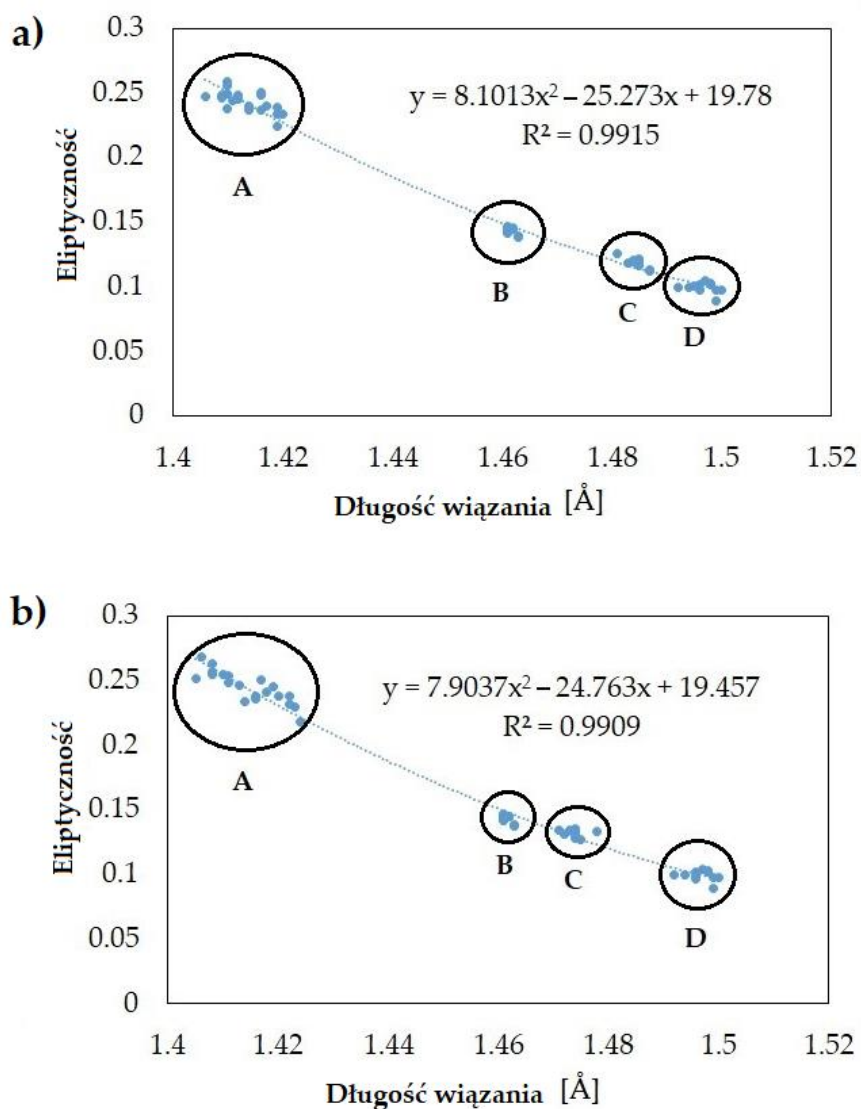
Rysunek 5 Korelacje eliptyczności z długością wiązań dla 1,8-dihydroksy-9-antronu i 1,8-dihydroksy-9-antranolu gdzie: a- wiązanie C8a-C9, b- wiązanie C9a-C9. Region A stanowi formy enolowe, region B- formy ketonowe z dwoma wiązaniami wodorowymi, region C- formy ketonowe z jednym wiązaniem wodorowym, region D- formy ketonowe bez wiązań wodorowych

Podobną korelację wyznaczono dla antronów i antrachinonów. Substytucja grup aminowych w bocznym pierścieniu aromatycznym antronów powoduje wzrost eliptyczności większości wiązań środkowego pierścienia. Największy wpływ na eliptyczność wiązań położonych najbliżej pierścienia podstawianego ma wpływ jednokrotne podstawienie grupą aminową. Podobnie jak dla antronów, największy wpływ na eliptyczność wiązań w środkowym pierścieniu antrachinonów ma podstawienie aminowe w bocznym pierścieniu. Podstawienie grup nitrowych w bocznym pierścieniu w większości przypadków również powoduje wzrost eliptyczności w grupie antronów i an-

trachinonów. Odstępstwa zaobserwowano dla wiązań środkowego pierścienia znajdujących się najbliżej grupy karbonylowej zarówno w antronach jak i antrachinonach. Brak grupy karbonylowej przy węglu C10 powoduje mniejszy przepływ gęstości elektronowej między pierścieniem bocznym a pierścieniem środkowym. Dlatego też podstawienie pierścienia aromatycznego za pomocą podstawników oddających i akceptujących elektrony nie wpływa znacząco na wiązania sąsiadujące z węglem C10. Zauważono, że substytucja w bocznym pierścieniu antronów i antrachinonów nieznacznie wpływa na wiązania wspólne dla pierścienia aromatycznego i alifatycznego. Różny charakter chemiczny oraz wielkość podstawników w środkowym pierścieniu antronów ma znaczący wpływ na długość i eliptyczność wiązań sąsiadujących z podstawianym atomem węgla.

Lokalna energia jonizacji

Aby określić obszary zawierające wysoce reaktywne elektrony w układach 1,8-dihydroksy-9-antronu i 1,8-dihydroksy-9-antranolu wyznaczono średnie lokalne energie jonizacji (ALIE-Average Local Ionization Energy) [14]. Jasnoniebieskie obszary odpowiadają minimom ALIE na izopowierzchni, wskazując korzystne miejsca ataku elektrofilowego. Ciemniejszy niebieski kolor wskazuje stosunkowo niskie wartości parametru ALIE, gdzie elektrony mają wysoką reaktywność. Podsumowując otrzymane wyniki: w strukturach w formie enolowej miejscem ataku elektrofilowego są atomy węgla w pierścieniach bocznych, które nie są współdzielone z pierścieniem środkowym. W przypadku formy enolowej podstawionej atomem wodoru miejscem ataku elektrofilowego jest także atom C10 (Rysunek 6). Te same miejsca ataku elektrofilowego stają się mniej wrażliwe w formach keto.
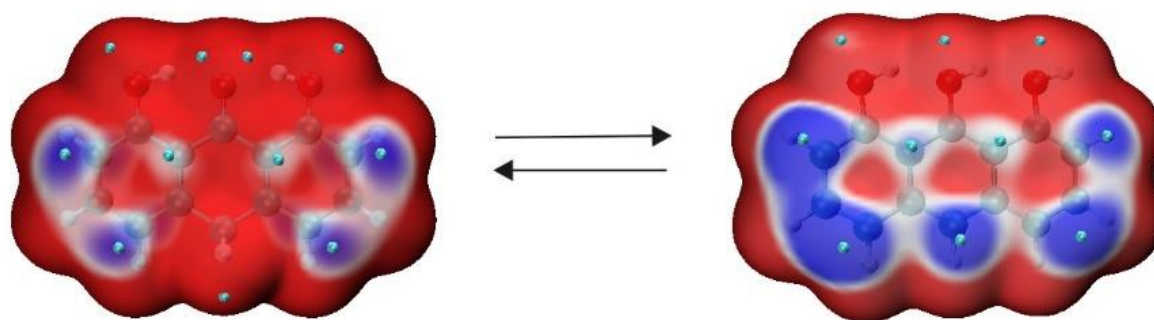
Rysunek 6 Lokalna energia jonizacji dla formy ketonowej i enolowej z atomem wodoru w pozycji C10.

Entalpia dysocjacji wiązania

Entalpia dysocjacji wiązania OH (BDE) [17] to jeden z parametrów pomocnych w przewidywaniu właściwości przeciwutleniających substancji. W związku z tym zbadano wpływ podstawników na entalpię dysocjacji wiązania OH przy atomie C10 w 1,8-dihydroksy-9-antranolu. Dodatkowo wyznaczono entalpię dysocjacji wiązania CH przy atomie C10 w 1,8-dihydroksy-9-antronie. Entalpie dysocjacji wiązań badano dla struktur z jednym i dwoma wewnątrzcząsteczkowymi wiązaniami wodorowymi.

Podstawianie środkowego pierścienia podstawnikiem charakteryzującym się właściwościami elektronoakceptorowymi powoduje wzrost BDE (O-H) i BDE(C-H) w strukturach z dwoma wewnątrzcząsteczkowymi wiązaniami wodorowymi. Substytucja tego samego podstawnika do struktur z jednym wiązaniem wodorowym spowodowała niewielki wzrost BDE(O-H) i niewielki spadek BDE(C-H). W związku z tym obecność takiego podstawnika jak NO_2 wraz z dwoma wiązaniami wodorowymi wpływa na trudniejsze oderwanie atomu wodoru od grupy OH i CH.

Zbadano również wpływ podstawnika o charakterze elektronodonorowym- NH_2 na BDE. Jego substytucja spowodowała niewielki spadek BDE(O-H) w stosunku do struktury niepodstawionej z jednym oraz dwoma wiązaniami wodorowymi co oznacza, że łatwiej jest oderwać wodór od grupy OH w strukturze enolowej. W strukturze w formie ketonowej podstawnik NH_2 spowodował niewielki wzrost BDE (C-H) co wpływa na trudniejsze oderwanie wodoru względem struktury niepodstawionej.

Wpływ obecności wewnątrzcząsteczkowych wiązań wodorowych

Analizując entalpie dysocjacji wiązań O-H i C-H zauważono, że na ich wartości ma wpływ obecność wewnątrzcząsteczkowych wiązań wodorowych. Struktury z dwoma wiązaniami wodorowymi mają niższe wartości BDE(O-H) i BDE(C-H) co wpływa na łatwiejsze oderwanie atomu wodoru od OH i CH. Porównując różnice entalpii swobodnej pomiędzy dwoma formami tautomerycznymi zaobserwowano, że jest ona większa dla struktur z dwoma wiązaniami wodorowymi niż z jednym. Wynika z tego, że łatwiej przesunąć równowagę w kierunku formy ketonowej w strukturach z dwoma wewnątrzcząsteczkowymi wiązaniami wodorowymi.

Zbadano wpływ ilości wewnątrzcząsteczkowych wiązań wodorowych na energię w serii związków 1,8-dihydroksy-9-antronu i 1,8-dihydroksy-9-anranolu (Rysunek 7). Związki z wewnątrzcząsteczkowym wiązaniem wodorowym mają najwyższą energię w strukturach w formie ketonowej z dwoma wiązaniami wodorowymi. Energia wiązania wodorowego w strukturach ketonowych w większości przypadków wynosi 12 kcal/mol a dla form enolowych 8 kcal/mol. Warto zaznaczyć, że na energię we-

wnątrzcząsteczkowego wiązania wodorowego ma wpływ nie tylko forma tautome-ryczna, ale także podstawniki w środkowym pierścieniu. Energia wiązania wodoro-wego dla związków w formie ketonowej z podstawnikami COOH, CH_3, Cl i CH_2CH_3 mieści się w zakresie 8-19kcal/mol.
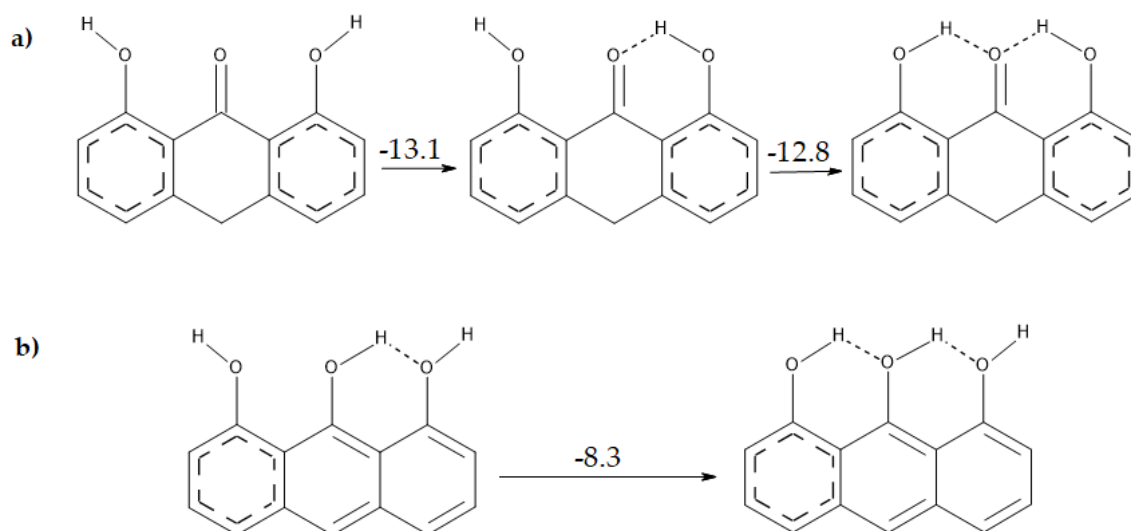

Rysunek 7 Energie struktur z wiązaniem wodorowym podstawionych atomem wodoru w pozycji C10, gdzie a- forma ketonowa, b- forma enolowa
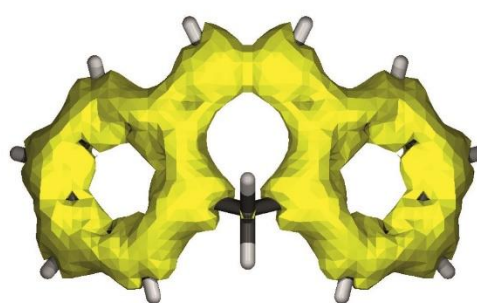
ACID

Zmiany delokalizacji gęstości elektronowej, które determinują reaktywność czą-steczki a także jej właściwości fizyczne i chemiczne wpływają na zmiany aromatycz-ności opisywane przez parametry HOMA i HOMED. Doskonałą metodą wizualizacji delokalizacji elektronów jest anizotropia gęstości indukowanej prądem- ACID [9]. Po-równując struktury z atomem azotu i podwójnym wiązaniem w środkowym pierście-niu do struktur bez azotu i z wiązaniem pojedynczym pozwala na zobrazowanie de-lokalizacji elektronów π w pierścieniach i określenie charakteru wiązań.

Na wygenerowanej powierzchni ACID struktury 5H-dibenzo[b,f]azepiny, która w pierścieniu środkowym zawiera zarówno wiązanie podwójne jak i atom azotu zaob-serwowano, że środkowy pierścień to nierozerwalna „obręcz" co oznacza delokalizo-wanie się elektronów (Rysunek 8). Wpływa to na częściowo aromatyczny charakter środkowego pierścienia. Zastąpienie atomu azotu atomem węgla w 5H-di-benzo[a,d][7]annulenie powstrzymuje delokalizację elektronów centralnego pierście-nia.
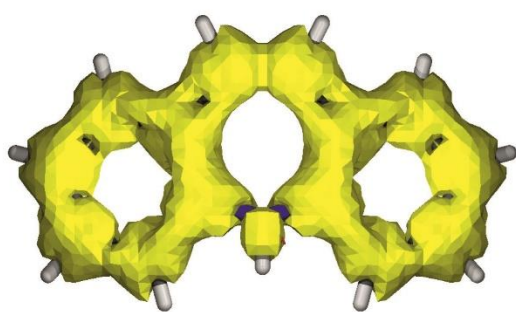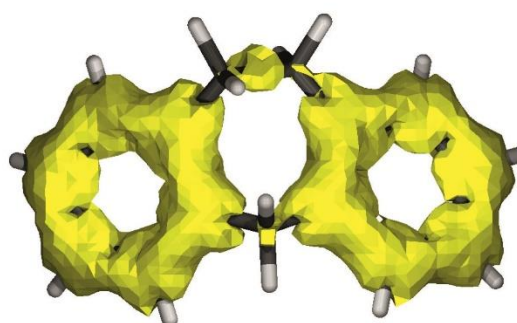
5H-dibenzo[b,f]azepina **5H-dibenzo[a,d][7]annulen**
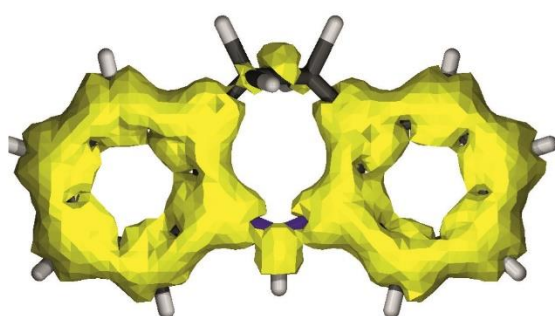
10,11-dihydro-5H-dibenzo[b,f]azepina **10,11-dihydro-5H-dibenzo[a,d][7]annulen**
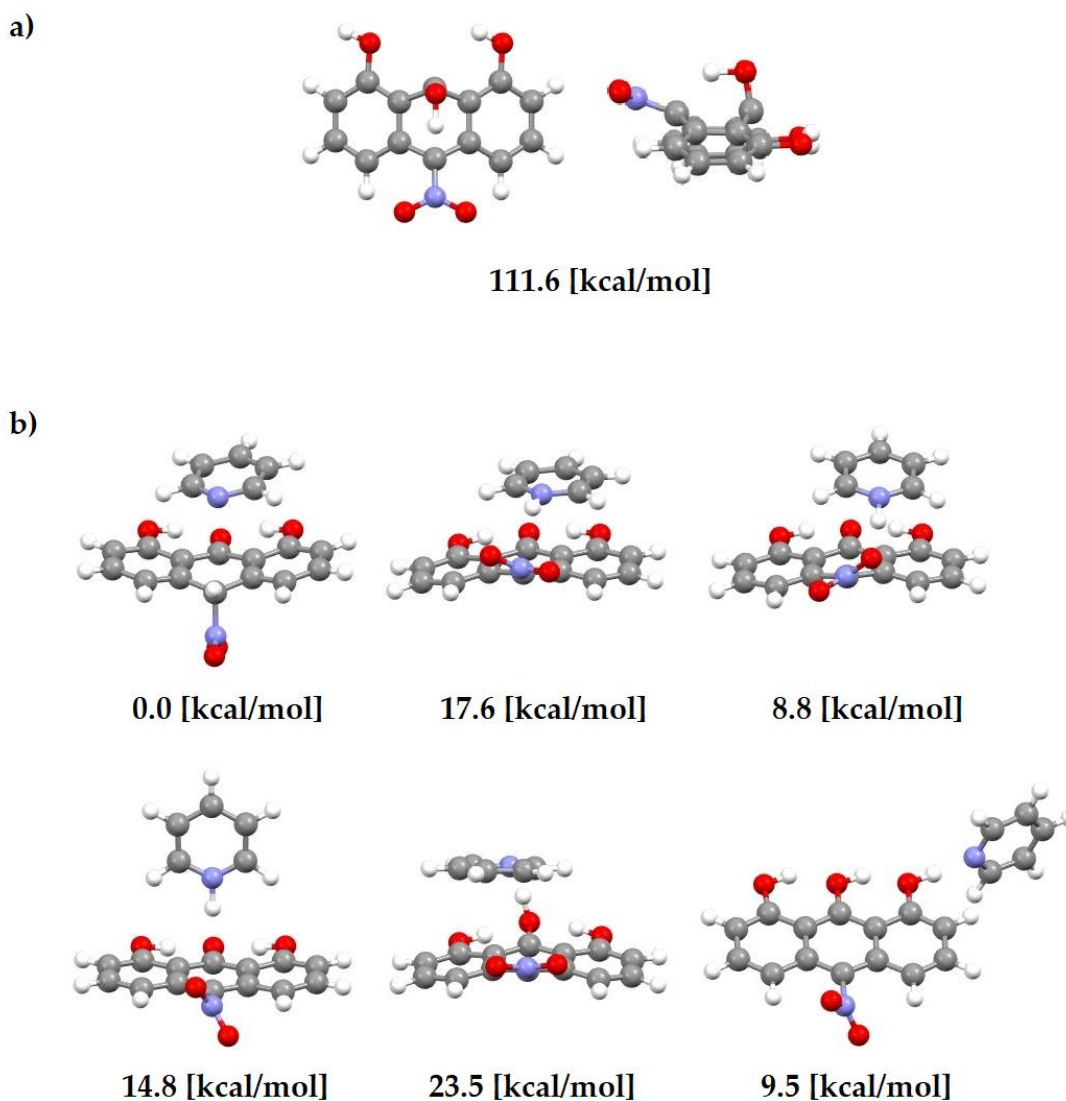
Rysunek 8 Wyznaczone powierzchnie ACID

Badanie mechanizmu tautomerii keto-enolowej

Ponieważ dla dihydroksyantronów możliwe jest przeniesienie protonu z grupy OH do atomu węgla C10, tym samym możliwe jest występowanie dwóch form tautomerycznych. Ponieważ równowaga keto-enolowa zasadniczo zmienia strukturę związku i jego właściwości fizykochemiczne, możliwość jej występowania powinna być zbadana dla wszystkich substancji o charakterze leczniczym. W reakcji keto-enolowej możliwe są dwa mechanizmy transferu protonu i oba zostały zbadane w niniejszej pracy. Pierwsza droga dotyczy wewnątrzcząsteczkowego transferu protonu. Z powodu wygięcia się środkowego pierścienia podczas przenoszenia protonu energia stanu przejściowego wynosi około 105-111 kcal/mol (Rysunek 9) [14]. W drugim mechanizmie reakcji wykorzystano cząsteczkę pirydyny jako nośnik protonu, przez co reakcja stała się wieloetapowa. Ma to wpływ na zmniejszenie energii stanu przejściowego do 17-23 kcal/mol [14].

Aby zbadać wpływ podstawników na transfer protonu w reakcji keto-enolowej dla obu mechanizmów reakcji zoptymalizowano stany przejściowe z różnymi podstawni-

kami w środkowym pierścieniu alifatycznym. W przypadku wewnątrzcząsteczkowego przeniesienia protonu nie zauważono znaczących różnic w energii stanów przejściowych w przypadku podstawienia centralnego pierścienia grupami o charakterze elektronodorowym i elektronoakceptorowym.

a)

111.6 [kcal/mol]

b)

0.0 [kcal/mol]   **17.6 [kcal/mol]**   **8.8 [kcal/mol]**

14.8 [kcal/mol]   **23.5 [kcal/mol]**   **9.5 [kcal/mol]**

Rysunek 9 Energie stanów przejściowych w reakcji keto-enolowej a- z wewnątrzcząsteczkowym przeniesieniem protonu, b- mechanizm reakcji z wykorzystaniem pirydyny jako nośnika protonu.

Druga ścieżka przeniesienia protonu ze względu na większą ilość etapów charakteryzuje się znacznie mniejszymi energiami stanów przejściowych. Pierwszym krokiem reakcji jest przeniesienie protonu z C10 na atom azotu w cząsteczce pirydyny. Kolejnym etapem jest utworzenie jonu. Cząsteczka pirydyny obraca się tak, aby atom

azotu znajdował się w pobliżu atomu tlenu w środkowym pierścieniu w wyniku czego tworzy się wiązanie wodorowe. Aby doszło do przeniesienia protonu z atomu azotu w cząsteczce pirydyny na tlen w analizowanej strukturze dając enolową formę tautomeryczną, potrzebna jest niewielka energia swobodna (Rysunek 9).

Równowaga keto-enolowa to szybka reakcja, która często silnie faworyzuje jeden z tautomerów. Obliczenia wskazują, że to forma ketonowa dominuje w mieszaninie w fazie gazowej. Ze względu na niewielkie energie stanów przejściowych na ścieżce z udziałem pirydyny ta reakcja przeniesienia protonu jest bardziej prawdopodobna.

Wnioski

Głównym celem pracy było wyznaczenie parametrów, które w znaczący sposób odzwierciedlają zmiany geometryczne analizowanych związków co w konsekwencji może mieć wpływ na ich właściwości fizykochemiczne. Właściwości fizykochemiczne związków leczniczych są związane z ich przyswajalnością oraz działaniem jako leki. Ponieważ większość właściwości fizykochemicznych oraz biodostępność związku wynika z jego struktury molekularnej, znajomość struktury oraz zmian w geometrii spowodowanych różnymi czynnikami może pozytywnie wpłynąć na projektowanie nowych leków o oczekiwanych właściwościach.

Najczulszym parametrem opisującym geometrię badanych struktur był kąt pomiędzy dwoma pierścieniami aromatycznymi. Jego wartość zależała od charakteru elektronodonorowego lub elektronoakcpetorowego podstawników w środkowym pierścieniu alifatycznym. Ułożenie podstawników w przestrzeni również miało wpływ na geometrię badanych związków. Energie struktur z podstawnikami ułożonymi ekwatorialnie i aksjalnie były zbliżone. Zmiana wartości kąta α przyczynia się do zmiany konformacji centralnego pierścienia alifatycznego. Gęstość elektronowa, energia kinetyczna i potencjalna elektronów w RCP są czułe na zmiany kąta α.

Na wartość kąta α wpływ ma także obecność wewnątrzcząsteczkowych wiązań wodorowych w 1,8-dihydroksy-9-antronie oraz 1,8-dihydroksy-9-antranolu. Obecność dwóch wewnątrzcząsteczkowych wiązań wodorowych powoduje zmniejszenie kąta motylkowego co jest efektem wypłaszczania się struktury.

Podstawienie bocznego pierścienia aromatycznego podstawnikami o charakterze elektronodonorowym i elektronoakceptorowym wpłynęło na zmianę struktury centralnego pierścienia a co za tym idzie także parametru aromatyczności.

Analizując serię pochodnych dibenzoazepin zbadano wpływ atomu azotu oraz podwójnego wiązania w środkowym pierścieniu na jego aromatyczność. Okazało się,

że obecność atomu azotu i podwójnego wiązania wpływa na delokalizację elektronów w środkowym pierścieniu zwiększając tym samym parametr aromatyczności HOMED co doskonale obrazują wygenerowane powierzchnie ACID.

Kolejnym istotnym parametrem, który w doskonały sposób opisuje geometrię cząsteczki jest odległość atomów azotu/węgla od płaszczyzny wyznaczonej przez cztery atomy węgla środkowego pierścienia uwspólnione z pierścieniami zewnętrznymi. Oprócz podstawników w środkowym pierścieniu na strukturę oraz aromatyczność centralnego pierścienia mają wpływ podwójne wiązania oraz heteroatomy. Częściowo aromatyczny charakter jest związany z obecnością wolnej pary elektronowej na atomie azotu, delokalizacją wiązania podwójnego a także udział aromatycznych elektronów, które pochodzą z bocznych pierścieni.

Analizując wpływ podstawników o różnym charakterze chemicznym na właściwości antyoksydacyjne badanych związków stwierdzono, że najlepszych właściwości przeciwutleniających można spodziewać się po związku z podstawnikiem NH_2. Dzięki wyznaczeniu energii stanów przejściowych zaobserwowano, że zmienia się ona nieznacznie w zależności od podstawnika. Na szybkość reakcji keto-enolowej istotny wpływ ma wykorzystana ścieżka przeniesienia protonu. Z tego względu przemiana keto-enolowa zachodzi znacznie szybciej w obecności pirydyny jako nośnika protonu.

Bibliografia

1. Prisinzano, T. E. Medicinal Chemistry: A Molecular and Biochemical Approach. Third Edition By Thomas Nogrady and Donald F. Weaver. Oxford University Press, New York. 2005. ISBN 978-0-19-510456 (Paperback). *J. Med. Chem.* **49**, 3428–3428 (2006).

2. Mosnaim, A.D., Ranade, V.V, Wolf, M.E., Puente, J., Valenzuela, A.M., Phenothiazinemolecule provides the basic chemical structure for various classes of pharmacotherapeutic agents, Am. J. Therapeut. 13 (2006) 261e273

3. Marsden, J. R., Coburn, P. R., Marks, J., Shuster, S. Measurement of the response of psoriasis to short-term application of anthralin. *Br J Dermatol* **109**, 209–218 (1983).

4. Rodríguez-Gamboa, T. *et al.* Anthrone and oxanthrone C,O-diglycosides from Picramnia teapensis. *Phytochemistry* (2000) doi:10.1016/S0031-9422(00)00323-X.

5. Krygowski, T. M. Crystallographic Studies of Inter- and Intramolecular Interactions Reflected in Aromatic Character of π-Electron Systems. *Journal of Chemical Information and Computer Sciences* (1993) doi:10.1021/ci00011a011.

6. Frisch, M.J. et al. Gaussian Inc 16, Revision A.03. Wallingford CT. (2016).

7. Grimme, S., Antony, J., Ehrlich, S., Krieg, H. A consistent and accurate ab initio parametrization of density functional dispersion correction (DFT-D) for the 94 elements H-Pu. *Journal of Chemical Physics* (2010) doi:10.1063/1.3382344.

8. Bader, R.F.W. Atoms in Molecules: A Quantum Theory, Oxford University Press, New York, 1990

9. Herges, R.; Geuenich, D. Delocalization of Electrons in Molecules. J. Phys. Chem. A **2001**, 105, 3214–3220

10. Allen, F. H. The Cambridge Structural Database: A quarter of a million crystal structures and rising. *Acta Crystallographica Section B: Structural Science* (2002) doi:10.1107/S0108768102003890.

11. Szymańska, M., Majerz, I. Theoretical Study of the Geometry of Dibenzoazepine Analogues. *Molecules* **27**, 790 (2022).

12. Szymańska, M., Majerz, I. Geometry and electron density of phenothazines. *Journal of Molecular Structure* (2020) doi:10.1016/j.molstruc.2019.127095.

13. Szymańska, M., Majerz, I. Effect of Substitution of Hydrogen Atoms in the Molecules of Anthrone and Anthraquinone. *Molecules (Basel, Switzerland)* **26**, (2021).

14. Szymańska, M., Majerz, I. Prototropy, Intramolecular Interactions, Electron Delocalization, and Physicochemical Properties of 1,8-dihydroxy-9-anthrone—DFT-D3 Study of Substituent Effects. *Molecules* **28**, 344 (2023).

15. Raczyńska, E. D., Hallman, M., Kolczyńska, K., Stępniewski, T. M. On the Harmonic Oscillator Model of Electron Delocalization (HOMED) Index and its Application to Heteroatomic π-Electron Systems. *Symmetry* **2**, 1485–1509 (2010).

16. Dominikowska, J., Palusiak, M. EL: the new aromaticity measure based on one-electron density function. *Structural Chemistry* **23**, 1173–1183 (2012).

17. Nazarparvar, E., Zahedi, M. & Klein, E. Density functional theory (B3LYP) study of substituent effects on O-H bond dissociation enthalpies of trans -resveratrol derivatives and the role of intramolecular hydrogen bonds. *Journal of Organic Chemistry* **77**, 10093–10104 (2012).

Konferencje

1. Szymańska Małgorzata, Majerz Irena: Teoretyczne badanie struktur pochodnych dibenzoazepiny, W: V Ogólnopolska Konferencja Naukowa "Współczesne zastosowanie metod analitycznych w farmacji i medycynie". [Online], 27 listopada 2020 r. Książka abstraktów, 2020, s.37-38

2. Szymańska Małgorzata, Majerz Irena: Theoretical study of monoanthrones, W: 4th International Wroclaw Scientific Meetings. Wrocław, 09-10 October 2020 / Kulbacka Julita, Rembiałkowska Nina, Weżgowiec Joanna (*red.*), 2020, Wrocław, Wydawnictwo Naukowe TYGIEL sp. z o.o., s.239-240, ISBN 978-83-66489-37-0

3. Polesiak Małgorzata, Majerz Irena: Wykorzystanie metod obliczeniowych do analizy struktury dikumarolu, W: IV Ogólnopolska Konferencja Naukowa "Współczesne zastosowanie metod analitycznych w farmacji i medycynie". Wrocław, 12 kwietnia 2019 r. Książka abstraktów, 2019, s.[36]

Wykaz publikacji wchodzących w skład rozprawy

Szymańska Małgorzata, Majerz Irena: Geometry and electron density of phenothazines, Journal of Molecular Structure, 2020, vol. 1200, art.127095 [15 s.]. DOI:10.1016/j.molstruc.2019.127095

Szymańska Małgorzata, Majerz Irena: Effect of substitution of hydrogen atoms in the molecules of anthrone and anthraquinone, Molecules, 2021, vol. 26, nr 2, art.502 [23 s.]. DOI:10.3390/molecules26020502

Szymańska Małgorzata, Majerz Irena: Theoretical study of the geometry of dibenzoazepine analogues, Molecules, 2022, vol. 27, nr 3, art.790 [23 s.]. DOI:10.3390/molecules27030790

Szymańska Małgorzata, Majerz Irena: Prototropy, intramolecular interactions, electron delocalization, and physicochemical properties of 1,8-dihydroxy-9-anthrone - DFT-D3 study of substituent effects, Molecules, 2023, vol. 28, nr 1, art.344 [24 s.]. DOI:10.3390/molecules28010344
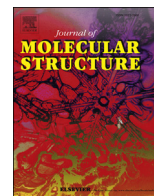
Geometry and electron density of phenothazines

Małgorzata Szymańska, Irena Majerz*

Faculty of Pharmacy, Wroclaw Medical University, Borowska 211a, 50-556, Wroclaw, Poland

ARTICLE INFO

ABSTRACT

A systematic theoretical analysis of the structural parameters of 9,10-dihydroanthracene, *9H*-thioxanthene and phenothiazine was performed at DFT B3LYP/6-311++G**-GD3 level. The main structural parameter determining the conformation and the electron density at the ring-critical point of the central ring is the angle between the aromatic rings. Although the axial orientation of the substituent at the central ring is preferred, both directions of the substituent are characterized by similar energy and can be realized in the solid state.

© 2019 Elsevier B.V. All rights reserved.

1. Introduction

Phenothiazine derivatives play an important role in many areas of medicine since they have an affinity for many receptors, enzymes and proteins [1–4]. Because phenothiazine derivatives take part in a wide variety of biological processes and are characterized by low toxicity, they are commonly used as popular medicines to treat a wide variety of diseases. Currently about 150 derivatives of phenothiazines are used in medicine and efforts are constantly being made to produce new derivatives.

Phenothiazine derivatives have antipsychotic [1,5–10], sedative [8], antihistamine [8], antidepressant [11], antiemetic [8], antibacterial [2,8], anesthetic [8], analgesic [8], anti-migraine [8,12], spasmolytic [8], anti-schizophrenic [8,10,13,14], and anticancer effects [15–19]. They are also used in the treatment of Alzheimer's disease [3,20]. Phenothiazines have properties that modify multidrug resistance (MDR), which is especially significant in anticancer therapy [15,21,22].

The antipsychotic effect of phenothiazines is related to their affinity to dopaminergic and serotoninergic receptors [1,5,7–10,23]. Blockage of dopaminergic receptors also affects antischizophrenic activity [8,13,14]. Many of the phenothiazine derivatives have an affinity for adrenergic receptors, which may also affect the anti-schizophrenic effect [8,10] Phenothiazine derivatives

have antiallergic, antiemetic and sedative effects due to the fact that they are histamine-receptor antagonists [8]. Chlorpromazine blocks peripheral adrenergic receptors and acts on the smooth muscles of the arterial walls, which affects the expansion of blood vessels [24]. Phenothiazine derivatives are antagonists of calmodulin, which is a protein involved in cell proliferation [4,25]. In view of the fact that phenothiazines are P-glycoprotein inhibitors, they also find applications in the modification of multi-drug resistance [15,21]. Phenothiazines are inhibitors of the butyrylcholinesterase enzyme that catalyzes dissociation of acetylcholine and is important in the treatment of Alzheimer's [20].

Phenothiazines are a group of neuroleptics with a tricyclic structure where two rings of benzene are connected by nitrogen and sulphur atoms. To the nitrogen atom a carbon chain containing a tertiary amine is attached. The affinity of phenothiazine derivatives to many biological structures is possible due to their unique conformation [26]. The structure of phenothiazines is not planar. It takes the form of a "butterfly" and the angle between the side aromatic rings can be different [10,26–31]. The structure of phenothiazine is presented in Scheme 1.

Modification of phenothiazine to obtain new derivatives consists of introducing of a new aminoalkyl chain in the N10 position [11,13] and this change can provide both electrostatic and hydrophobic interactions with the receptor. Positively charged nitrogen may bind to the anionic shape of the receptor and the end of the aminoalkyl chain may have hydrophobic interactions with the nonpolar regions of the inside channel wall near of the anionic site [8]. The length of the carbon chain affects the conformation and the

---

* Corresponding author.
 E-mail addresses: majerz@yahoo.com, irena.majerz@umed.wroc.pl (I. Majerz).
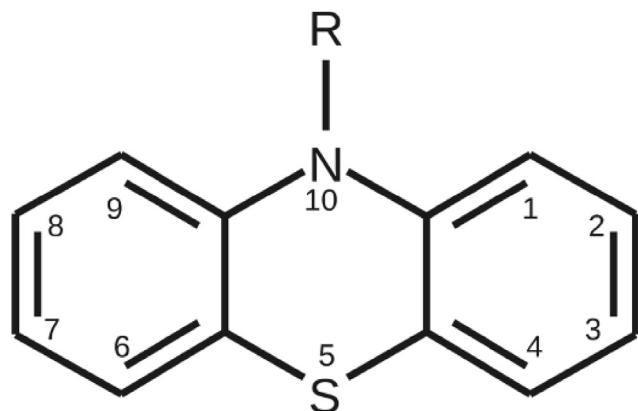
Scheme 1. Molecular structure of phenothiazine.

volume of the molecule. According to Darvesh [32], phenothiazine derivatives that have 5 or more carbon atoms in the N10 position inhibit butyrylcholinesterase enzyme without inhibiting acetylcholinesterase. It is similar when the substituent is a cyclic ring with 6 or more carbon atoms. Derivatives with a cyclic ring having 6 or more carbon atoms inhibit only butyrylcholinesterase enzyme [32]. The active site volume in acetylcholinesterase is smaller than in butyrylcholinesterase enzyme [20]. The presence of an additional substituent in the C2 position is not obligatory. However, it increases the antipsychotic activity. These substituents increase the lipophilicity of the molecules, making phenothiazines more easily cross the blood-brain barrier [33] and have a positive effect on antibacterial activity [8].

The structure of phenothiazine has a big influence on the antitumor effect, which is related to the affinity to calmodulin. Compounds that inhibit calmodulin have two aromatic rings and chain with an amine group. It is suggested that the structure of the molecule plays an important role in the interaction with this protein. The N10 aminoalkyl chain plays a significant role in anticancer treatment. Its length determines the strength of action of the drug, while the nature of the substituent in the C2 position determines the way in which the tumor line works with a drug [34].

Some authors [10,13,23,35] connect the affinity of phenothiazines for dopaminergic and histamine receptors with their similar structure to the structure of dopamine and histamine [10,13,23,35] Feinberg et al. [14] suggested that van der Waals interactions between the side chain and the C2 substituent might explain the ability of phenotiazines to adopt a dopamine-like conformation [14].

The spatial structure of the molecule plays an important role [7,13,36] Sungwoon Choi et al. [7], suggested that the particular mesoridazine enantiomers may have different pharmacodynamic, pharmacokinetic and toxicological properties. The stereochemistry of sulfoxide played a dominant role in structure-activity relationships [7]. These observations indicate also the stereospecificity of phenothiazine derivatives.

The non-planar structure of phenothiazines is associated with the direction of the electron pair on the nitrogen atom. Despite the fact that, according to many authors [11,20,37], there is no direct correlation between the dihedral angle and the phenothiazines' properties [11,20,37] the non-planar structure seems to be indispensable for neuroleptic action [11].

In this work we have undertaken a systematic theoretical study to analyze the structural parameters of phenothiazine (Scheme 2). The most characteristic is the angle between the side benzene-ring planes α_1 determined as the angle between the side aromatic ring plane including all the carbon atoms belonging to the side benzene ring. Independent of the substituent in the side benzene ring, the deviation from the benzene ring plane is not higher than 0.0154 Å. The second structural parameter important for the phenothiazine pharmaceutical activity is the angle between the planes containing four carbon atoms of the central aliphatic ring and the plane formed by the nitrogen and two carbon α_2 atoms. Also the direction of the N-R bond against the plane α_2 seems to be important for the pharmaceutical properties of phenothiazine (α_3).

Taking into account the importance of the molecular volume and the role of heteroatoms, we have investigated the influence of the heteroatoms in the phenothiazine central ring, and compared a series of phenothiazine, 9H-thioxanthene and 9,10-dihydroanthracene. To investigate the influence of possible conformations of the aliphatic chain linked to the central ring, the derivatives of 9H-thioxanthene and 9,10-dihydroanthracene with a different conformation of the substituents at the central ring have been optimized.

Systematic study of the structural parameters in Scheme 3 is connected with the optimization of the structures with the substituents with electron-donor and electron-withdrawing properties connected to the aliphatic carbon joining the benzene rings (the nitrogen atom for phenothiazine). In the case of phenothiazine, besides the typical substituents, the molecules used as popular drugs have also been optimized. Because it can be expected that the change of the angle between the aromatic rings should be connected with the change of the electron density, we have used the QTAIM method to perform systematic investigation of the electron density.

2. Computational details

The investigated molecules were optimized using a Gaussian 16 package [38] at DFT B3LYP/6-311++G** level [39,40], which included Grimme dispersion [41]. To check that the resultant geometry reached the energy minimum, vibrational frequencies were calculated. The wave function evaluated for the optimized molecules was used as the input to the AIMALL program [42].

3. Results

3.1. Geometry of investigated compounds

The angles most characteristic for the investigated molecules: α_1, α_2 and α_3 presented in Fig. 2 are collected in Table 1. The butterfly angle α_1 is very sensitive to the substituent connected to the carbon or nitrogen atom located between the benzene rings and changes in the range of $20-60°$.

The α_2 and α_3 angles change in a similar range. The α_1 and α_2 angles are related with a common relationship that includes all the investigated compounds, regardless of the presence of heteroatoms in the central ring: $\alpha_2 = 0.8369\alpha_1 + 2.6839$ ($R^2 = 0.8947$). This correlation shows that mutual location of the side benzene rings is connected with the change of geometry of the central ring. To compare the optimized and X-ray structures, this same correlation has been split into three groups to present the comparison in more detail (Fig. 1).

For 9,10-dihydroanthracene the α_1 and α_2 angles for X-ray structures follow the correlation for the optimized molecules. For 9H-thioxanthene the only structure with a tertbutyl substituent in CSD is far from the correlation line for the optimized molecules. In the case of phenothiazines the compounds with very low and very high α_1 do not follow the correlation so it can be used to predict the α_2 values for the compounds with α_1 in the range of $25-40°$. The packing of molecules in the crystal structure of 10H-phenothiazine
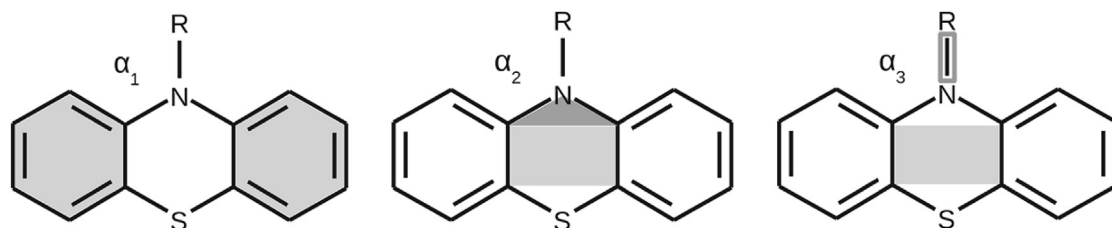
Scheme 2. The analyzed geometrical parameters of phenothiazine.

9,10-dihydroanthracene   9H-thioxanthene   phenothiazine
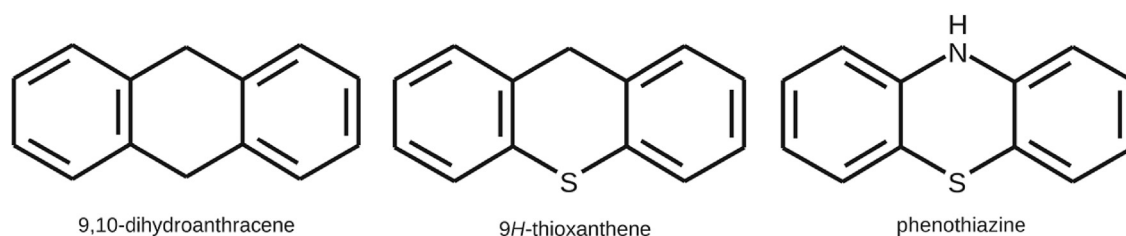
Scheme 3. Molecular structure of the investigated compounds.

(PHESAZ01) [6] is determined by the N−H⋯S interaction of 2.618 Å. 10-ethylphenothiazine crystallizes in Pna2$_1$ (NEPTAZ) [43], Pbca (NEPTAZ01) [44] and Pna2$_1$ (NEPTAZ02) [45] groups and the polymorphism is an evidence of flexibility of the phenothiazine aliphatic ring. In the crystal cell of 10-[2-(1-methylpiperidin-2-yl) ethyl]-2-methylsulfanyl-phenothiazine (TORDAZ) [46], two molecules with different geometry are present.

A substituent linked to the carbon atom of the central ring of 9,10-dihydroanthracene or 9H-thioxanthene can be located equatorially or axially against the ring. Also, for phenothiazine derivatives, the direction of the N-R bond to the central ring can be different. To check a preferable substituent location, for the model compounds the geometry with axial and equatorial locations of the substituents has been optimized and the geometrical parameters for 9,10-dihydroanthracenes and 9H-thioxanthenes have been compared in Table 2.

According to the energy change connected with the reorientation of the substituent from equatorial to axial orientation, for the majority of the compounds in Table 2 the preferred orientation of the substituent linked to the aliphatic carbon atom between the benzene rings is axial. The small energy connected with reorientation of the substituent suggests that every direction of the substituent against the central plane is possible. The energy difference between the equatorial and axial structure is especially low when the butterfly angle is small. It suggests that reorientation of the substituent is easier for the flat structures. Reorientation of the substituent from axial to equatorial orientation influences the geometry of 9,10-dihydroanthracene and 9H-thioxanthene so the α_1 and α_2 angles change but are still related according to the general correlation common for all compounds. The changes of α_1 and α_2 angle upon the substituent reorientation are related and can be expressed as: $\Delta\alpha_2 = 0.8857\Delta\alpha_1 - 0.1043$ ($R^2 = 0.8771$).

In the case of phenothiazine derivatives the typical angle between the N-R bond and the plane determined by four benzene carbons of the central ring (α_3) is in the range of 70−90° including the drug molecules with big substituents at the nitrogen. Among the drug molecules only N,N-dimethyl-3-(phenothiazin-10-yl)-propan-1-amine is characterized by the equatorial location of the substituent at the nitrogen so it can be expected that the axial substituent is typical for drug phenothiazines. Common correlations for the compounds with simple substituents at the central

ring and the drug molecules are evidence that substitution at the side benzene ring is not essential for the main geometrical parameters of the phenothiazine drugs.

Substitution of the central ring of 9,10-dihydroanthracene, 9H-thioxanthene and phenothiazine can change the butterfly angle and, as a consequence, other molecular angles. Despite the sensitivity of the angles, the bond lengths of the investigated compounds do not depend on the substitution and changes of the molecular conformation. The only change of the bond lengths can be seen for 9,10-dihydroanthracene and 9H-thioxanthene. The bonds common for the central ring and the benzene rings are elongated with the butterfly-angle increase, but the change is limited from 1.399 to 1.409 Å (CC = 0.0003α_1 + 1.3916, $R^2 = 0.8533$). Analogous changes for phenothiazine derivatives with a bulky substituent at the nitrogen atom are irregular.

3.2. Comparison of the optimized and X-ray structure

The optimized structure is very useful for investigation of the ideal structural parameters characterizing the single molecule in a vacuum. Besides the effects of substituents which influence the molecular bond lengths and angles, packing of the molecules in the crystal can also significantly change the molecular geometry. To check whether the molecules in the crystal meet the correlations found for the single molecules in a vacuum, Table 3 compares the α_1, α_2 and α_3 angles for the optimized molecules and analogous molecules in a crystal retrieved from CSD [47].

An axial location of similar substituents is typical for phenothiazine derivatives. Despite the fact that, according to the energy difference, the substituent at the central ring should be axially located, in the case of 9,10-dihydroanthracene and 9H-thioxanthene, in the crystal structure the methyl and tert-butyl substituents are close to being parallel to the central ring.

3.3. Electron density at central ring-critical point

Substitution of the central ring of phenothiazine, 9,10-dihydroanthracene and 9H-thioxanthene changes the interplanar angles but does not influence the bond lengths so it can be expected that the electron densities characterizing the chemical bonds are insensitive to the substituent at the central ring. In any case, the

Table 1
Geometrical parameters of the investigated compounds. α_1, α_2 and α_3 angles according to Scheme 2. The compounds in Table 1 are arranged in ascending order relative to butterfly angle α_1.

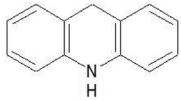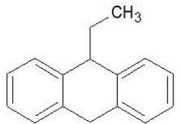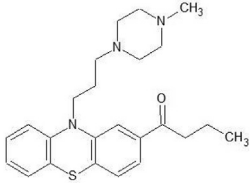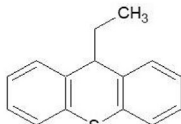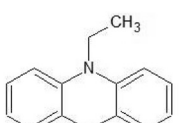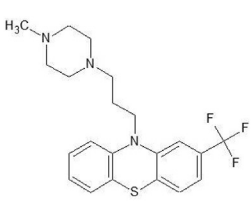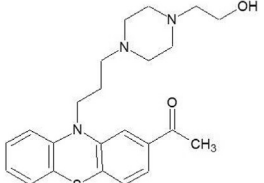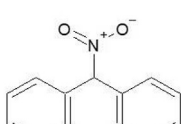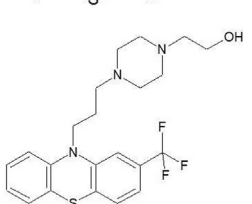| Compound name	α_1	α_2	α_3	Structure
9,10-dihydroacridine	25.616	21.867	82.863	
9-ethyl-9,10-dihydroanthracene	26.345	22.663	18.762	
1-[10-[3-(4-methylpiperazin-1-yl)propyl]phenothiazin-2-yl] butan-1-one	26.83	25.58	77.857	
9-ethyl-9*H*-thioxanthene	27.276	26.763	16.06	
10-ethylphenothiazine	27.705	25.748	76.58	
10-[3-(4-methylpiperazin-1-yl)propyl]-2-(trifluoromethyl) phenothiazine	28.207	26.871	76.964	
1-[10-[3-[4-(2-hydroxyethyl)piperazin-1-yl]propyl]phenothiazin-2-yl]ethanone	28.262	27.057	76.667	
9-nitro-9*H*-thioxanthene	28.276	28.767	8.138	
2-[4-[3-[2-(trifluoromethyl)phenothiazin-10-yl]propyl]piperazin-1-yl]ethanol	28.545	27.173	77.033	

Table 1 (*continued*)

Compound name	α_1	α_2	α_3	Structure
10-[3-(4-hydroxypiperidin-1-yl)propyl]phenothiazine-2-carbonitrile	28.597	27.337	76.423	
10*H*-pyrido[3,2-*b*] [1,4]benzothiazine	28.75	26.596	85.672	
2-[4-[3-(2-chlorophenothiazin-10-yl)propyl]piperazin-1-yl]ethanol	29.268	27.324	76.734	
N,N-dimethyl-10-[3-(4-methylpiperazin-1-yl)propyl] phenothiazine-2-sulfonamide	29.317	27.501	76.964	
2-chloro-10-[3-(4-methylpiperazin-1-yl)propyl] phenothiazine	29.33	27.414	76.541	
10-[3-(4-methylpiperazin-1-yl)propyl]phenothiazine	29.462	27.607	76.399	
9-nitro-9,10-dihydroanthracene	29.839	25.374	9.585	
9-nitro-9,10-dihydroanthracene	29.850	25.389	9.563	
9,10-dihydroanthracene-9-carbaldehyde	30.595	25.86	9.256	

(*continued on next page*)

Table 1 (*continued*)
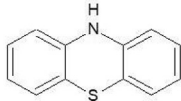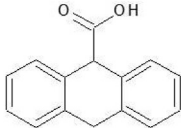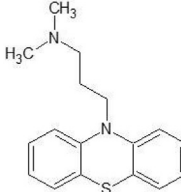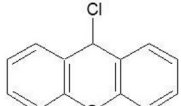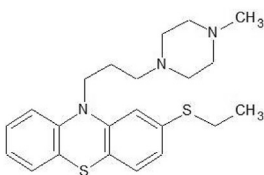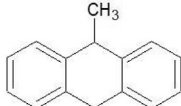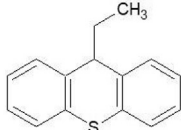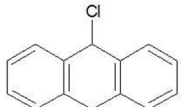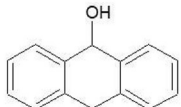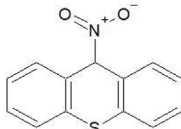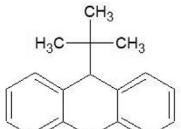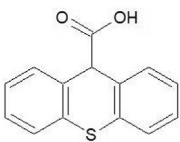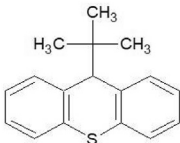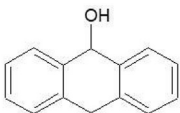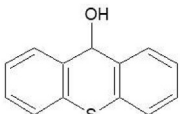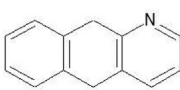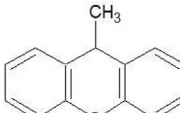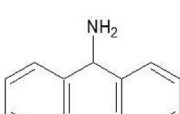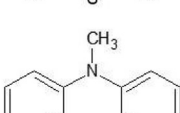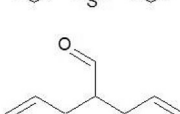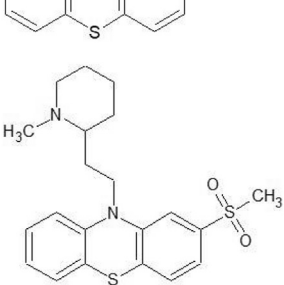
Compound name	α_1	α_2	α_3	Structure
10*H*-phenothiazine	30.997	30.063	87.113	
9,10-dihydroanthracene-9-carboxylic acid	31.529	25.618	13.505	
N,N-dimethyl-3-(phenothiazin-10-yl)-propan-1-amine	31.792	27.542	39.194	
9-chloro-9*H*-thioxanthene	32.161	31.666	4.685	
2-ethylsulfanyl-10-[3-(4-methylpiperazin-1-yl)propyl] phenothiazine	32.74	29.974	75.858	
9-methyl-9,10-dihydroanthracene	34.491	29.771	8.762	
9-ethyl-9*H*-thioxanthene	34.974	36.305	83.97	
9-chloro-9,10-dihydroanthracene	35.27	28.961	6.456	
9,10-dihydroanthracen-9-ol	35.549	29.538	72.674	
9-nitro-9*H*-thioxanthene	36.055	35.734	1.864	
9-tert-butyl-9,10-dihydroanthracene	36.686	28.74	15.408	

Table 1 (*continued*)

Compound name	α_1	α_2	α_3	Structure
9H-thioxanthene-9-carboxylic acid	36.701	31.857	10.282	
9-tert-butyl-9H-thioxanthene	36.794	32.358	13.418	
9,10-dihydroanthracen-9-ol	37.053	33.181	2.249	
9H-thioxanthene-9-ol	37.113	37.531	2.445	
5,10-dihydrobenzo[g]quinoline	37.143	30.306		
9-methyl-9H-thioxanthene	37.222	35.972	3.212	
9H-thioxanthene-9-amine	37.373	37.298	3.373	
10-Methylphenothiazine	37.861	35.618	76.49	
9H-thioxanthene-9-carbaldehyde	38.262	37.07	76.047	
10-[2-(1-methylpiperidin-2-yl)ethyl]-2-methylsulfonyl-phenothiazine	38.45	37.216	73.702	

Table 1 (*continued*)
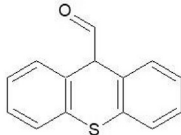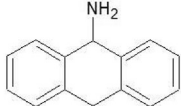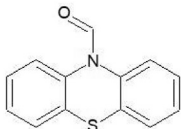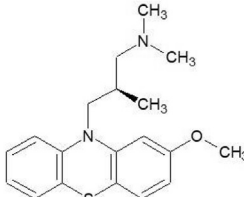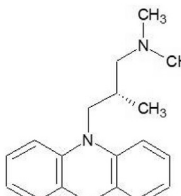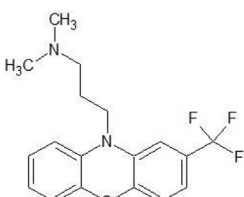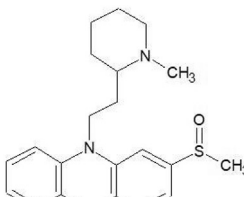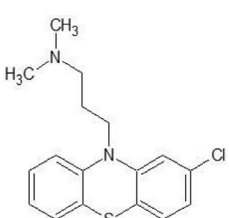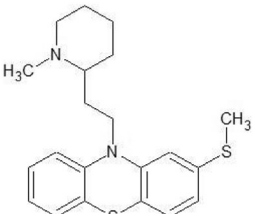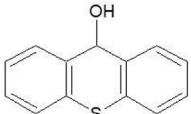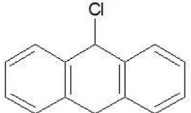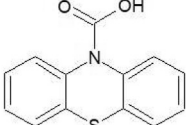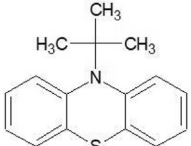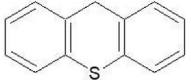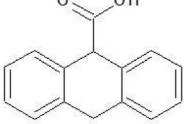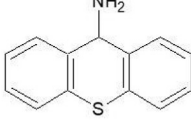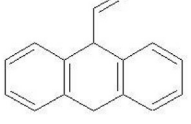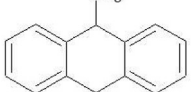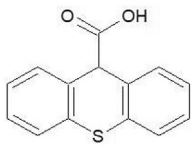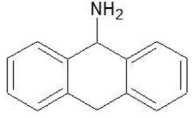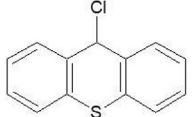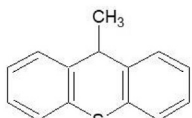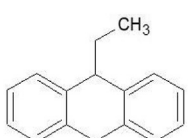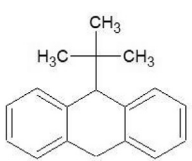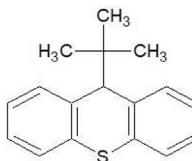
Compound name	α_1	α_2	α_3	Structure
9*H*-thioxanthene-9-carbaldehyde	38.509	37.757	2.829	
9,10-dihydroanthracene-9-amine	38.841	33.903	0.613	
9,10-dihydroanthracene	39.036	32.238		
Phenothiazine-10-carbaldehyde	39.445	37.283	49.023	
(2R)-3-(2-methoxyphenothiazin-10-yl)-*N,N*,2-trimethyl-propan-1-amine	40.304	36.874	69.037	
(2S)−N,N,2-Trimethyl-3-(phenothiazin-10-yl)-propan-1-amine	40.37	37.096	68.605	
N,N-dimethyl-3-[2-(trifluoromethyl)phenothiazin-10-yl] propan-1-amine	40.438	37.401	70.153	
10-[2-(1-methylpiperidin-2-yl)ethyl]-2-methylsulfinyl phenothiazine	40.493	37.626	72.369	
3-(2-chlorophenothiazin-10-yl)-N,N-dimethyl-propan-1-amine	40.862	37.5	70.176	

Table 1 (*continued*)

Compound name	α_1	α_2	α_3	Structure
10-[2-(1-methylpiperidin-2-yl)ethyl]-2-methylsulfanyl-phenothiazine	41.225	37.737	71.447	
9H-thioxanthene-9-ol	41.236	38.457	82.2	
9-chloro-9,10-dihydroanthracene	42.059	38.164	82.034	
Phenothiazine-10-carboxylic acid	43.129	39.63	41.061	
10-tert-butyl-phenothiazine	43.269	38.508	33.613	
9H-thioxanthene	43.527	40.417		
9,10-dihydroanthracene-9-carboxylic acid	43.597	38.748	81.454	
9H-thioxanthene-9-amine	45.593	41.914	87.341	
9,10-dihydroanthracene-9-carbaldehyde	45.803	39.714	87.477	
9-methyl-9,10-dihydroanthracene	46.543	38.497	84.326	

(*continued on next page*)

Table 1 (*continued*)

Compound name	α_1	α_2	α_3	Structure
9*H*-thioxanthene-9-carboxylic acid	47.963	46.497	89.697	
9,10-dihydroanthracene-9-amine	48.048	40.938	83.102	
9-chloro-9*H*-thioxanthene	48.557	46.937	88.623	
9-methyl-9*H*-thioxanthene	48.787	44.69	89.153	
9-ethyl-9,10-dihydroanthracene	51.81	41.778	89.404	
9-tert-butyl-9,10-dihydroanthracene	55.366	45.547	78.938	
9-tert-butyl-9*H*-thioxanthene	57.182	50.538	76.215	

QTAIM parameters [54] of the central-ring-critical point located in the center of the aliphatic ring are sensitive to the heteroatoms and strongly depend on the butterfly ring. Fig. 2 presents the correlations of main electron-density parameters for the central-ring-critical points.

Besides the electron density at the ring-critical point (RCP), a very illustrative parameter delivered by QTAIM theory is the potential (V(r)) and kinetic (G(r)) energy of the electrons at the critical point [55,56]. Potential energy is connected with the pressure exerted on the electrons at the RCP by other electrons. Kinetic energy is related to the pressure exerted by the electrons at the RCP on other electrons and illustrates the mobility of the electrons at the RCP. According to the correlations in Fig. 2, bending of the central ring causes an increase of the electron density at the RCP and the electrons at RCP become more mobile and influenced by the pressure of other electrons. When the correlations of the butterfly angle with other geometrical parameters of the investigated molecules were common for 9,10-dihydroanthracene, 9*H*-thioxanthene and phenothiazine, the correlations of electron density and kinetic and potential energy of the electrons at the RCP are different and dependent on the heteroatoms in the central ring. The slope of the

correlation lines shows that the electron-density parameters are more sensitive to the geometry changes in the case of phenothiazine derivatives than 9,10-dihydroanthracene and 9*H*-thioxanthene.

4. Conclusions

The angle between the aromatic ring of 9,10-dihydroanthracene, 9*H*-thioxanthene and phenothiazine (butterfly angle) is the main structural parameter determining the conformation of the central ring. The substituent at the central ring of 9,10-dihydroanthracene and 9*H*-thioxanthene at the nitrogen atom of phenothiazine can be directed axially or equatorially and both directions are characterized by similar energy and can be realized in the solid state. Correlation of α_1 and α_2 angles causes a change of the butterfly angle to result in a change of the conformation of the central ring of 9,10-dihydroanthracene, 9*H*-thioxanthene and phenothiazine. The electron density and potential and kinetic energy of the electrons at the central-ring-critical point are sensitive to the butterfly angle and the ring heteroatoms.

Fig. 1. Correlation of α_1 and α_2 angles for 9,10-dihydroanthracene (a), *9H*-thioxanthene (b) and phenothiazine (c). Red points − X-ray structure.
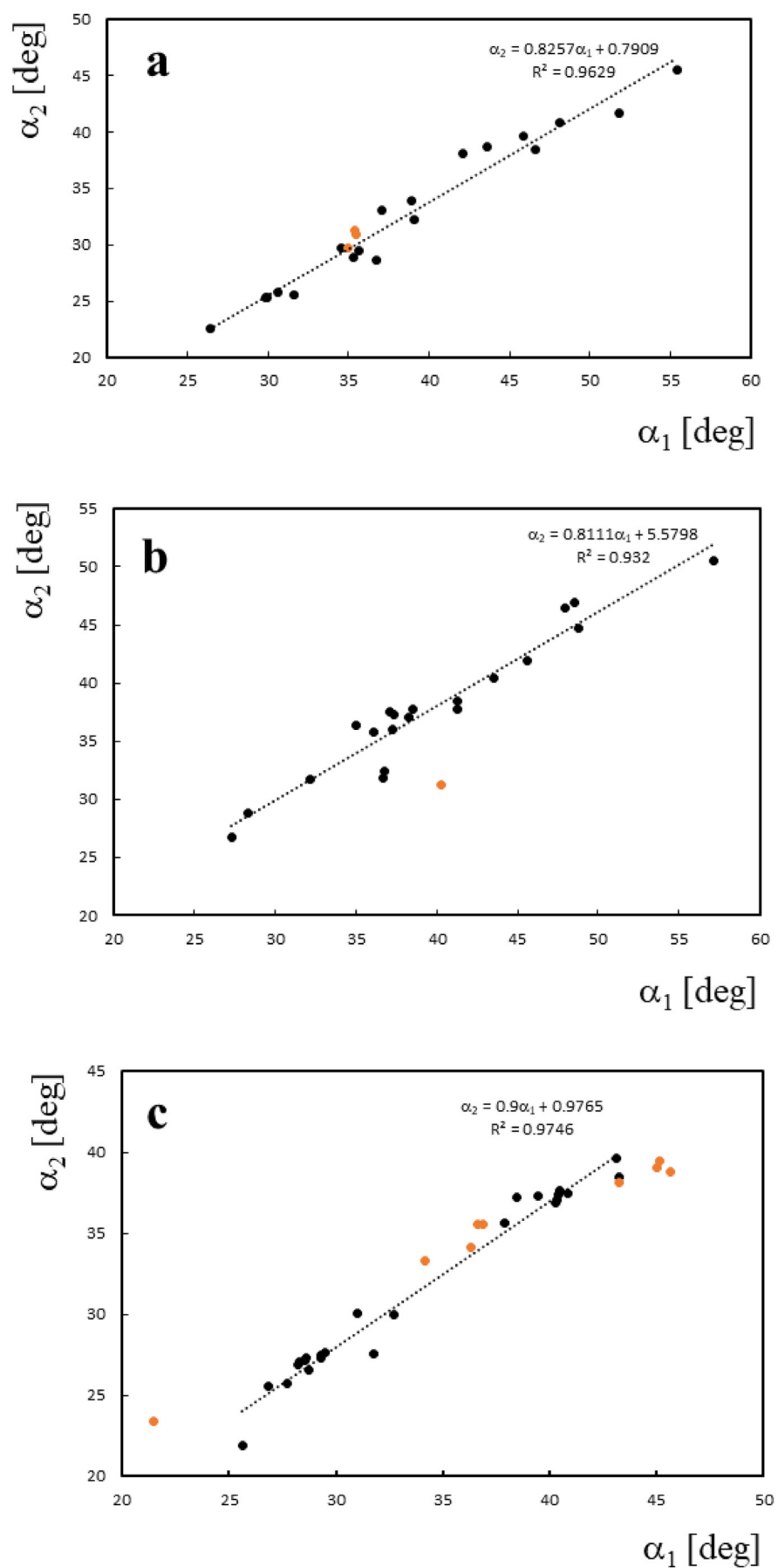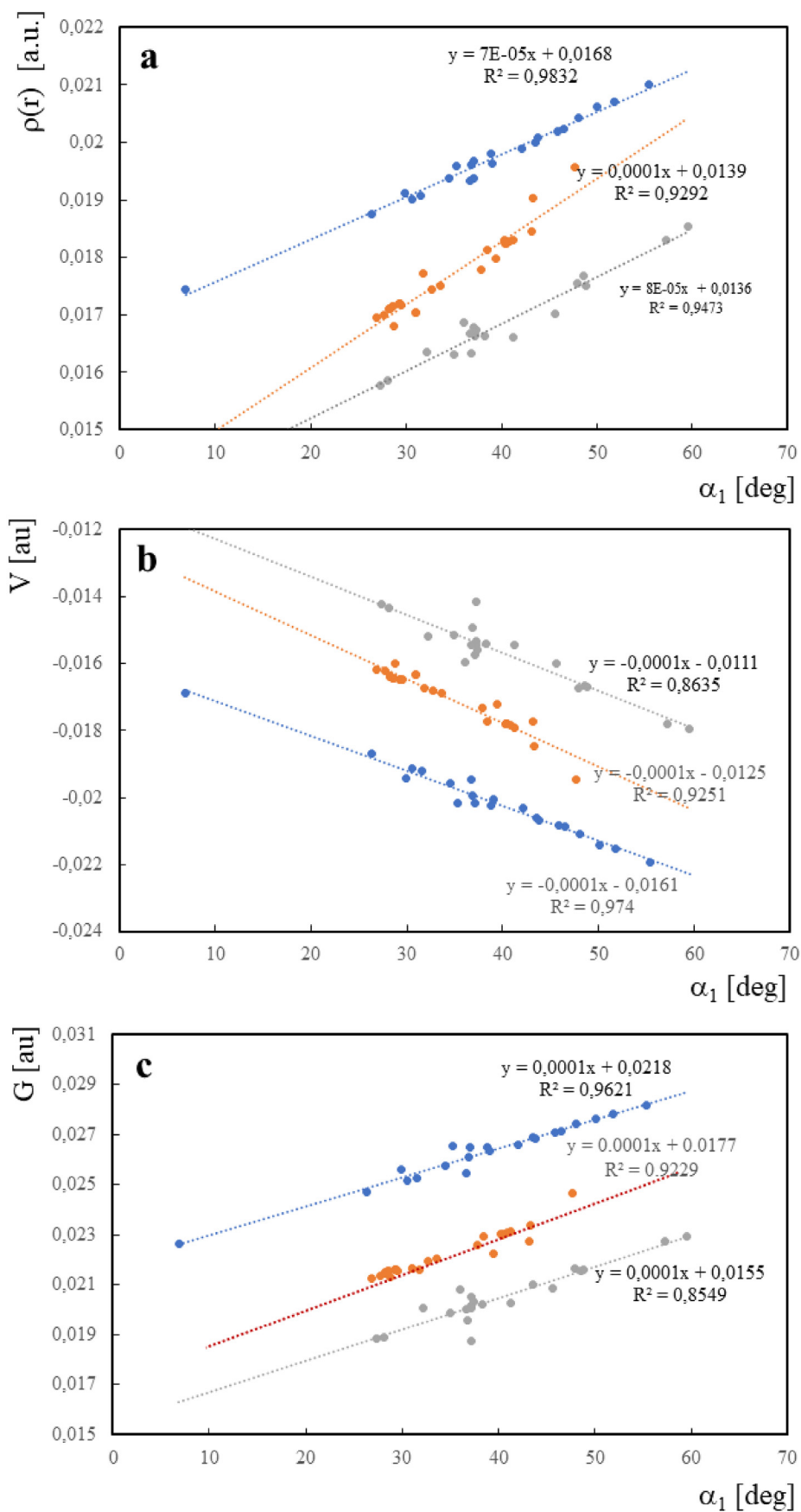
Fig. 2. Correlations of QTAIM parameters at the ring-critical point in the central ring of 9,10-dihydroanthracene (blue), *9H*-thioxanthene (grey) and phenothiazine (red). a -electron density, b − kinetic energy, c − potential energy of electron density.

Table 2
Geometrical parameters for the optimized structures with axial and equatorial location of the substituents for 9,10-dihydroanthracene and *9H*-thioxanthene derivatives and energy difference between the structure with equatorial and axial substituent orientation.

Compound name	axial			equatorial			ΔE [kcal/mol]
	α_1	α_2	α_3	α_1	α_2	α_3	
9-nitro-9,10-dihydroanthracene	29.85	25.389	9.563				
9,10-dihydroanthracen-9-ol	37.053	33.181	2.249	35.549	29.538	72.674	−0.89
9-methyl-9,10-dihydroanthracene	34.491	29.771	8.762	46.543	38.497	84.326	1.87
9,10-dihydroanthracene-9-carbaldehyde	30.595	25.86	9.256	45.803	39.714	87.477	6.16
9-chloro-9,10-dihydroanthracene	35.27	28.961	6.456	42.059	38.164	82.034	4.78
9,10-dihydroanthracene-9-carboxylic acid	31.529	25.618	13.505	43.597	38.748	81.454	3.97
9-ethyl-9,10-dihydroanthracene	26.345	22.663	18.762	51.81	41.778	89.404	4.05
9,10-dihydroanthracene-9-amine	38.841	33.903	0.613	48.048	40.938	83.102	2.34
9-nitro-9,10-dihydroanthracene	29.839	25.374	9.585				
9-tert-butyl-9,10-dihydroanthracene	36.686	28.74	15.408	55.366	45.547	78.938	11.24
9*H*-thioxanthene-9-carbaldehyde	38.509	37.757	2.829	38.262	37.07	76.047	2.64
9-chloro-9*H*-thioxanthene	32.161	31.666	4.685	48.557	46.937	88.623	4.1
9*H*-thioxanthene-9-carboxylic acid	36.701	31.857	10.282	47.963	46.497	89.697	0.9
9-ethyl-9*H*-thioxanthene	27.276	26.763	16.06	34.974	36.305	83.97	4.34
9*H*-thioxanthene-9-amine	37.373	37.298	3.373	45.593	41.914	87.341	0.7
9-nitro-9*H*-thioxanthene	36.055	35.734	1.864	28.276	28.767	8.138	−0.12
9*H*-thioxanthene-9-ol	37.113	37.531	2.445	41.236	38.457	82.2	0.38
9-tert-butyl-9*H*-thioxanthene	36.794	32.358	13.418	57.182	50.538	76.215	9.61
9-methyl-9*H*-thioxanthene	37.222	35.972	3.212	48.787	44.69	89.153	1.67

Table 3
Comparison of α_1, α_2 and α_3 angles for optimized compounds with axial (upper) and equatorial (down) substituent location the angles for the crystal structure.

Compound name/REFCODE	α_1	α_2	α_3
9,10-dihydroanthracene	39.036	32.238	71.318
			2.393
DITBOX [48]	35.355(161)	31.336(405)	70.195(2244)
			3.465(2318)
DITBOX01 [49]	35.452(121)	30.963(243)	71.206(1641)
			0.599(1934)
9-methyl-9,10-dihydroanthracene	46.543	38.497	84.326
9-methyl-9,10-dihydroanthracene	34.491	29.771	8.762
YAKGOG [50]	34.969(89)	29.677(189)	8.929(146)
9-tert-butyl-9*H*-thioxanthene	57.182	50.538	76.215
9-tert-butyl-9*H*-thioxanthene	36.794	32.358	13.418
TBTXAN [51]	40.282	31.275	15.127
10*H*-phenothiazine	30.997	30.063	87.113
PHESAZ01 [6]	21.493(6)	23.401(27)	84.406(14)
10-Methylphenothiazine	37.861	35.618	76.49
MPHTAZ10 [52]	36.337	34.15	79.758
MPHTAZ11 [53]	36.643(70)	35.561(193)	79.049(116)
MPHTAZ12 [45]	36.890(197)	35.579(501)	80.476(313)
10-ethylphenothiazine	27.705	25.748	76.58
NEPTAZ [43]	45.02	39.05	75.543
NEPTAZ01 [44]	43.278(44)	38.184(128)	76.496(77)
NEPTAZ02 [45]	45.117(171)	39.470(357)	75.085(244)
10-[2-(1-methylpiperidin-2-yl)ethyl]-2-methylsulfanyl-phenothiazine	41.225	37.737	71.447
TORDAZ [46]	45.622	38.839	73.665
	34.156	33.315	72.396

Acknowledgments

References

[1] N.M. Richtand, J.A. Welge, A.D. Logue, P.E. Keck Jr., S.M. Strakowski, R.K. Mcnamara, Dopamine and serotonin receptor binding and antipsychotic efficacy, Neuropsychopharmacology 32 (2007) 1715−1726, https://doi.org/10.1038/sj.npp.1301305.

[2] N. Motohashi, M. Kawase, S. Saito, H. Sakagami, Antitumor potential and possible targets of phenothiazine-related compounds, Curr. Drug Targets 1

(2000) 237−245, https://doi.org/10.2174/1389450003349191.

[3] G.F. Makhaeva, S.V. Lushchekina, N.P. Boltneva, O.G. Serebryakova, E.V. Rudakova, A.A. Ustyugov, S.O. Bachurin, A.V. Shchepochkin, O.N. Chupakhin, V.N. Charushin, R.J. Richardson, 9-Substituted acridine derivatives as acetylcholinesterase and butyrylcholinesterase inhibitors possessing antioxidant activity for Alzheimer's disease treatment, Bioorg. Med. Chem. 25 (2017) 5981−5994, https://doi.org/10.1016/j.bmc.2017.09.028.

[4] S.Z. Khan, C.L. Longland, F. Michelangeli, The effects of phenothiazines and other calmodulin antagonists on the sarcoplasmic and endoplasmic reticulum Ca^{2+} pumps, Biochem. Pharmacol. 60 (2000) 1797−1806, https://doi.org/10.1016/S0006-2952(00)00505-0.

[5] W.W. Shen, A history of antipsychotic drug development, Compr. Psychiatr. 40 (1999) 407−414, https://doi.org/10.1016/S0010-440X(99)90082-2.

[6] J.J.H. McDowell, The crystal and molecular structure of phenothiazine, Acta Crystallogr. B 32 (1976) 5−10, https://doi.org/10.1107/S0567740876002215.

[7] S. Choi, D. Haggart, L. Toll, G.D. Cuny, Synthesis, receptor binding and functional studies of mesoridazine stereoisomers, Bioorg. Med. Chem. Lett 14 (2004) 4379−4382, https://doi.org/10.1016/j.bmcl.2004.06.078.

[8] A.D. Mosnaim, V.V. Ranade, M.E. Wolf, J. Puente, A.M. Valenzuela, Phenothiazine molecule provides the basic chemical structure for various classes of pharmacotherapeutic agents, Am. J. Therapeut. 13 (2006) 261−273, https://doi.org/10.1097/01.mjt.0000212897.20458.63.

[9] A. Jaszczyszyn, K. Gasiorowski, P. Świątek, W. Malinka, K. Cieślik-Boczula, J. Petrus, B. Czarnik-Matusewicz, Chemical structure of phenothiazines and their biological activity, Pharmacol. Rep. 64 (2012) 16−23, https://doi.org/10.1016/S1734-1140(12)70726-0.

[10] S.G. Dahl, E. Hough, P.A. Hals, Phenothiazine drugs and metabolites: molecular conformation and dopaminergic, alpha adrenergic and muscarinic cholinergic receptor binding, Biochem. Pharmacol. 35 (1986) 1263−1269, https://doi.org/10.1016/0006-2952(86)90269-8.

[11] C. García, R. Oyola, L.E. Piñero, R. Arce, J. Silva, V. Sánchez, Substitution and solvent effects on the photophysical properties of several series of 10-alkylated phenothiazine derivatives, J. Phys. Chem. A 109 (2005) 3360−3371, https://doi.org/10.1021/jp044530j.

[12] N.E. Kelley, D.E. Tepper, Rescue therapy for acute migraine, part 2: neuroleptics, antihistamines, and others, Headache 52 (2012) 292−306, https://doi.org/10.1111/j.1526-4610.2011.02070.x.

[13] A.S. Horn, S.H. Snyder, Chlorpromazine and dopamine: conformational similarities that correlate with the antischizophrenic activity of phenothiazine drugs, Proc. Natl. Acad. Sci. U. S. A 68 (1971) 2325−2328, https://doi.org/10.1073/pnas.68.10.2325.

[14] A.P. Feinberg, S.H. Snyder, Phenothiazine drugs: structure-activity relationships explained by a conformation that mimics dopamine, Proc. Natl. Acad. Sci. U. S. A 72 (1975) 1899−1903, https://doi.org/10.1073/pnas.72.5.1899.

[15] K. Michalak, O. Wesolowska, N. Motohashi, J. Molnar, A. Hendrich, Interactions of phenothiazines with lipid bilayer and their role in multidrug resistance reversal, Curr. Drug Targets 7 (2006) 1095−1105, https://doi.org/10.2174/138945006778226570.

[16] B. Morak-Młodawska, K. Pluta, M. Latocha, M. Jeleń, D. Kuśmierz, Synthesis and anticancer and lipophilic properties of 10-dialkylaminobutynyl derivatives of 1,8- and 2,7-diazaphenothiazines, J. Enzym. Inhib. Med. Chem. 31 (2016) 1132−1138, https://doi.org/10.3109/14756366.2015.1101092.

[17] I. Gil-Ad, B. Shtaif, Y. Levkovitz, J. Nordenberg, M. Taler, I. Korov, A. Weizman, Phenothiazines induce apoptosis in a B16 mouse melanoma cell line and attenuate in vivo melanoma tumor growth, Oncol. Rep. 15 (2006) 107−112, https://doi.org/10.3892/or.15.1.107.

[18] T.S. Lialiaris, F. Papachristou, C. Mourelatos, M. Simopoulou, Antineoplastic and cytogenetic effects of chlorpromazine on human lymphocytes in vitro and on Ehrlich ascites tumor cells in vivo, Anti Canccer Drugs 20 (2009) 746−751, https://doi.org/10.1097/CAD.0b013e32832f567b.

[19] P.B. Mortensen, The occurrence of cancer in first admitted schizophrenic patients, Schizophr. Res. 12 (1994) 185−194, https://doi.org/10.1016/0920-9964(94)90028-0.

[20] S. Darvesh, R.S. McDonald, A. Penwell, S. Conrad, K.V. Darvesh, D. Mataija, G. Gomez, A. Caines, R. Walsh, E. Martin, Structure-activity relationships for inhibition of human cholinesterases by alkyl amide phenothiazine derivatives, Bioorg. Med. Chem. 13 (2005) 211−222, https://doi.org/10.1016/j.bmc.2004.09.059.

[21] M. Schmidt, M. Teitge, M.E. Castillo, T. Brandt, B. Dobner, A. Langner, Synthesis and biochemical characterization of new phenothiazines and related drugs as MDR reversal agents, Arch. Pharm. (Weinheim) 341 (2008) 624−638, https://doi.org/10.1002/ardp.200800115.

[22] I. Tsakovska, I.K. Pajeva, Phenothiazines and structurally related compounds as modulators of cancer multidrug resistance, Curr. Drug Targets 7 (2006) 1123−1134, https://doi.org/10.2174/138945006778226660.

[23] B. Varga, A. Csonka, A. Csonka, J. Molnar, L. Amaral, G. Spengler, Possible biological and clinical applications of phenothiazines, Anticancer Res. 37 (2017) 5983−5993, https://doi.org/10.21873/anticanres.12045.

[24] U. Elkayam, W. Frishman, Cardiovascular effects of phenothiazines, Am. Heart J. 100 (1980) 397−401. https://doi.org/10.1016/0002-8703(80)90153-2.

[25] B. Weiss, W.C. Prozialeck, T.L. Wallace, Interaction of drugs with calmodulin. Biochemical, pharmacological and clinical implications, Biochem. Pharmacol. 31 (1982) 2217−2226, https://doi.org/10.1016/0006-2952(82)90104-6.

[26] C.L. Klein, J. Lear, S. O'Rourke, S. Williams, L. Liang, Crystal and molecular structures of tricyclic neuroleptics, J. Pharm. Sci. 83 (1994) 1253−1256,

https://doi.org/10.1002/jps.2600830914.

[27] J. Jia, Y. Wu, Alkyl length dependent reversible mechanofluorochromism of phenothiazine derivatives functionalized with formyl group, Dyes Pigments 147 (2017) 537−543, https://doi.org/10.1016/j.dyepig.2017.08.049.

[28] A. Karuppasamy, C. Udhaya Kumar, M. Velayutham Pillai, C. Ramalingan, Synthesis, spectral, structural and DFT studies of novel dialkylfluorene decorated phenothiazine-3-carbaldehyde, J. Mol. Struct. 1133 (2017) 154−162, https://doi.org/10.1016/j.molstruc.2016.12.002.

[29] A. Karuppasamy, K. Gokula Krishnan, M. Velayutham Pillai, C. Ramalingan, Synthesis, molecular structure and vibrational analysis of D-D-A based carbazole decorated phenothiazine-3-carbaldehyde: experimental (FT-IR, UV and NMR) and density functional theory (DFT) calculations, J. Mol. Struct. 1128 (2017) 674−684, https://doi.org/10.1016/j.molstruc.2016.09.026.

[30] M. Malińska, J. Nowacki, A. Kapturkiewicz, K. Woźniak, Differences in electron densities of phenoxazine and phenothiazine derivatives - charge density studies, RSC Adv. 2 (2012) 4318−4328, https://doi.org/10.1039/c2ra01148d.

[31] V.L.S. Freitas, J.R.B. Gomes, M.D.M.C. Ribeiro Da Silva, Structural, energetic and reactivity properties of phenoxazine and phenothiazine, J. Chem. Thermodyn. 73 (2014) 110−120, https://doi.org/10.1016/j.jct.2013.11.013.

[32] S. Darvesh, I.R. Pottie, K.V. Darvesh, R.S. McDonald, R. Walsh, S. Conrad, A. Penwell, D. Mataija, E. Martin, Differential binding of phenothiazine urea derivatives to wild-type human cholinesterases and butyrylcholinesterase mutants, Bioorg. Med. Chem. 18 (2010) 2232−2244, https://doi.org/10.1016/j.bmc.2010.01.066.

[33] S. Darvesh, R.S. McDonald, K.V. Darvesh, D. Mataija, S. Conrad, G. Gomez, R. Walsh, E. Martin, Selective reversible inhibition of human butyrylcholinesterase by aryl amide derivatives of phenothiazine, Bioorg. Med. Chem. 15 (2007) 6367−6378, https://doi.org/10.1016/j.bmc.2007.06.060.

[34] N. Motohashi, M. Kawase, K. Satoh, H. Sakagami, Cytotoxic potential of phenothiazines, Curr. Drug Targets 7 (2006) 1055−1066, https://doi.org/10.2174/138945006778226624.

[35] C.J. Grol, H. Rollema, H.W. Asselbergs, The effect of 2-substitution on conformations and brain concentrations of phenothiazine-neuroleptics in relation to dopamine-antagonism, J. Pharm. Pharmacol. 31 (1979) 667−671, https://doi.org/10.1111/j.2042-7158.1979.tb13625.x.

[36] S.J. Enna, J.P. Bennett, D.R. Burt, I. Creese, S.H. Snyder, Stereospecificity of interaction of neuroleptic drugs with neurotransmitters and correlation with clinical potency, Nature 263 (1976) 338−341, https://doi.org/10.1038/263338a0.

[37] P. Borowicz, J. Herbich, A. Kapturkiewicz, R. Anulewicz-Ostrowska, J. Nowacki, G. Grampp, Nature of the lowest triplet states of 4'-substituted N-phenyl-phenothiazine derivatives, Phys. Chem. Chem. Phys. 2 (2000) 4275−4280, https://doi.org/10.1039/b005058j.

[38] M.J. Frisch, et al., Gaussian Inc 16, Revision A.03, 2016. Wallingford CT.

[39] A.D. Becke, Density-functional thermochemistry. III. The role of exact exchange, J. Chem. Phys. 98 (1993) 5648−5652, https://doi.org/10.1063/1.464913.

[40] C. Lee, W. Yang, R.G. Parr, Development of the Colle-Salvetti correlation-energy formula into a functional of the electron density, Phys. Rev. B. B37 (1988) 785−789, https://doi.org/10.1103/PhysRevB.37.785.

[41] S. Grimme, J. Antony, S. Ehrlich, H. Krieg, A consistent and accurate ab initio parametrization of density functional dispersion correction (DFT-D) for the 94 elements H-Pu, J. Chem. Phys. 132 (2010) 154104, https://doi.org/10.1063/1.3382344.

[42] T.A. Keith, TK Gristmill Software, K.S. Overland Park, aim.tkgristmill.com, 2014. (Accessed 7 October 2016).

[43] S.S.C. Chu, D. der Helm, The crystal structure of N-ethylphenothiazine, Acta Crystallogr. B 31 (1975) 1179−1183, https://doi.org/10.1107/S056774087500475X.

[44] S. Ergun, C.F. Elliott, A.P. Kaur, S.R. Parkin, S.A. Odom, Overcharge performance of 3,7-disubstituted N-ethylphenothiazine derivatives in lithium-ion batteries, Chem. Commun. 50 (2014) 5339−5341, https://doi.org/10.1039/C3CC47503D.

[45] J. Yang, X. Gao, Z. Xie, Y. Gong, M. Fang, Q. Peng, Z. Chi, Z. Li, Elucidating the excited state of mechanoluminescence in organic luminogens with room-temperature phosphorescence, Angew. Chem. Int. Ed. 56 (2017) 15299−15303, https://doi.org/10.1002/anie.201708119.

[46] J.J.H. McDowell, The crystal and molecular structure of thioridazine, a derivative of phenothiazine, Acta Crystallogr. B 31 (1975) 2256−2264, https://doi.org/10.1107/S0567740875007352.

[47] F.H. Allen, The Cambridge Structural Database: a quarter of a million crystal structures and rising, Acta Crystallogr. B 58 (2002) 380−388, https://doi.org/10.1107/S0108768102003890.

[48] F.H. Herbstein, M. Kapon, G.M. Reisner, Molecular compounds and complexes. XVI. 9,10-Dihydroanthracene (I) (C14H12) (a redetermination) and 9,10-dihydroanthracene:bis(1,3,5-trinitrobenzene) (II) (C14H12.C6H3N3O6), Acta Crystallogr. B 42 (1986) 181−187, https://doi.org/10.1107/S0108768186098385.

[49] J.P. Reboul, Y. Oddon, C. Caranoni, J.C. Soyfer, J. Barbe, G. Pèpe, Structure du dihydro-9,10 anthracène. Support tricyclique de médicaments psychotropes, Acta Crystallogr. C 43 (1987) 537−539, https://doi.org/10.1107/S010827018709512X, 537−539.

[50] R.K. Dhar, A. Sygula, F.R. Fronczek, P.W. Rabideau, An investigation of substituent effects on the conformation of 9,10-dihydroanthracenes by molecular mechanics calculations and X-ray structure analysis, Tetrahedron 48 (1993)

9417–9426, https://doi.org/10.1016/S0040-4020(01)88310-1.

[51] S.S.C. Chu, W.W. Kou, 9-tert-Butylthioxanthene, Acta Crystallogr. B 34 (1978) 2348–2350, https://doi.org/10.1107/S0567740878008146.

[52] S.S.C. Chu, D. der Helm, The refinement of the crystal structure of N-methylphenothiazine, Acta Crystallogr. B 30 (1974) 2489–2490, https://doi.org/10.1107/S0567740874007394.

[53] P. Malikireddy, G. Siddan, S. Madurai, S. Chandramouleeswaran, L. Srinivasakannan, 10-Methyl-10H-phenothiazine, IUCrData 1 (2016) x161299, https://doi.org/10.1107/S2414314616012992.

[54] R.F.W. Bader, Atoms in Molecules: A Quantum Theory, Oxford University Press, New York, 1990.

[55] E. Espinosa, E. Molins, C. Lecomte, Hydrogen bond strengths revealed by topological analyses of experimentally observed electron densities, Chem. Phys. Lett. 285 (1998) 170–173. https://doi.org/10.1016/S0009-2614(98)00036-0.

[56] E. Espinosa, I. Alkorta, I. Rozas, J. Elguero, E. Molins, About the evaluation of the local kinetic, potential and total energy densities in closed-shell interactions, Chem. Phys. Lett. 336 (2001) 457–461. https://doi.org/10.1016/S0009-2614(01)00178-6.

Article

Effect of Substitution of Hydrogen Atoms in the Molecules of Anthrone and Anthraquinone

Małgorzata Szymańska [ID] and Irena Majerz *

Faculty of Pharmacy, Wroclaw Medical University, Borowska 211a, 50-556 Wroclaw, Poland;
m.szymanska@umed.wroc.pl
* Correspondence: irena.majerz@umed.wroc.pl; Tel.: +48-717-840-305; Fax: +48-717-1784-0307

Abstract: The geometry of anthrone and anthraquinone—natural substances of plant origin—was investigated under the substitution of hydrogen atoms in side aromatic ring and, for anthrone, also in the central ring. A significant influence of substitution on geometry expressed by the angle between the side rings was shown. The geometry changes are connected with the changes of electron density and aromaticity of the anthrone and anthraquinone rings. The flexibility of the investigated compounds was confirmed by comparison of the optimized molecules and the molecules in the crystal state where the packing forces can influence the molecular geometry.

Keywords: anthrone; anthraquinone; aromaticity; QTAIM

1. Introduction

Anthrones are compounds of natural origin extracted from plants. The broad spectrum of biological and medical properties [1,2] means that interest in monoanthrones has not diminished over the years. Monoanthrones have antimicrobial [3], cytotoxic [4], anti-HIV [4], antifungal [5], antiviral [6], phototoxic [7,8], antioxidant [9,10], anticancer [11,12], and anti-inflammatory [13] properties. Anthraquinones have antifungal [1], cytotoxic [4], anti-HIV [4], antioxidant [1], antibacterial, antiviral, and antitumor [6,14] properties.

Anthrones and anthraquinones are tricyclic compounds (Scheme 1). Two side rings have an aromatic character, while the central ring is aliphatic. The aliphatic character of the central ring affects the non-planar structure of anthrones. It can be expected that the oxygen atom substituted to the central ring flattens the molecule.
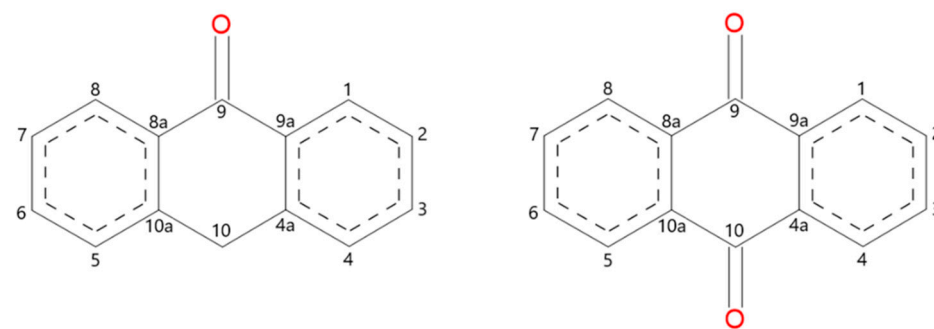
Scheme 1. Molecular structure and atom numbering of anthrone and anthraquinone.

In the literature, there is a lot of information linking the physical and pharmaceutical properties of anthrones and anthraquinones with substituents of the aliphatic and aromatic ring and molecular geometry. According to Gow-Chin Yen [10], there is a relationship between the presence of the ketone groups in the central ring and substitution of the lateral aromatic rings and the antioxidant properties of anthrones. The antioxidant with one ketone group at the central ring showed the strongest antioxidant activity. The antioxidant

activity of numerous compounds results from the presence of the OH group. Moreover, unsubstituted anthraquinone showed the least antioxidant properties. Kamei [15], who studied the effect of anthraquinones on inhibiting cell growth, came to similar conclusions. It turned out that the presence of OH groups attached to lateral aromatic rings can have a significant impact on the antitumor properties of the tested compounds. The activity of anthrones is influenced not only by the number of the OH groups in the aromatic rings, but also by their location. According to Cai [16], ortho-dihydroxy substitution in the anthraquinone molecule significantly increases the scavenging effect. Marković [17] performed an analysis of the bond dissociation enthalpy (BDE) for all OH sites of emodin. In his opinion, a significant role in antioxidant properties is played by the OH group substituted to the third carbon atom [17] (Scheme 1).

The physicochemical properties and reactivity of the cyclohexa-2,5-dienone analogs with the heteroatom in the ring indicate a partially aromatic nature of the ring [18]. In the case of anthrone, the partially aromatic character of the central ring can be additionally influenced by the presence of side aromatic rings with mobile π electrons. It has been evidenced that the enol form present in anthrone stabilizes the aromaticity of the rings [19] and high π-electron delocalization in the condensed rings suggests that the central ring in anthrone and anthraquinone may change aromaticity under the influence of electron density change in the molecule caused by the presence of substituents.

For a better understanding of the therapeutic and physicochemical properties and mechanism of action of anthrones and anthraquinones, it is necessary to perform an analysis of the geometry of the single molecule and its electronic structure. In this work, we have undertaken a systematic theoretical study to analyse the structural parameters of anthrones and anthraquinones under substitution with electron donating and electron withdrawing groups. The electron donating the NH_2 group characterized by the strongest donating properties ($\sigma_p = -0.66$) was chosen. (The substituent constant σ_p is a measure of the total polar effect exerted by substituent in para position. It is positive for electron withdrawing and negative for electron donating substituent.) Similarly, the electron withdrawing NO_2 group has the strongest electron withdrawing properties ($\sigma_p = 0.77$) among the substituents. Because it can be expected that a substituent attached to the aromatic ring can affect the geometry of the investigated molecules, a systematic study of the structural parameters under substitution was performed. By single and multiple substitutions in the aromatic ring of each of these groups, a systematic study of the effect of donating or withdrawing the charge to the ring was carried out.

The main structural parameter for anthrones and anthraquinones is the alpha angle (Scheme 2) between two planes formed by four atoms of the middle ring. To investigate the influence of substitution on the geometry of the anthrone, the structures with NO_2, CHO, COOH, CH_3, CH_2CH_3, NH_2, OH, Cl, and $C(CH_3)_3$ substituents in the central ring were also optimized. An additional group of the compounds used in the analysis are the structures delivered from the Cambridge Structural Database (CSD) [20], which were optimized and compared with the X-ray structures. The difference between the solid state structure and the optimal structure shows how much changes in the environment of a molecule can affect its geometry. The structures of anthrones and anthraquinones with electron-donor and electron-withdrawing substituents at the aromatic side ring were optimized (Scheme 3). The aliphatic character of the central ring of anthrones and anthraquinones determines the non-planarity of the molecules.

The presence of two ketone groups in the aliphatic ring causes its flattening, which, together with the aromatic CC bonds common with the aromatic side rings, can influence the aliphatic character of the central ring. It can be assumed that the flattening of the central ring is related to changes in the electron density. To characterize these changes, the QTAIM (quantum theory of atom in molecule) [21] method was used, which enables the description of the electron density both in the centre of the molecule ring and on the aromatic chemical bonds. Because it can be assumed that the electron density in the middle ring is sensitive to substitution, the electron density parameters for the central ring critical

point were correlated with the α angle. As the changes in geometry are related to changes in the electron density, and these in turn are related to changes in aromaticity, for all rings in the investigated compounds, the aromaticity was characterized using the HOMA (*harmonic oscillator model of aromaticity*) [22].
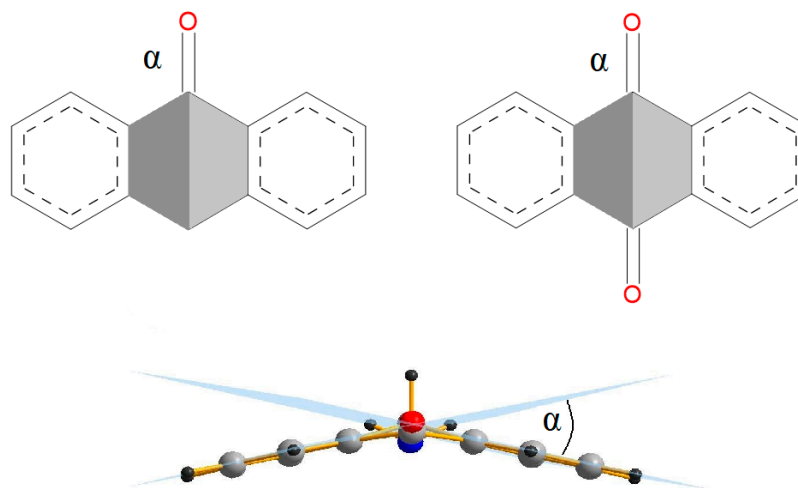
Scheme 2. Definition of the α angle for monoanthrones and anthraquinones.
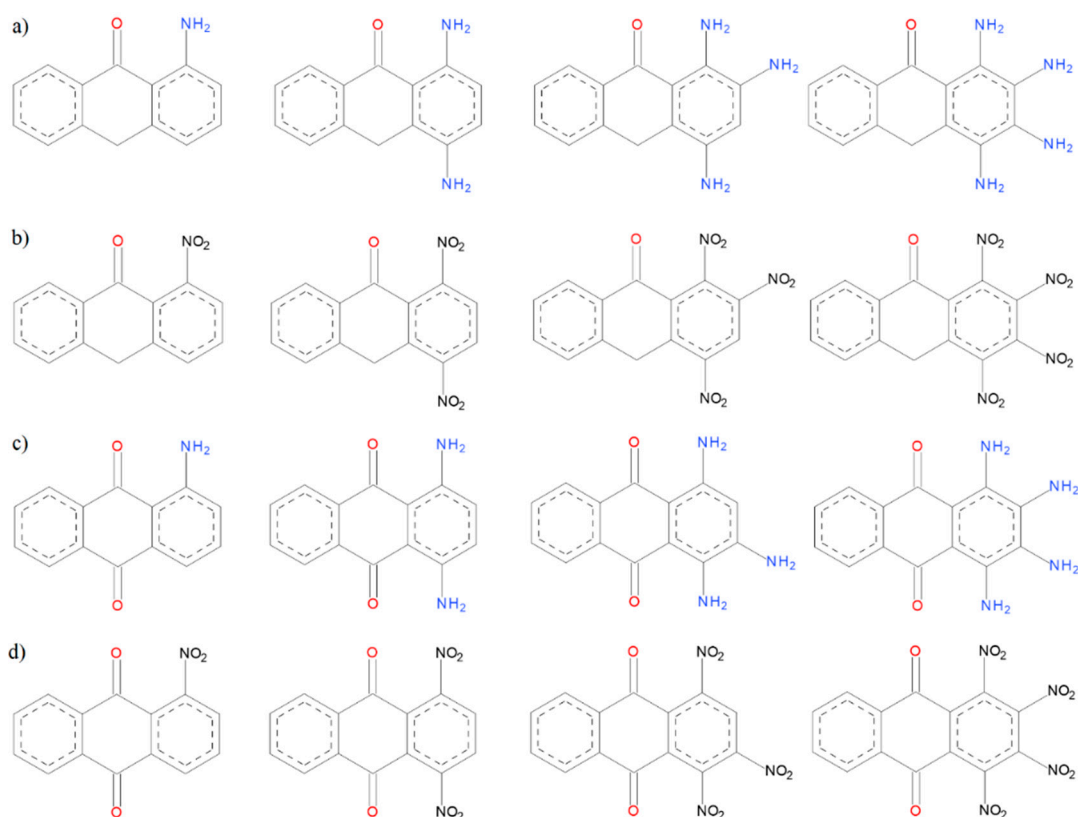
Scheme 3. (**a**) Anthrone structures with the substituents with electron-donor properties, (**b**) anthrone structures with substituents with electron-withdrawing, (**c**) anthraquinone structures with substituents with electron-donor properties, and (**d**) anthraquinone structures with substituents with electron-withdrawing.

Computational Details

The investigated molecules were optimized using a Gaussian 16 package [23] at DFT-D3 B3LYP/6-311++G** level [24,25], which included Grimme dispersion [26]. To check that the resultant geometry reached the energy minimum, vibrational frequencies were calculated. The wave function evaluated for the optimized molecules was used as the input to the AIMALL program [21].

2. Results

2.1. Geometry of Investigated Compounds

The main geometric parameter for the studied molecules—the angle α—is presented in Scheme 2 and collected in Table S1 (Supplementary Materials). The α angle is very sensitive to the substitution in the aliphatic and aromatic ring and changes from 0 to 41°. The values of the α angle for optimized anthrone and anthraquinone molecules as well as for the structures in the crystal are collected in Table 1. The α angle is more sensitive to substitution in the anthrone central ring and is affected not only by the character of the substituent, but also by its size and axial or equatorial orientation. Most of the computed structures have a substituent in the axial position. The exception is 10-amino-10*H*-anthracen-9-one, for which the structure with the axial substituent, as well as 10-*tert*-butyl-10H-anthracen-9-one, could not be obtained. For two 10-*t*-butyl-9,10-dihydro-9-anthracenone structures, the difference between the α angle for the axial and equatorial substituent location is 13.321°. In the 10-methyl-10*H*-anthracen-9-one structure taken from the CSD database [27], the slope angle for the methyl substituent and for the hydrogen atom in relation to the plane of the middle ring is very similar. Therefore, it cannot be clearly stated that it is a structure with a substituent in the axial or equatorial position. More limited changes of the α angle are observed for structures with substituents in the side ring. Minimal changes of the α angle were obtained for anthraquinone structures with substituents in the benzene ring. It is interesting to note the multiple substitution of the aromatic ring with electron-donor and electron-withdrawing substituents because of the steric hindrances between adjacent groups causes bending of the substituted ring. To better understand how substituents with electron-donor and electron-withdrawing properties are arranged against the ring plane, the β angle between the plane of the substituted ring and the substituent plane (Scheme 4) was determined (Table 2). Substitution of the amino group next to the ketone group causes formation of weak hydrogen bonds (H···O 1.87–1.89 Å), which reduces the β angle. Close location of the amino groups causes an increase of the β angle, which is associated with the steric hindrance. It is known that the nitro group tends to be located in the plane of the aromatic ring to which the group is substituted. Substitution to the anthrone side ring of a nitro group located next to the ketone group of the middle ring causes the nitro group to swing out the plane of the benzene ring and the β angle increases. The β angle decreases by about 30° when the nitro group is not close to the ketone or another nitro group. The nitro groups are larger than the amino groups; therefore, substitution of four nitro groups to the aromatic ring causes the ring to become non-planar and the β angles for the substituted groups to be larger than in the case of amino substitution. Another interesting feature of the structures substituted with many amino and nitro groups is elongation of the C–N bond linking the substituent with the aromatic ring. The close location of amino and carbonyl groups reduces the length of the C–N bond in both anthrones and anthraquinones. The bond is more elongated if the number of substituents increases and the elongation is more significant for amino groups substituted to anthrones when, for the substitution with the nitro group, the elongation of the C–N bond is more significant for anthraquinones.

Table 1. α angle defined according to Scheme 2 for the investigated compounds. Angles for the optimized compounds (upper) and the angles for the crystal structure (lower).
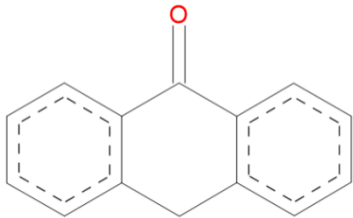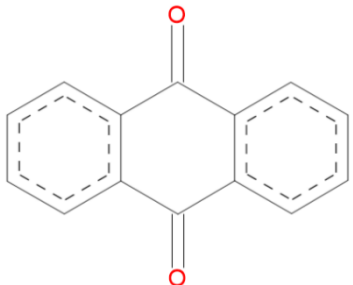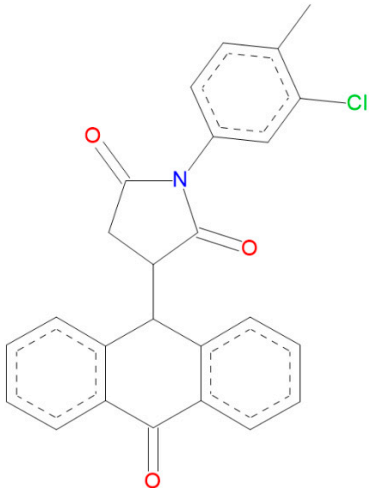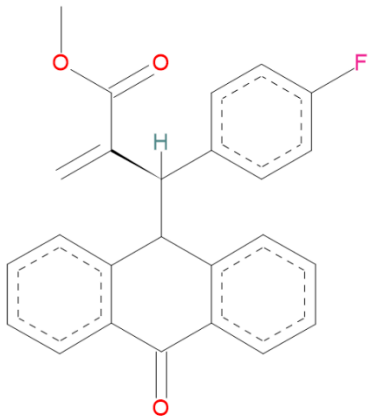
	Name	α [°]	Structure
1	10*H*-anthracen-9-one	0.023	
2	anthracene-9,10-dione	0.003	
3	1-(3-chloro-4-methylphenyl)-3-(10-oxo-9,10-dihydroanthracen-9-yl)pyrrolidine-2,5-dione	18.346 14.252 [28]	
4	Methyl (*R*)-2-((4-fluorophenyl)(10-oxo-9,10-dihydroanthracen-9-yl)methyl)acrylate	18.715 25.727 [29]	

Table 1. *Cont.*

	Name	α [°]	Structure
5	10-((1*S*,2*S*)-1-(4-Bromophenyl)-2-methyl-3-oxobutyl)anthracen-9(10*H*)-one	21.432 18.895 [29]	
6	9-Oxo-10-diphenylphosphinoylanthracene	23.705 26.869 [30]	
7	(*S*)-10-(1-(4-Chlorophenyl)-3-oxobutyl)anthracen-9(10*H*)-one	23.330 23.095 [31]	
8	10-methyl-10*H*-anthracen-9-one	16.168 4.920 [27]	

<div align="center">**Table 1.** *Cont.*</div>

	Name	α [°]	Structure
9	10-Isopropyl-9,10-dihydro-9-anthracenone	21.684 22.692 [27]	
10	10-tert-butyl-10*H*-anthracen-9-one (axial position)	28.177 26.680 [27]	
11	1,8-dihydroxy-10-(1-hydroxy-1,2-dihydronaphthalen-2-yl)anthracen-9(10*H*)-one	19.281 19.764 [32]	
12	10-(6,7-dibromo-1-hydroxy-5,8-dimethyl-1,2-dihydronaphthalen-2-yl)anthracen-9(10*H*)-one	25.498 25.296 [32]	

Table 1. *Cont.*

	Name	α [°]	Structure
13	10-(6,7-difluoro-1-hydroxy-1,2-dihydronaphthalen-2-yl)-1,8-dihydroxyanthracen-9(10*H*)-one	19.547 18.505 [32]	
14	10-carbaldehyde-10*H*-anthracen-9-one	15.369	
15	10-chloro-10*H*-anthracen-9-one	14.876	
16	9-oxo-10*H*-anthracene-10-carboxylic acid	15.617	

<div align="center">Table 1. <i>Cont.</i></div>
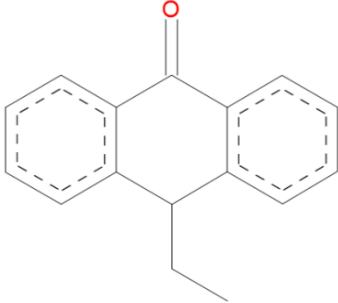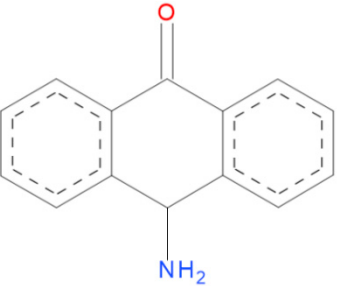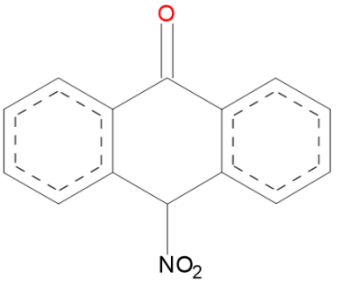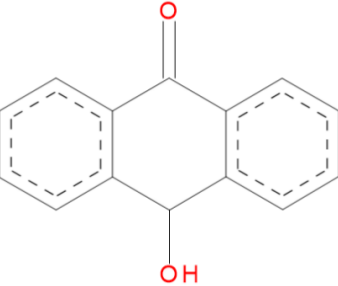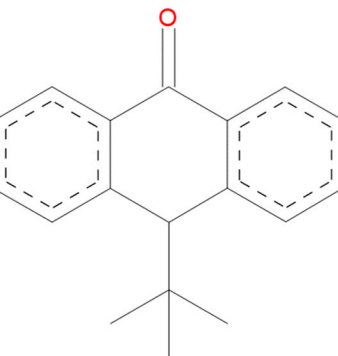
	Name	α [°]	Structure
17	10-ethyl-10*H*-anthracen-9-one	22.978	
18	10-amino-10*H*-anthracen-9-one	28.192	
19	10-nitro-10*H*-anthracen-9-one	16.168	
20	10-hydroxy-10*H*-anthracen-9-one	15.267	
21	10-tert-butyl-10*H*-anthracen-9-one (equatorial position)	41.498	

Table 1. *Cont.*

	Name	α [°]	Structure
22	1-amino-10*H*-anthracen-9-one	7.569	
23	1,4-diamino-10*H*-anthracen-9-one	4.074	
24	1,2,4-triamino-10*H*-anthracen-9-one	2.752	
25	1,2,3,4-tetraamino-10*H*-anthracen-9-one	0.357	
26	1-aminoanthracene-9,10-dione	0.008	

Table 1. *Cont.*
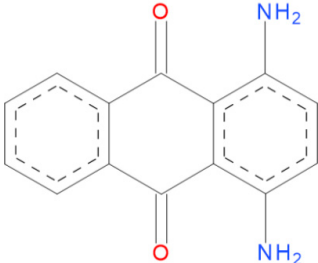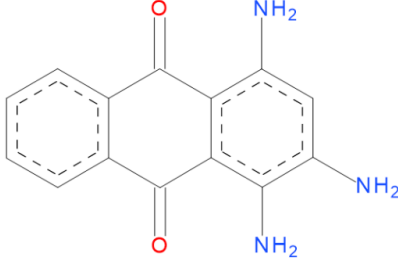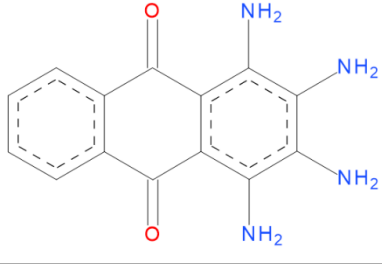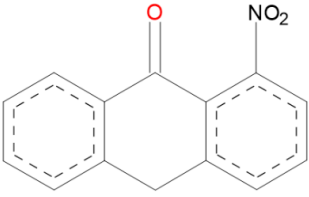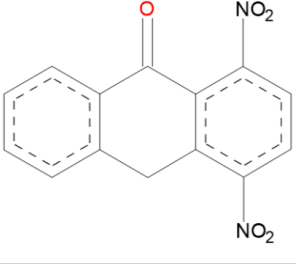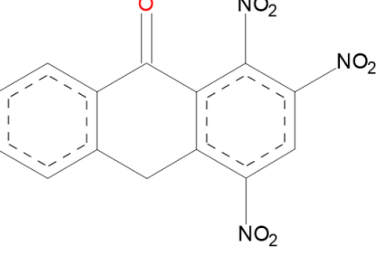
	Name	α [°]	Structure
27	1,4-diaminoanthracene-9,10-dione	0.094	
28	1,3,4-triaminoanthracene-9,10-dione	0.269	
29	1,2,3,4-tetraaminoanthracene-9,10-dione	0.053	
30	1-nitro-10*H*-anthracen-9-one	16.812	
31	1,4-dinitro-10*H*-anthracen-9-one	16.22	
32	1,2,4-trinitro-10*H*-anthracen-9-one	3.137	

Table 1. *Cont.*
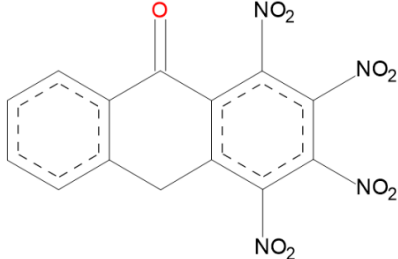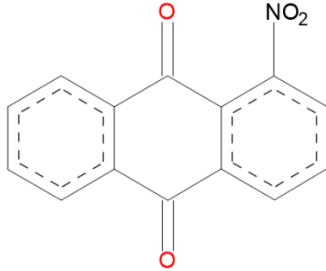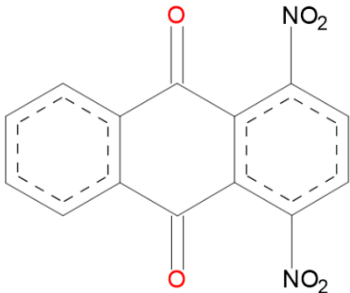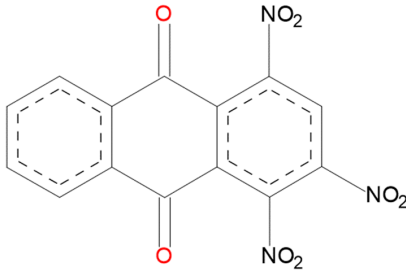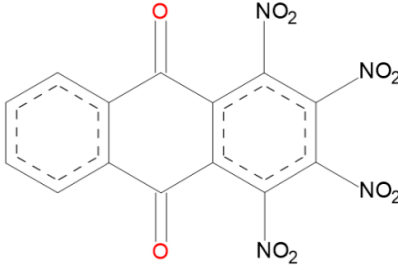
	Name	α [°]	Structure
33	1,2,3,4-tetranitro-10*H*-anthracen-9-one	17.452	
34	1-nitroanthracene-9,10-dione	6.528	
35	1,4-dinitroanthracene-9,10-dione	1.008	
36	1,3,4-trinitroanthracene-9,10-dione	14.116	
37	1,2,3,4-tetranitroanthracene-9,10-dione	1.305	

Table 2. β angle and C–N bond length for substituents in the aromatic side ring.

Molecule	The Number of the Carbon Atom to Which Substituent Is Attached	Single Substitution		Double Substitution		Triple Substitution		Quadruple Substitution	
		β Angle [°]	C–N Bond Length [Å]	β Angle [°]	C–N Bond Length [Å]	β Angle [°]	C–N Bond Length [Å]	β Angle [°]	C–N Bond Length [Å]
Anthrone with amino substituents	1	8.287	1.361	18.275	1.369	41.642	1.388	48.021	1.398
	2	—	—	—	—	48.465	1.410	52.29	1.415
	3	—	—	—	—	—	—	45.828	1.408
	4	—	—	43.760	1.415	42.485	1.412	46.847	1.414
Anthrone with nitro substituents	1	65.671	1.486	69.204	1.486	72.621	1.493	69.097	1.494
	2	—	—	—	1.486	33.269	1.485	53.625	1.488
	3	—	—	—	—	—	—	53.408	1.488
	4	—	—	34.192	1.482	38.135	1.486	58.199	1.486
Anthraquinone with amino substituents	1	0.588	1.358	11.006	1.362	8.797	1.361	33.212	1.370
	2	—	—	—	—	43.815	1.394	49.769	1.410
	3	—	—	—	—	—	—	50.137	1.402
	4	—	—	11.072	1.362	41.063	1.382	43.981	1.388
Anthraquinone with nitro substituents	1	70.053	1.486	70.416	1.487	73.663	1.488	67.81	1.494
	2	—	—	70.416	1.487	—	—	55.286	1.490
	3	—	—	—	—	34.506	1.487	55.309	1.489
	4	—	—	70.271	1.487	73.092	1.493	67.802	1.493
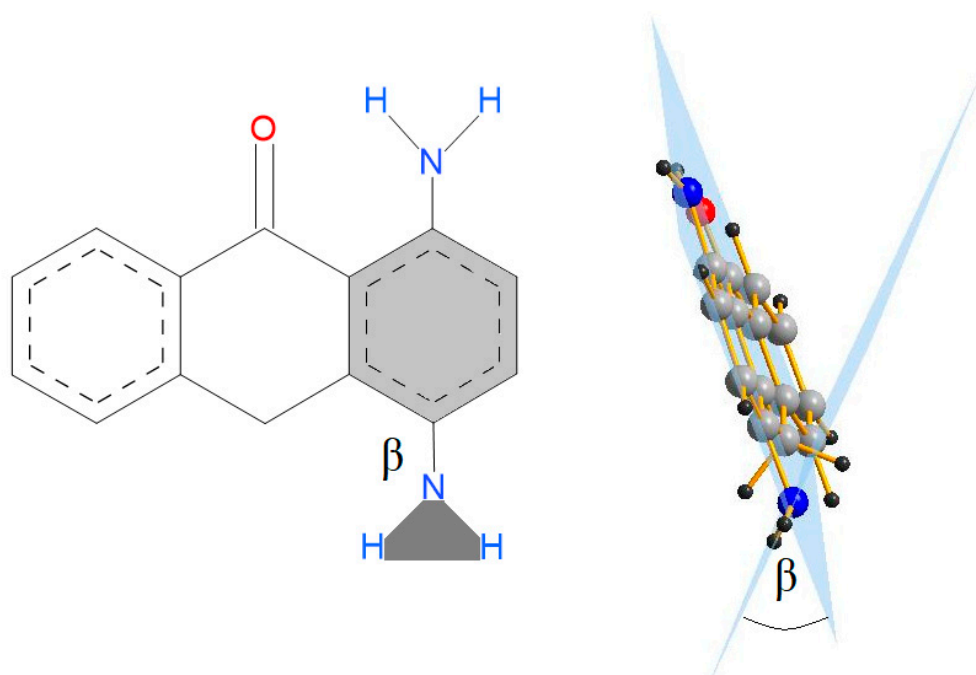
Scheme 4. Definition of the β angle.

It is characteristic that the carbonyl group substituted in the central ring of the anthrone causes significant flattening of the molecule compared with 9,10-dihydroanthracene, investigated previously, for which the α angle is 39.036° [33]. The aliphatic ring of anthraquinone is planar with an α angle of 0.003°. The α angle is very sensitive to substitution, especially in the anthrone central ring, but also to the substitution in the aromatic side ring. Changes of the α angle are more prominent for anthrone than for anthraquinone. Substitution of the side ring with an NH_2 and NO_2 group influences the α angle, and these changes are more significant for the NO_2 group and for anthrone compared with anthraquinone. Multiple substitution of the aromatic ring is connected with twisting of the substituent group against the aromatic ring and elongation of the C–N bond length between the aromatic ring and the substituent. Comparison of the α angle for the optimized molecule and the same molecule in crystal (Table 1) confirms the flexibility of this angle, which can be changed as a result of packing in the crystal lattice. For 10-methyl-9,10-dihydro-9-anthracenone, the angle of 16.168° for the optimized molecule changes by up to 4.92°.

2.2. Electron Density at Central-Ring-Critical Point

In the frame of quantum theory of atoms in molecules (QTAIM), the molecule is treated as electron density, $\varrho(r)$, characterized by a system of critical points (CP) for which the gradient of the electron density vanishes. Diagonalization of the Hessian of electron density gives non-zero eigenvalues and their number and the sum of their signs describes a characteristic of the critical point. The maximum of $\varrho(r)$ represents the nucleus when the minimum of $\varrho(r)$ corresponds to the cage critical point. The bond critical point (BCP) and ring critical point (RCP) are the saddle points of the electron density. The gradient path of electron density linking the atoms located at its maximum is a chemical bond with a BCP at the minimum along the bond path and maximum along the directions perpendicular to the bond path [34]. From the BCP, two gradient paths extend to the atoms linked by the chemical bond. Except for the chemical bond, depending on the BCP parameters, the gradient path is also important for an interaction between two atoms [35,36]. The quantitative description of the molecule is connected with the analysis of the topological parameters of critical points [37].

Changes of the molecular geometry are usually reflected in the changes of electron density. Looking at the geometric changes of the investigated anthrone and anthraquinone

molecules, it can be expected that the significant changes of electron density will be related to the central aliphatic ring, especially to the ring-critical point (RCP) of the aliphatic ring, and can be correlated with the α angle. The aromaticity of a ring may be related to its electron density. It has been shown that the parameters used in the QTAIM theory to describe the electron density, such as electron density and potential and kinetic energy at the critical point of the ring, can be used as parameters describing the aromaticity of the ring [38].

Electron density at the critical point of the central ring ($\varrho(r)$), potential-energy density ($V(r)$), and kinetic-energy density ($G(r)$) for the electrons at the critical point of the central ring have been correlated with the α ring, and is presented in Figure 1. The substitution of both the central-aliphatic and side-aromatic ring affects the α angle. Therefore, it is interesting to determine the relationship between the electron density of the central-ring-critical point (RCP) and the α angle. The potential energy density ($V(r)$) is affected by the pressure exerted on the electrons at the RCP by other electrons. In contrast, kinetic energy density ($G(r)$) is related to the pressure exerted by the electrons in the RCP on other electrons [39]. The QTAIM parameters for the RCP located in the centre of the aliphatic ring are the most sensitive to the substituent in the central ring and strongly depend on the α angle. For most investigated structures, an increase in the α angle causes an increase in the electron density at the RCP for the aliphatic ring. The value of the potential energy density of electrons at the ring-critical point for the central ring decreases as the value of the α angle for the above-mentioned structures increases, while the kinetic energy density of electrons at the critical point of the central ring increases as the value of the α angle increases. Similar correlations were obtained in a previous work [33], where the effect of substituents on the α angle of phenothiazine, 9H-thioxanthene, and 9,10-dihydroanthracene derivatives was studied. No correlation was found for the QTAIM parameters of the RCP and the α angle for anthraquinones with a substituent in the side ring. This is most likely due to the bending of the substituted aromatic ring.

The correlations in Figure 1 show that the electron density as well as potential and kinetic-energy density at the RCP of the aliphatic ring are sensitive to the α angle. The planarity of the anthrone molecule is connected with the decreasing of the electron density and mobility of the electrons at the RCP when, for nonplanar compounds, the electron density and mobility of electrons are higher. The reverse tendency is observed for potential-energy density at the RCP. The general correlation of the QTAIM parameters can be split into categories corresponding to individual compounds. The most sensitive to the α angle are the QTAIM parameters for the aliphatic RCP for the anthrones substituted in the aliphatic ring when substitution of the side ring causes only limited changes of the electron density at the aliphatic RCP. Substitution of the anthraquinone side ring does not influence the electron density of the central ring.
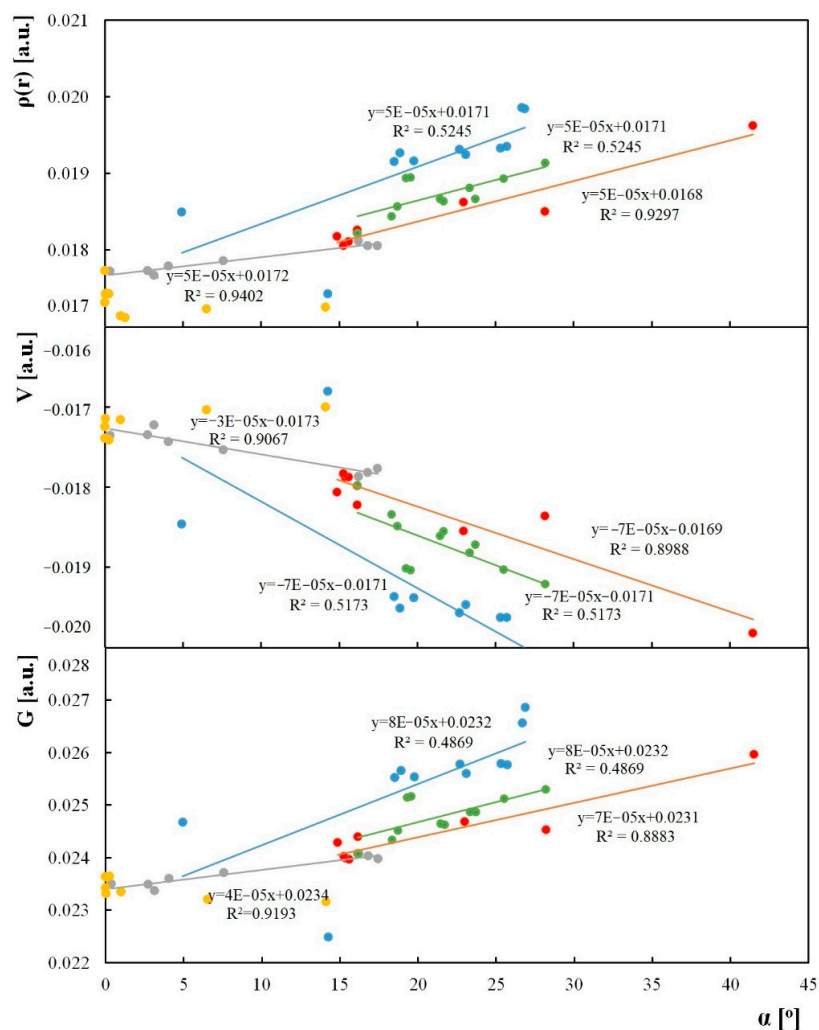
Figure 1. Correlations of quantum theory of atoms in molecules (QTAIM) parameters at the ring-critical point of the central ring. A-electron density, b-kinetic-energy density, c-potential-energy density, where blue-structures from the Cambridge Structural Database (CSD); red-anthrones with a substituent in the central ring, grey anthrones with substituent NO_2 and NH_2, yellow-anthraquinones with substituent NO_2 and NH_2, and green-optimized experimental structures from CSD.

2.3. Bond Ellipticity

Other fragments of the molecule sensitive to changes in flatness of the central aliphatic ring are the C–C bonds common for the aliphatic and aromatic ring. Participation in the aromatic ring is connected with the increasing of electron density compared with a typical aliphatic bond. Ellipticity of the electron density at the bond-critical point (BCP) gives information about the π-nature of the C–C bond. It is not possible to characterize the heteroatom—carbon bonding the measure of the π-nature—because of the free electron pair on the heteroatom [40], although ellipticity changes for the C=O bond are noticeable. The ellipticity and the length of the C–C bonds in the central ring are affected by substituents in both the middle and the side-aromatic ring. In order to better understand the change of ellipticity of the aliphatic ring under substitution, the ellipticity was compared with these for the unsubstituted structures.

Symmetrical substituents in the central ring cause the same changes in ellipticity and length in the bonds C8a–C10a and C4a–C9a, C8a–C9 and C9–C9a, and C10a–C10 and C10–C4a (atom numbering according to Scheme 1) relative to the unsubstituted molecule.

The highest ellipticity suggesting the π-nature of the bonds was observed for the bonds C8a–C10a and C4a–C9a, with lengths in the range of 1.38–1.44 Å. The C10a–C10 and

C10–C4a bonds are characterized by the lowest ellipticity and the lengths within the range of 1.46–1.54 Å typical for single bonds.

Substitution of the amino groups in the aromatic side ring of anthrones causes an increase of ellipticity for most bonds. The exceptions are the C10a–C10 and C10–C4a bonds with a single amino substitution. This substitution has the greatest effect on the ellipticity of the bonds located closer to the substituted side ring (i.e., C10–C4a, C4a–C9a, and C9–C9a). A particularly large increase of ellipticity is observed for the C9–C9a bond.

Amino groups substituted in the anthraquinone side ring also cause an increase of the ellipticity for most bonds. Only for the C8a–C10a bond is the ellipticity very close to the ellipticity for the same bond in the unsubstituted molecule. However, a single substitution of the amino group in anthraquinones caused a slight decrease of ellipticity of the C10–C4a bond. As with anthrones, amino substitution has the greatest effect on the ellipticity of the bonds closer to the substituted side ring. The largest increase in ellipticity is observed for the C9–C9a bond.

Substitution of nitro groups in anthrones causes an increase of the ellipticity of the C8a–C9, C8a–C10a, C10a–C10, and C10–C4a bonds. In the case of the C4a–C9a bond, an increase of ellipticity occurs for one and disubstituted structures. On the other hand, substitution with nitro groups of the side ring causes a decrease of the ellipticity of the C9–C9a bond. The greatest changes in ellipticity relative to the unsubstituted molecule were observed for the C9–C9a bond.

The substitution of nitro groups in anthraquinones causes an increase of the ellipticity of the C8a–C9, C8a–C10a, C10a–C10, and C4a–C9a bonds. For the C10–C4a and C9–C9a bonds, ellipticity decreased. In this case, substitution also has the most significant effect on change of the C9–C9a bond ellipticity relative to the unsubstituted structure.

Substitution with amino and nitro groups influences the geometry of anthrones and anthraquinones, so a correlation of ellipticity of electron density at BCP and bond lengths can be expected. Correlations of the bond length and ellipticity for the central-ring bonds with the correlation lines are presented in Figure 2. The best fit was obtained for the C9–C9a bond. For bonds C8a–C10a and C4a–C9a, no correlation was found. For the C9=O bond, three trend lines were drawn: for structures with substituents NH_2 and NO_2 and for structures with substituents in the middle ring. The same was done with regard to the C10=O bond. The C8a–C9 bond for anthrones substituted with the NH_2 group in the side ring was not included in the trend line. A lack of oxygen at C10 carbon results in less electron-density flow between the side, substituted aromatic rings and the central-aliphatic ring in anthrone. Therefore, substitution of the anthrone lateral ring with electron-donor and electron-withdrawing substituents slightly affects the C10a–C10 and C10–C4a bonds. In addition, the different nature and size of substituents in the central ring has a significant impact on the ellipticity and length of the C10a–C10 and C10–C4a bonds. The trend line for the C10a–C10 and C10–C4a bonds was determined on the basis of anthraquinones with NH_2 and NO_2 substituents in the side-aromatic ring and two anthrone structures with a substituent in the central-aliphatic ring (NH_2 and $C(CH_3)_3$). The changes of ellipticity confirm that substitution of the side ring of anthrones and anthraquinones does not significantly influence the bonds common for the aliphatic and aromatic ring.
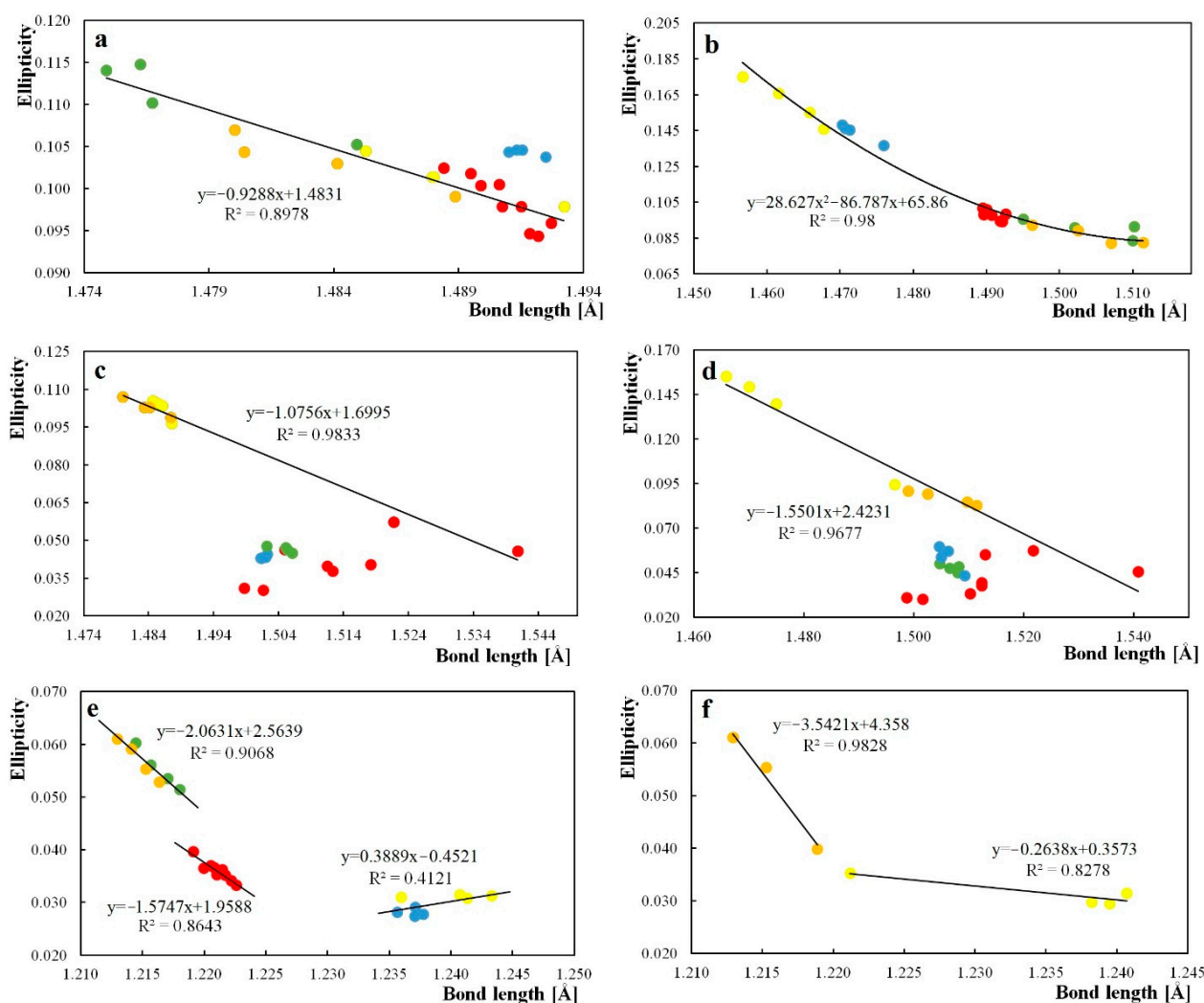
Figure 2. Correlations between ellipticity and bond length of the central aliphatic ring, (**a**)—C8a–C9 bond, (**b**)—C9–C9a bond, (**c**)—C10a–C10 bond, (**d**)—C10–C4a bond, (**e**)—C9=O bond, and (**f**)—C10=O bond, where red-anthrones with a substituent in the central ring, blue-anthrones with a substituent NH_2, green-anthrones with a substituent NO_2, yellow-anthraquinones with a substituent NH_2, and orange-anthraquinones with a substituent NO_2. The C8a–C9 bond for anthrones substituted with the NH_2 group in the side ring was not included in the trend line.

2.4. Harmonic *Oscillator Model of Aromaticity*

In order to study the effect of substituents on ring aromaticity, the HOMA geometric index was proposed [22]. For the benzene aromatic ring, the HOMA index is equal to 1; for cyclohexane, it is zero; and for the antiaromatic ring, it is negative.

$$HOMA = 1 - \alpha/n\sum_{i=1}^{n}\left(R_{opt} - R_{ij}\right)^2 \tag{1}$$

R_{opt}—the optimized CC bond length of a perfectly aromatic system and equals 1.388 Å
R_{ij}—determined bond length
α—standardization constant of 257.7
n—number of bonds

The HOMA parameters for the investigated compounds are shown in Figures 3 and 4 and the correlation of HOMA with α angle is shown in Figure 5. Analogous calculations of the aromaticity of the anthrone rings confirmed the aliphatic character of the central ring [19].
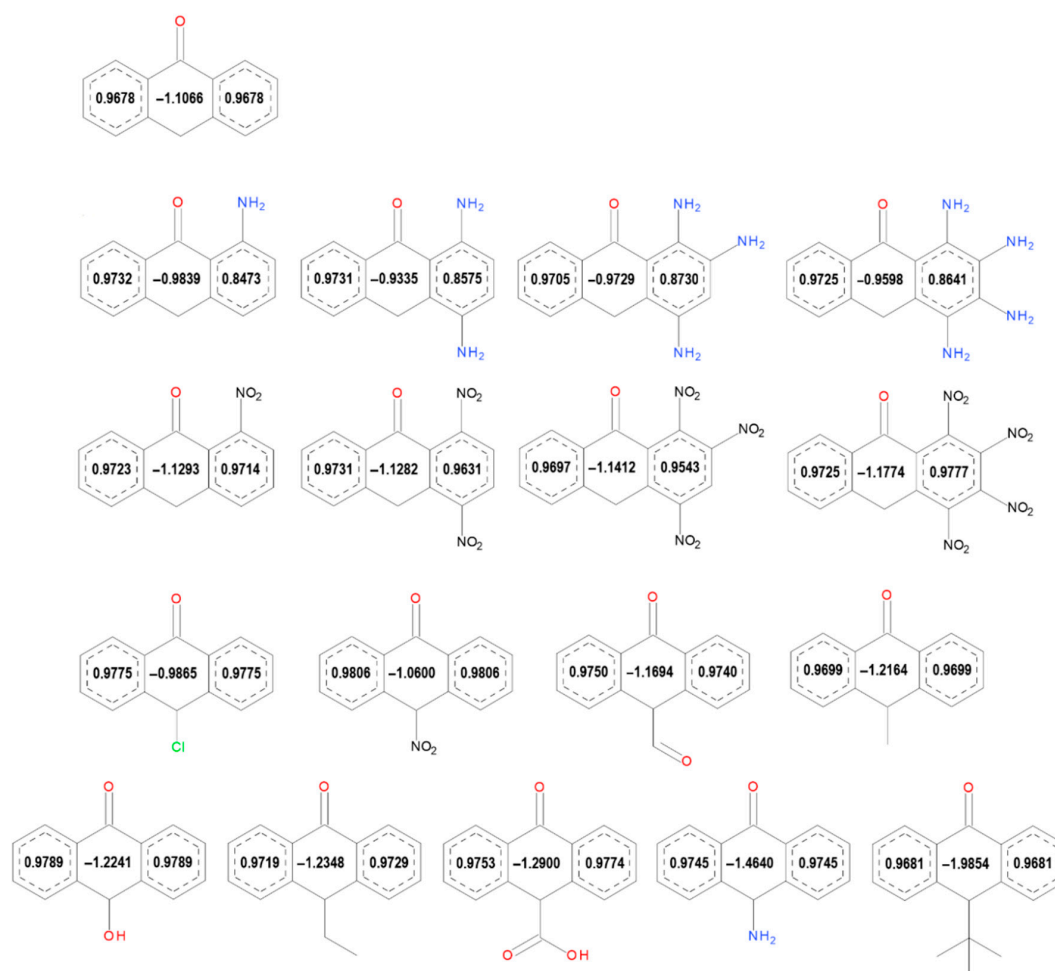
Figure 3. *Harmonic* oscillator model of aromaticity (HOMA) parameters for anthrone structures with a substituent in the side aromatic ring and in the central aliphatic ring.
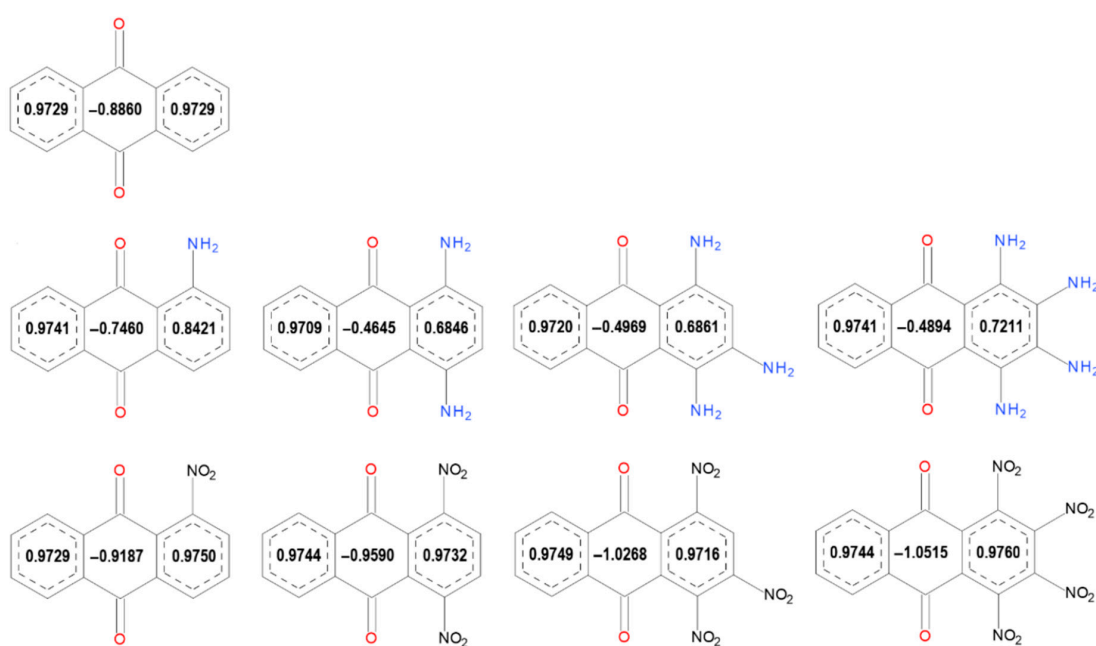
Figure 4. HOMA parameters for anthraquinone structures with a substituent in the side aromatic.
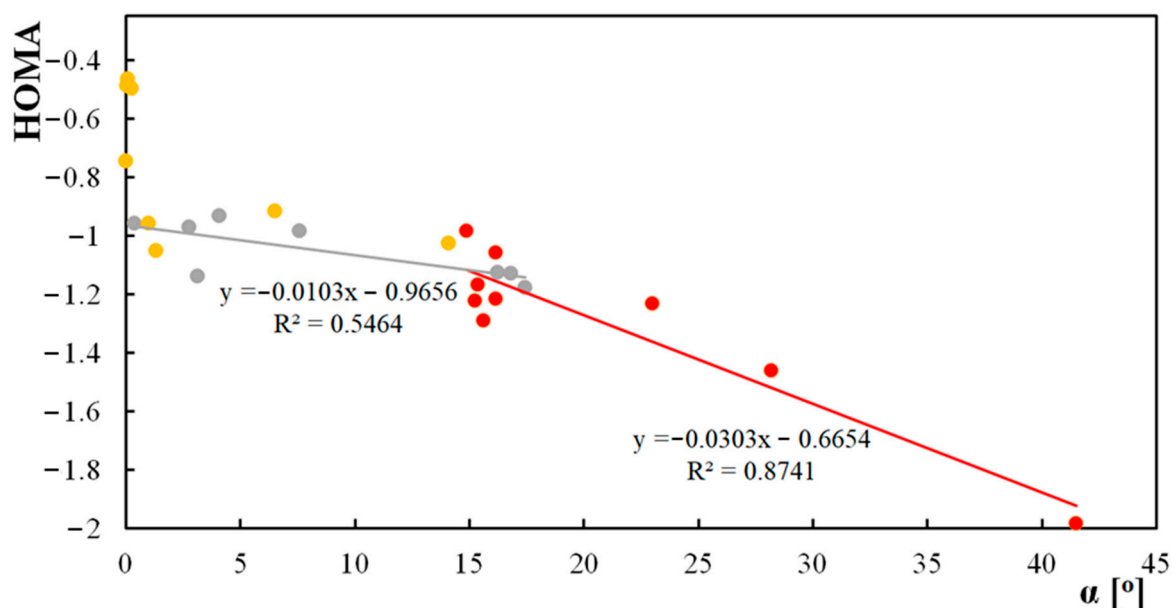
Figure 5. Correlations between HOMA parameters for the central ring and α angle: yellow-anthraquinones with a substituent NH_2 and NO_2, red-anthrones with a substituent in the central ring, and grey-anthrones with a substituent NH_2 and NO_2 in the side ring.

Of particular interest is the influence of substituents in the lateral aromatic ring on the aromaticity, not only of the aliphatic ring, but also on the aromaticity of the second, unsubstituted aromatic ring. This phenomenon was observed for all investigated compounds. The lowest HOMA value in the central ring was observed for the anthrone molecule substituted with four nitro groups in the aromatic side ring. The largest increase of the HOMA index for the central ring of anthraquinone was observed in the case of substitution of the aromatic side ring with two amino groups in para position. Electron density at the RCP of the central ring is significantly affected by the presence of the C=O. This is due to the formation of weak hydrogen bonds (H$\cdots$O = 1.85 Å) between the carbonyl oxygen and the hydrogen of the amine substituent closest to the middle ring. Greater changes of the HOMA value relative to the unsubstituted structure were observed for the structures with substituents in the side ring of anthraquinones than for anthrones.

Changes of the HOMA values under substitution show that aromaticity of the side rings is influenced by donor and acceptor properties of the substituents as well as the size of the substituent. Substitution of the middle ring with Cl, NO_2, CH_3, OH, NH_2, and $C(CH_3)_3$ does not influence the electron-density distribution in the aromatic rings, and the HOMA value for both aromatic side rings is the same.

A correlation between the HOMA parameter and the α angle was determined (Figure 5). For both anthrones with a substituent in the middle ring and anthrones with NO_2 and NH_2 substituents in the central ring, the HOMA value decreases as the alpha angle increases. When the alpha angle is low, the molecule is flat and the electron density in the central ring increases. Because, in anthraquinones, multiple substitution of the aromatic ring with electron-donor and electron-withdrawing substituents causes the substituted ring to be bend, no correlation between the HOMA parameter and the α angle was found. The value of the HOMA parameter of the central aliphatic ring shifts towards aromaticity after substitution of the side ring with an electron-donating substituent, while substitution of the side ring with an electron-withdrawing group causes a shift of the HOMA parameter value towards anti-aromaticity.

The demonstrated effect of the substitution, and especially the substitution in the central ring of anthrones, on changes in aromaticity and the correlated changes in geometry expressed by the α angle, shows the flexibility of the central ring. Consequently, a substitution can significantly change the geometry of the molecule and its properties. One of the

most important problems with anthrone is the balance between the ketone and hydroxyl forms. As this equilibrium is known to depend on many structural factors, changes in the aromaticity of the rings, and the environment of the molecule [19,41], it is expected that a change in the aromaticity of the rings will affect the keto-enol equilibrium. This is especially important for compounds with therapeutic properties; therefore, based on the known structure, theoretical studies of the keto-enol equilibrium for compounds used as drugs should be carried out.

3. Conclusions

The change of the angle between the anthrone aromatic rings is associated with the change in electron density at the RCP of the central ring. The value of the HOMA parameter of the central aliphatic ring shifts towards aromaticity after substitution of the side ring with an electron-donating substituent, while substitution of the side ring with an electron-withdrawing group causes a shift of the HOMA parameter value towards anti-aromaticity. Aromaticity of the anthrone rings is affected by the electron-donating and electron-withdrawing properties and the size of the substituent linked to the aromatic side ring as well as to the central aliphatic ring. Substituents in the anthrone aromatic ring affect the geometry and electronic structure of the central ring. Substitution in the central ring has the greatest impact on the structure of the entire molecule.

Supplementary Materials: The following are available online, Table S1: Bond length and ellipticity for the central ring of the optimized compounds.

Author Contributions: Investigation, M.S., I.M.; Methodology, M.S., I.M.; Software M.S., I.M., Data curation, M.S., I.M.; Writing-original draft preparation, M.S.; writing-review and editing, I.M.; Visualization, M.S., I.M.; Data curation, M.S., I.M.; Formal analysis, M.S., I.M., Funding acquisition, I.M. All authors have read and agreed to the published version of the manuscript.

Institutional Review Board Statement: Not applicable.

Informed Consent Statement: Not applicable.

Data Availability Statement: The data can be obtained from the authors.

Conflicts of Interest: The authors declare no conflict of interest.

Sample Availability: Samples of the molecular geometry are available from the authors.

References

1. Rodríguez-Gamboa, T.; Victor, S.R.; Fernandes, J.B.; Rodrigues Fo, E.; Das, G.F.; Da Silva, M.F.; Vieira, P.C.; Pagnocca, F.C.; Bueno, O.C.; Hebling, M.J.A.; et al. Anthrone and Oxanthrone C,O-Diglycosides from Picramnia Teapensis. *Phytochemistry* **2000**, *55*, 837–841. [CrossRef]
2. Flamini, G.; Catalano, S.; Caponi, C.; Panizzi, L.; Morelli, I. Three anthrones from Rubus Ulmifolius. *Phytochemistry* **2002**, *59*, 873–876. [CrossRef]
3. Bunbamrung, N.; Supong, K.; Intaraudom, C.; Dramae, A.; Auncharoen, P.; Pittayakhajonwut, P. Anthrone Derivatives from the Terrestrial Actinomycete, Actinomadura Sp. BCC47066. *Phytochem. Lett.* **2018**, *25*, 109–117. [CrossRef]
4. Feilcke, R.; Arnouk, G.; Raphane, B.; Richard, K.; Tietjen, I.; Andrae-Marobela, K.; Erdmann, F.; Schipper, S.; Becker, K.; Arnold, N.; et al. Biological Activity and Stability Analyses of Knipholone Anthrone, a Phenyl Anthraquinone Derivative Isolated from Kniphofia Foliosa Hochst. *J. Pharm. Biomed. Anal.* **2019**, *174*, 277–285. [CrossRef]
5. Jalab, M.; Critchley, M.E.; Taylor, C.M.; Lawrence, C.L.; Smith, R.B. 1,8-Substituted Anthraquinones, Anthrones and Bianthrones as Potential Non-Azole Leads against Fungal Infections. *Bioorg. Chem.* **2019**, *91*, 103151. [CrossRef]
6. Barnard, D.L.; Huffman, J.H.; Morris, J.L.B.; Wood, S.G.; Hughes, B.G.; Sidwell, R.W. Evaluation of the Antiviral Activity of Anthraquinones, Anthrones and Anthraquinone Derivatives against Human Cytomegalovirus. *Antivir. Res.* **1992**, *17*, 63–77. [CrossRef]

7.   Lin, H.D.; Li, K.T.; Duan, Q.Q.; Chen, Q.; Tian, S.; Chu, E.S.M.; Bai, D.Q. The Effect of Aloe-Emodin-Induced Photodynamic Activity on the Apoptosis of Human Gastric Cancer Cells: A Pilot Study. *Oncol. Lett.* **2017**, *13*, 3431–3436. [CrossRef] [PubMed]
8.   Tu, P.; Huang, Q.; Ou, Y.; Du, X.; Li, K.; Tao, Y.; Yin, H. Aloe-Emodin-Mediated Photodynamic Therapy Induces Autophagy and Apoptosis in Human Osteosarcoma Cell Line MG-63 through the ROS/JNK Signaling Pathway. *Oncol. Rep.* **2016**, *35*, 3209–3215. [CrossRef]
9.   Habtemariam, S. Antioxidant Activity of Knipholone Anthrone. *Food Chem.* **2007**, *102*, 1042–1047. [CrossRef]
10.   Yen, G.C.; Der Duh, P.; Chuang, D.Y. Antioxidant Activity of Anthraquinones and Anthrone. *Food Chem.* **2000**, *70*, 437–441. [CrossRef]
11.   Hu, W.; Zhou, W. Synthesis and Antitumor Activity of 10-Substituted Benzylidene Anthrone. *Bioorg. Med. Chem. Lett.* **2004**, *14*, 621–622. [CrossRef]
12.   Wei, W.T.; Lin, S.Z.; Liu, D.L.; Wang, Z.H. The Distinct Mechanisms of the Antitumor Activity of Emodin in Different Types of Cancer (Review). *Oncol. Rep.* **2013**, *30*, 2555–2562. [CrossRef]
13.   Park, M.Y.; Kwon, H.J.; Sung, M.K. Dietary Aloin, Aloesin, or Aloe-Gel Exerts Anti-Inflammatory Activity in a Rat Colitis Model. *Life Sci.* **2011**, *88*, 486–492. [CrossRef] [PubMed]
14.   Cudlín, J.; Blumauerová, M.; Steinbeová, N.; Matĕjů, J.; Zalabák, V. Biological Activity of Hydroxyanthraquinones and Their Glucosides toward Microorganisms. *Folia Microbiol.* **1976**, *21*, 54–57. [CrossRef] [PubMed]
15.   Kamei, H.; Koide, T.; Kojima, T.; Hashimoto, Y.; Hasegawa, M. Inhibition of Cell Growth in Culture by Quinones. *Cancer Biother. Radiopharm.* **1998**, *13*, 185–188. [CrossRef] [PubMed]
16.   Cai, Y.; Sun, M.; Xing, J.; Corke, H. Antioxidant Phenolic Constituents in Roots of Rheum Officinale and Rubia Cordifolia: Structure-Radical Scavenging Activity Relationships. *J. Agric. Food Chem.* **2004**, *52*, 7884–7890. [CrossRef]
17.   Marković, Z.S.; Manojlović, N.T. DFT Study on the Reactivity of OH Groups in Emodin: Structural and Electronic Features of Emodin Radicals. *Mon. Fur Chem.* **2009**, *140*, 1311. [CrossRef]
18.   Lumbroso, H.; Curé, J.; Evers, M. A Physical Study on the Aromaicity of 4H-Pyran-4-one, 9H-Xanthen-9-one and Related Sulphur Compounds. *Z. Naturforsch. Sect. A* **1986**, *41*, 1250–1257. [CrossRef]
19.   Ośmiałowski, B.; Raczyńska, E.D.; Krygowski, T.M. Tautomeric equilibria and π-electron delocalization for some monohydroxyarenes-quantum chemical studies. *J. Org. Chem.* **2006**, *71*, 3727–3736. [CrossRef]
20.   Allen, F.H. The Cambridge Structural Database: A Quarter of a Million Crystal Structures and Rising. *Acta Cryst. Sect. B Struct. Sci.* **2002**, *58*, 380–388. [CrossRef]
21.   Keith, T.A. *AIMALL*; Version 19.10.12; TK Gristmill Software: Overland Park, KS, USA, 2019.
22.   Krygowski, T.M. Crystallographic Studies of Inter- and Intramolecular Interactions Reflected in Aromatic Character of π-Electron Systems. *J. Chem. Inf. Comput. Sci.* **1993**, *33*, 70–78. [CrossRef]
23.   Frisch, M.J.; Trucks, G.W.; Schlegel, H.B.; Scuseria, G.E.; Robb, M.A.; Cheeseman, J.R.; Scalmani, G.; Barone, V.; Mennucci, B.; Petersson, G.A.; et al. *Gaussian Inc 16*; Revision A.03; Gaussian, Inc.: Wallingford, CT, USA, 2016.
24.   Becke, A.D. Density-Functional Thermochemistry. III. The Role of Exact Exchange. *J. Chem. Phys.* **1993**, *98*, 5648–5652. [CrossRef]
25.   Lee, C.; Yang, W.; Parr, R.G. Development of the Colle-Salvetti Correlation-Energy Formula into a Functional of the Electron Density. *Phys. Rev. B* **1988**, *B37*, 785–789. [CrossRef] [PubMed]
26.   Grimme, S.; Antony, J.; Ehrlich, S.; Krieg, H. A Consistent and Accurate Ab Initio Parametrization of Density Functional Dispersion Correction (DFT-D) for the 94 Elements H-Pu. *J. Chem. Phys.* **2010**, *132*, 154104. [CrossRef]
27.   Sygula, A.; Sygula, R.; Fronczek, F.R.; Rabideau, P.W. Crystal and Molecular Structure of 10-Substituted 9-Anthracenones. Substituent Size as the Controlling Factor for the Nonplanarity of the Central Ring. *J. Org. Chem.* **1992**, *57*, 3286–3291. [CrossRef]
28.   Goldberg, M.; Sartakov, D.; Bats, J.W.; Bolte, M.; Göbel, M.W. A chiral analog of the bicyclic guanidine TBD: Synthesis, structure and Brønsted base catalysis. *Beilstein J. Org. Chem.* **2016**, *12*, 1870–1876. [CrossRef]
29.   Ceban, V.; Tauchman, J.; Meazza, M.; Gallagher, G.; Light, M.E.; Gergelitsová, I.; Veselý, J.; Rios, R. Expanding the scope of Metal-Free enantioselective allylic substitutions: Anthrones. *Sci. Rep.* **2015**, *5*, 16886. [CrossRef]
30.   Liu, Q.X.; Song, H.B. 9-Oxo-10-diphenylphosphinoylanthracene. *Acta Cryst. Sect. E Struct. Rep. Online* **2005**, *E61*, 1489–1490. [CrossRef]
31.   Wu, C.; Li, W.; Yang, J.; Liang, X.; Ye, J. Asymmetric organocatalytic Michael addition of anthrone to enone. *Org. Biomol. Chem.* **2010**, *8*, 3244–3250. [CrossRef]
32.   Loh, C.C.J.; Fang, X.; Peters, B.; Lautens, M. Benzylic Functionalization of Anthrones via the Asymmetric Ring Opening of Oxabicycles Utilizing a Fourth-Generation Rhodium Catalytic System. *Chem. A Eur. J.* **2015**, *21*, 13883–13887. [CrossRef]
33.   Szymańska, M.; Majerz, I. Geometry and Electron Density of Phenothazines. *J. Mol. Struct.* **2020**, *1200*, 127095. [CrossRef]
34.   Bader, R.F.W. *Atoms in Molecules: A Quantum Theory*; Oxford University Press: New York, NY, USA, 1990.
35.   Bader, R.F.W. Bond paths are not chemical bonds. *J. Phys. Chem. A* **2009**, *113*, 10391–10396. [CrossRef] [PubMed]
36.   Bader, R.F.W. Definition of Molecular Structure: By Choice or by Appeal to Observation? *J. Phys. Chem. A* **2010**, *114*, 7431–7444. [CrossRef] [PubMed]
37.   Bader, R.F.W.; Essén, H. The characterization of atomic interactions. *J. Chem. Phys.* **1984**, *80*, 1943. [CrossRef]
38.   Palusiak, M.; Krygowski, T.M. Application of AIM parameters at ring critical points for estimation of π-electron delocalization in six-membered aromatic and quasi-aromatic rings. *Chem. A Eur. J.* **2007**, *13*, 7996–8006. [CrossRef]

39. Espinosa, E.; Alkorta, I.; Rozas, I.; Elguero, J.; Molins, E. About the Evaluation of the Local Kinetic, Potential and Total Energy Densities in Closed-Shell Interactions. *Chem. Phys. Lett.* **2001**, *336*, 457–461. [CrossRef]
40. Banting, L.; Clark, T. *Drug Design Strategies*; The Royal Society of Chemistry: Philadelphia, PA, USA, 2012; pp. 126–142.
41. Korth, H.G.; Mulder, P. Anthrone and related hydroxyarenes: Tautomerization and hydrogen bonding. *J. Org. Chem.* **2013**, *78*, 7674–7682. [CrossRef]

MDPI

Article

Theoretical Study of the Geometry of Dibenzoazepine Analogues

Małgorzata Szymańska * and Irena Majerz

Faculty of Pharmacy, Wroclaw Medical University, Borowska 211a, 50-556 Wroclaw, Poland;
irena.majerz@umw.edu.pl
* Correspondence: m.szymanska@umw.edu.pl; Tel.: +48-71-784-0646; Fax: +48-71-784-0307

Abstract: The geometry of dibenzoazepine analogues—typical multifunctional drugs—was investigated to find the geometrical parameters sensitive to the substitution of the central seven-membered ring. Exploration of the crystal structure database (CSD) shows that the geometrical parameter sensitive to the substitution of the carbon atom distance of the central ring not included in the aromatic rings to the plane through the carbon atoms common for the central ring and the aromatic side rings. Presence of the double bond in the central ring was reflected in its partial aromaticity expressed by the HOMED parameter. Some derivatives of 5*H*-dibenzo[b,f]azepine with flat conformation of the central ring are characterized by mobility of the electron density comparable to the mobility in the aromatic side rings. Influence of the surrounding on the investigated compounds was confirmed by comparison of the optimized molecules and the molecules in the crystal state where the packing forces can influence the molecular geometry.

1. Introduction

The subject of this work are the compounds presented in Scheme 1. Their common feature is the central seven-membered ring with which two benzene rings are accumulated. The conformation of the middle ring is closely related to the presence of a double bond and the presence of a nitrogen or carbon atom in the 5-position. This group of compounds is important because many derivatives are used as medicaments. In a previous work we studied the geometrical and electronic structure of phenothiazines [1]—neuroleptic drugs acting as dopamine blocker. Phenothiazines are tricyclic compounds. Two side rings are aromatic, and the middle ring is aliphatic. It was important to investigate the effect of the substituents in the middle ring on the structure of the phenothiazines. In this work, we investigate similar tricyclic compounds, but the middle ring is seven-membered, which influences its antidepressant properties [2]. The first effective drug for such ailments was imipramine [3]. Thanks to the interest in this group of compounds, further 10,11-dihydro-5*H*-dibenzo[b,f]azepine derivatives were created [4–6] expecting them to be drugs as well. Navdeep Kaur synthesized a series of 10,11-dihydro-5*H*-dibenzo[b,f]azepine hydroxamates, which may have a positive effect on the treatment of cognitive vascular disorders [4].
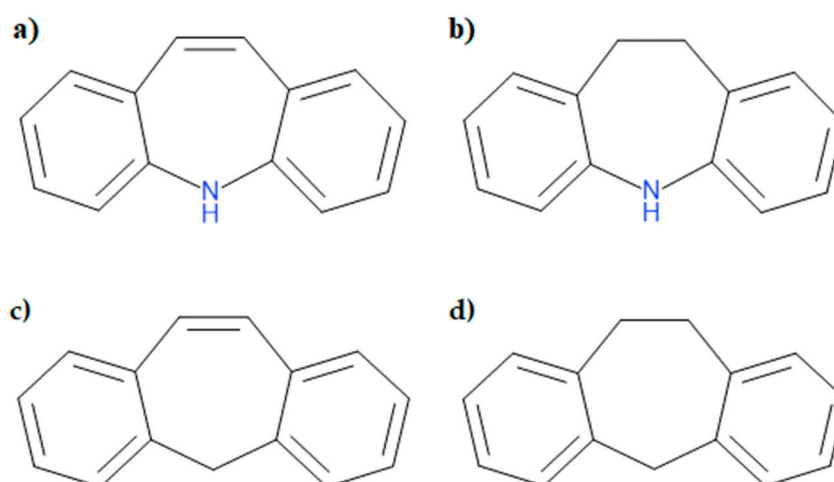
Scheme 1. Structure of the investigated compounds: 5*H*-dibenzo[b,f]azepine (**a**), 10,11-dihydro-5*H*-dibenzo[b,f]azepine (**b**), 5*H*-dibenzo[a,d][7]annulene (**c**), 10,11-dihydro-5*H*-dibenzo[a,d][7]annulene (**d**).

Another important drug belonging to dibenzazepines is carbamazepine. Carbamazepine has anti-epileptic properties [7,8] and additionally relieves the pain [9]. It is used in the treatment of neuroleptic malignant syndrome [10]. Ruaa Wassim prepared a series of 1,2,3-triazole derivatives basing on *N*-acetyl-5*H*-dibenzo[b,f]azepine-5-carboxamide. One of these compounds showed an excellent activity against P. aeruginoa [11]. Kumar Honnaiah prepared a series of 5*H*-dibenzo[b,f]azepine derivatives to evaluate the structure-antioxidant activity relationship [12,13]. Promising results were obtained with 10-methoxy-5*H*-dibenz[b,f]azepine. The presence of the electron donating group OCH_3 and the NH group in the middle ring may contribute to better antioxidant activity [12,13]. The derivative of 10,11-dihydro-5*H*-dibenzo[a,d][7]annulene is an antidepressant amineptine [14]. The interest in the derivatives of 10,11-dihydro-5*H*-dibenzo[a,d][7]annulene is quite large, as evidenced by numerous publications on the synthesis of new derivatives [15–18].

The last group of compounds which is worth attention are 5*H*-dibenzo[a,d][7]annulene derivatives with cytotoxic [19], antioxidant [20] and antimicrobial [21] properties. Kopanski confirmed effects of long-term treatment of rats with antidepressants on adrenergic-receptor sensitivity in cerebral cortex [22]. He observed that the sulfur or oxygen atom at the 10-position of dibenzocycloheptadienes (dibenzoazepine derivative) decreased the ability to induce down-regulation of the adrenergic receptor. He also noted that the effects of the drug were significantly influenced by changes in the chain substituted at the 5-position [22].

Because physicochemical and pharmaceutical properties as well as the mechanism of drug action in organisms are related to the molecular structure [12,13,23], we have undertaken a systematic theoretical study to analyze the structural parameters of 5*H*-dibenzo[b,f]azepine, 10,11-dihydro-5*H*-dibenzo[b,f]azepine, 5*H*-dibenzo[a,d][7]annulene and 10,11-dihydro-5*H*-dibenzo[a,d][7]annulene (Scheme 1). In the first step of the research, an analysis of the compounds available in the CSD crystallographic database [24] has been carried out. This analysis allowed for the determination of geometric parameters that change under substitution. The second step is comparison of the optimized structure with the experimental X-ray structure to check if the packing of the molecule in crystal can change the geometry of the molecule significantly. If so, it can be expected that also other factors resulting from the influence of the environment on the molecular geometry should be taken into account during the analysis of the environment of the drug in the living organism.

2. Computational Details

Geometries of the investigated compounds were retrieved from the 5.41 version of the CSD [24] with the updates in 2020. The search was performed without restrictions and gave 228 hits with 326 structures for 5*H*-dibenzo[b,f]azepine, 90 hits (126 structures) for 10,11-dihydro-5*H*-dibenzo[b,f]azepine, 428 hits (807 structures) for 5*H*-dibenzo[a,d][7]annulene and 277 hits (399 structures) for 10,11-dihydro-5*H*-dibenzo[a,d][7]annulene.

The investigated molecules were optimized using a Gaussian 16 package [25] at DFT-D3 B3LYP/6-311++G** level [26,27], with including Grimme dispersion [28]. DFT/B3LYP affords the best quality to predict the structure of organic compounds [29,30]. To check that the resultant geometry reached the energy minimum, vibrational frequencies were calculated. To visualize delocalization of electrons ACID program was used [31]. NBO analysis was performed using the ADF program [32–34].

3. Results and Discussion

3.1. Geometry of the Investigated Compounds

For 5*H*-dibenzo[b,f]azepine and 5*H*-dibenzo[a,d][7]annulene structures intramolecular proton transfer is possible [35,36]. For this purpose, the structures in Table 1 have been optimized. In order to decide which isomer 1 of 5*H*-dibenzo[b,f]azepine and 5*H*-dibenzo [a,d][7]annulene can exists in the investigated compounds, the energy of the isomers have been compared. The lowest energy structure indicates that, for the investigated compound, the isomer of the lowest energy is of a typical structure and the energy difference confirms that other isomers are not possible.

Table 1. Relative energies (ΔE in kcal $\times$ mol^{-1}) for 5*H*-dibenzo[b,f]azepine and 5*H*-dibenzo[a,d][7]annulene isomers.
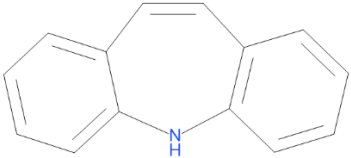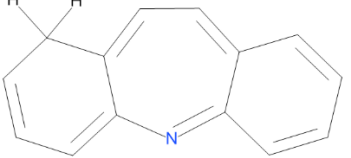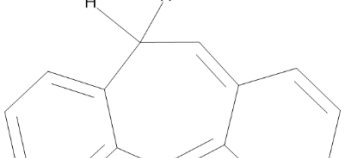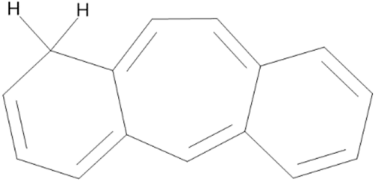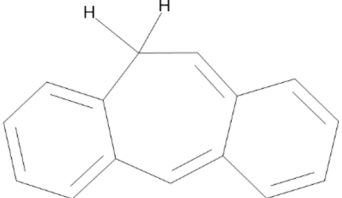
		Tautomer	ΔE [kcal $\cdot$ mol^{-1}]
5*H*-dibenzo[b,f]azepine	1		0
	2		47.71
	3		21.11
	1		0

Table 1. *Cont.*

	Tautomer	ΔE [kcal·mol^{-1}]
5*H*-dibenzo[a,d][7]annulene	2	47.29
	3	22.18

The analysis of geometry of the investigated compounds should result from the indication of a geometric parameters that are sensitive to substitution and potential geometry changes in different environment of the molecule. Scheme 2 shows the geometric parameters which seem to be the most sensitive to substitution of the analyzed compounds, as follows: the α and β angle (both angles are between the shaded planes), the distances of the carbons and the heteroatom from the A plane defined by the carbons in the plane of the central ring shared with the aromatic rings and the C10-C11 bond length.
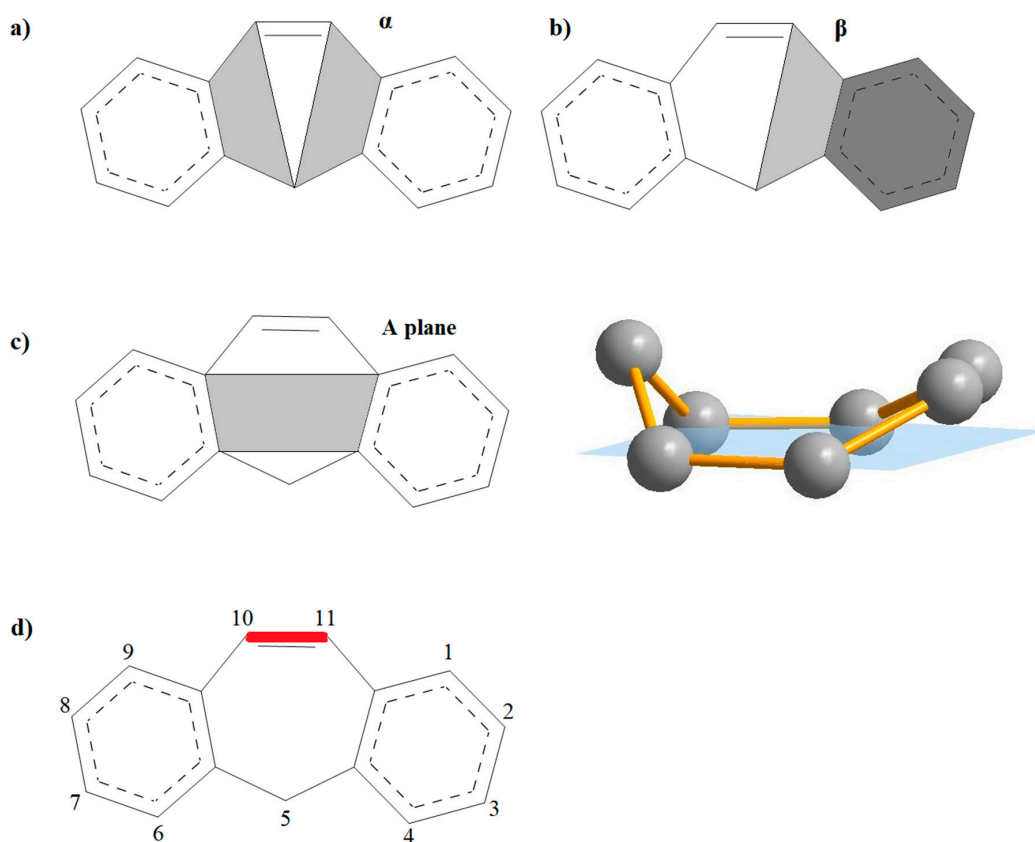
Scheme 2. Geometric parameters for the analyzed compounds. α angle (**a**), β angle (**b**) (both angles are defined between the shaded planes). The A plane is defined by 4 carbon atoms in common with the side aromatic rings (**c**) (for clarity aromatic rings are not included), C10-C11 bond length (**d**).

The results of the exploration of the CSD crystallographic base in relation to the above-mentioned geometric parameters are summarized in Table 2. The α angle for all the analyzed compounds does not reflect changes in geometry, because it changes slightly from 0 to 8 degrees for the analyzed compounds.

Table 2. Analyzed geometrical parameters for the investigated compounds.

Name	Minimum	Maximum	Mean	Variance	Std. Dev	Mean. Dev	Median
α angle							
5*H*-dibenzo[b,f]azepine	6.478	76.212	55.102	47.040	6.859	3.706	54.891
5*H*-dibenzo[a,d][7]annulene	1.196	72.078	54.257	192.096	13.860	9.081	58.611
10,11-dihydro-5*H*-dibenzo[b,f]azepine	7.035	82.424	53.577	180.502	13.435	9.313	57.400
10,11-dihydro-5*H*-dibenzo[a,d][7]annulene	5.028	83.931	59.767	206.198	14.36	11.258	60.169
$\beta1,\beta2$ angle							
5*H*-dibenzo[b,f]azepine	0.183	8.312	3.155	1.975	1.405	1.053	3.135
5*H*-dibenzo[b,f]azepine	0.273	9.489	3.117	2.428	1.558	1.178	3.107
5*H*-dibenzo[a,d][7]annulene	0.041	15.744	3.399	3.374	1.837	1.428	3.202
5*H*-dibenzo[a,d][7]annulene	0.044	11.373	3.449	3.161	1.778	1.41	3.251
10,11-dihydro-5*H*-dibenzo[b,f]azepine	0.416	19.911	3.094	6.373	2.525	1.627	2.42
10,11-dihydro-5*H*-dibenzo[b,f]azepine	0.441	15.258	2.967	5.078	2.253	1.508	2.266
10,11-dihydro-5*H*-dibenzo[a,d][7]annulene	0.136	12.738	3.433	4.439	2.107	1.608	3.062
10,11-dihydro-5*H*-dibenzo[a,d][7]annulene	0.072	12.512	3.21	4.658	2.158	1.636	2.736
Distance to the C12,C13,C14,C15 plane							
5*H*-dibenzo[b,f]azepine *C10*	0.004	0.884	0.537	0.008	0.087	0.056	0.527
5*H*-dibenzo[b,f]azepine *C11*	0.028	0.864	0.536	0.007	0.087	0.054	0.534
5*H*-dibenzo[b,f]azepine *N*	0.105	0.833	0.626	0.006	0.077	0.037	0.629
5*H*-dibenzo[a,d][7]annulene *C10*	0.002	1.003	0.525	0.025	0.158	0.114	0.556
5*H*-dibenzo[a,d][7]annulene *C11*	0.003	0.891	0.523	0.024	0.156	0.112	0.550
5*H*-dibenzo[a,d][7]annulene *C5*	0.005	0.818	0.632	0.025	0.158	0.101	0.677
10,11-dihydro-5*H*-dibenzo[b,f]azepine *C10*	0.000	0.873	0.532	0.034	0.184	0.125	0.587
10,11-dihydro-5*H*-dibenzo[b,f]azepine *C11*	0.015	0.980	0.554	0.103	0.32	0.295	0.514
10,11-dihydro-5*H*-dibenzo[b,f]azepine *N*	0.015	1.008	0.611	0.100	0.316	0.294	0.698
10,11-dihydro-5*H*-dibenzo[a,d][7]annulene *C10*	0.003	1.247	0.642	0.111	0.333	0.296	0.727
10,11-dihydro-5*H*-dibenzo[a,d][7]annulene *C11*	0.001	1.235	0.693	0.098	0.314	0.268	0.806
10,11-dihydro-5*H*-dibenzo[a,d][7]annulene *C5*	0.011	0.930	0.627	0.035	0.186	0.137	0.644
C10C11 bond length							
5*H*-dibenzo[b,f]azepine *C10=C11*	1.240	1.473	1.35	0.001	0.034	0.023	1.341
5*H*-dibenzo[a,d][7]annulene *C10=C11*	1.252	1.499	1.371	0.002	0.044	0.040	1.348
10,11-dihydro-5*H*-dibenzo[b,f]azepine *C10-C11*	1.332	1.606	1.519	0.001	0.038	0.022	1.524
10,11-dihydro-5*H*-dibenzo[a,d][7]annulene *C10-C11*	1.299	1.711	1.524	0.002	0.041	0.026	1.526

It can be expected that the C10C11 bond length should be typical for single or double CC bond. The data in Table 1 show that, depending on the substitution, the C10C11 bond can change in relatively wide range. In general, this bond is longer for azepine than for annulene derivatives.

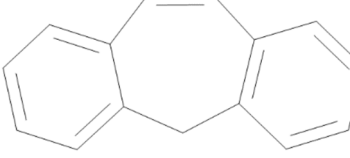The histograms of the α angle performed for the compounds found in the CSD crystallographic database, as follows: 5*H*-dibenzo[b,f]azepine, 5*H*-dibenzo[a,d][7]annulene 10,11-dihydro-5*H*-dibenzo[b,f]azepine and 10,11-dihydro-5*H*-dibenzo[a,d][7]annulene are presented in Figure 1. The α angle covers a wide range of variation. For each group of compounds, the most frequent value can be detected except for 10,11-dihydro-5*H*-dibenzo[a,d][7]annulene. The α angle could be used as the parameter which describes nonplanarity of the central ring of the investigated compounds, but analysis of Table 2 suggests that the best geometrical parameters illustrating nonplanarity of the central ring are the distances of N, C5, C10 and C11 to the plane formed by the carbon atoms common with the aromatic rings (Scheme 2c).

According to the results in Table 2, the distances of the carbon and nitrogen atoms of the middle ring to the plane formed by the carbon atoms of the central ring shared with the aromatic rings vary widely. It is characteristic that very often the distance of these atoms from the plane is close to zero, which proves that the central ring becomes flat. Linear correlations between the distances of the C10 and C11 atoms from the A plane confirm the potential flattening of the middle ring. For 5*H*-dibenzo[b,f]azepine there is a straight line described by the following equation: $y = 0.9217x + 0.0416$, $R^2 = 0.8544$. The mutual correlations of the distances from the plane of atoms C10 and N as well as C11 and N are described by a third-order polynomial, as follows: $y = 5.5627x^3 - 7.5677x^2 + 3.822x - 0.2636$, $R^2 = 0.6713$ and $y = 5.0552x^3 - 6.9641x^2 + 3.6504x - 0.2673$, $R^2 = 0.6732$, respectively. These correlations indicate that the shortening of the distances of the C10 and C11 atoms to the plane is coordinated, but not always associated with the placement of the nitrogen atom in the A plane.
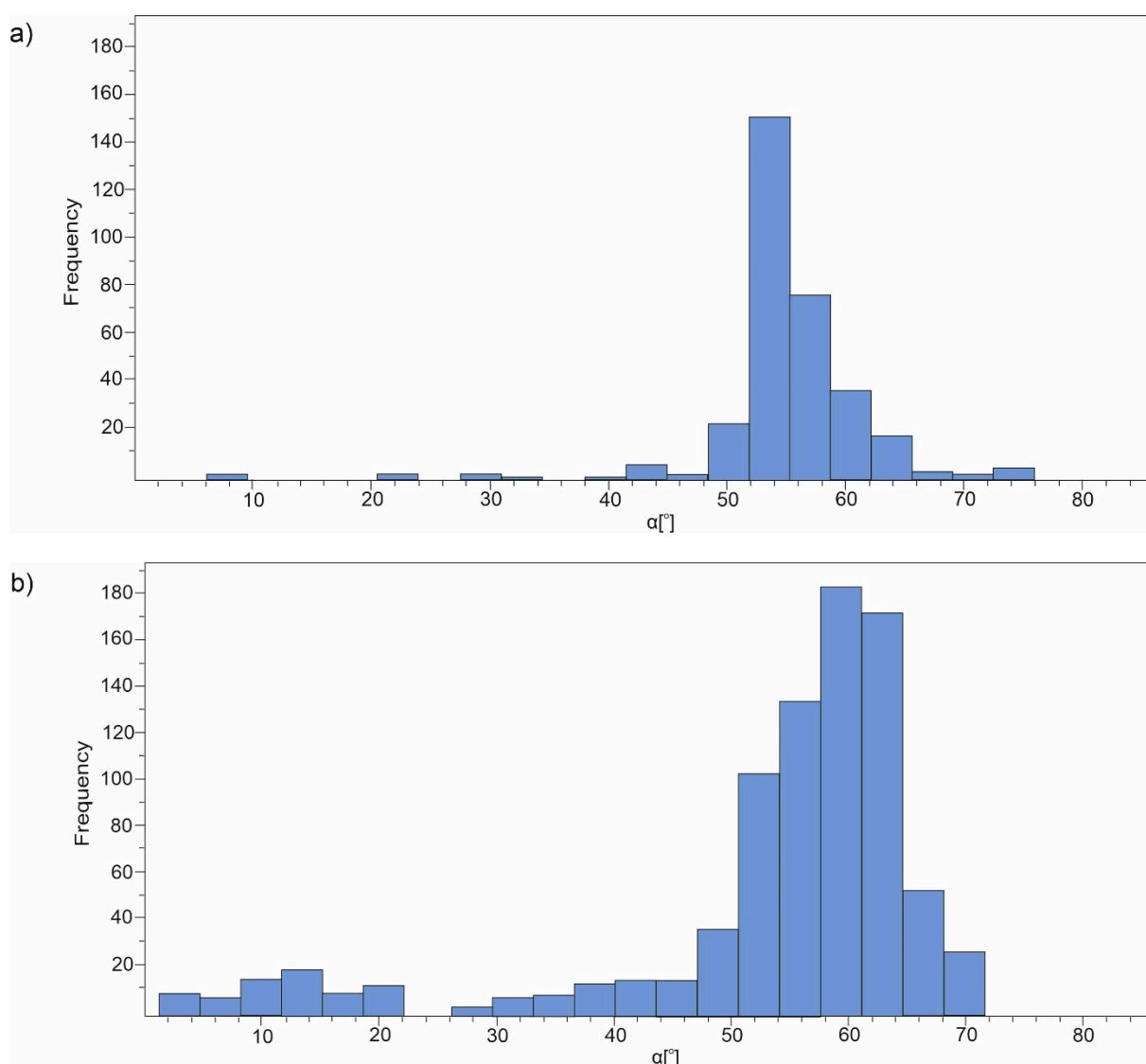
Figure 1. *Cont.*
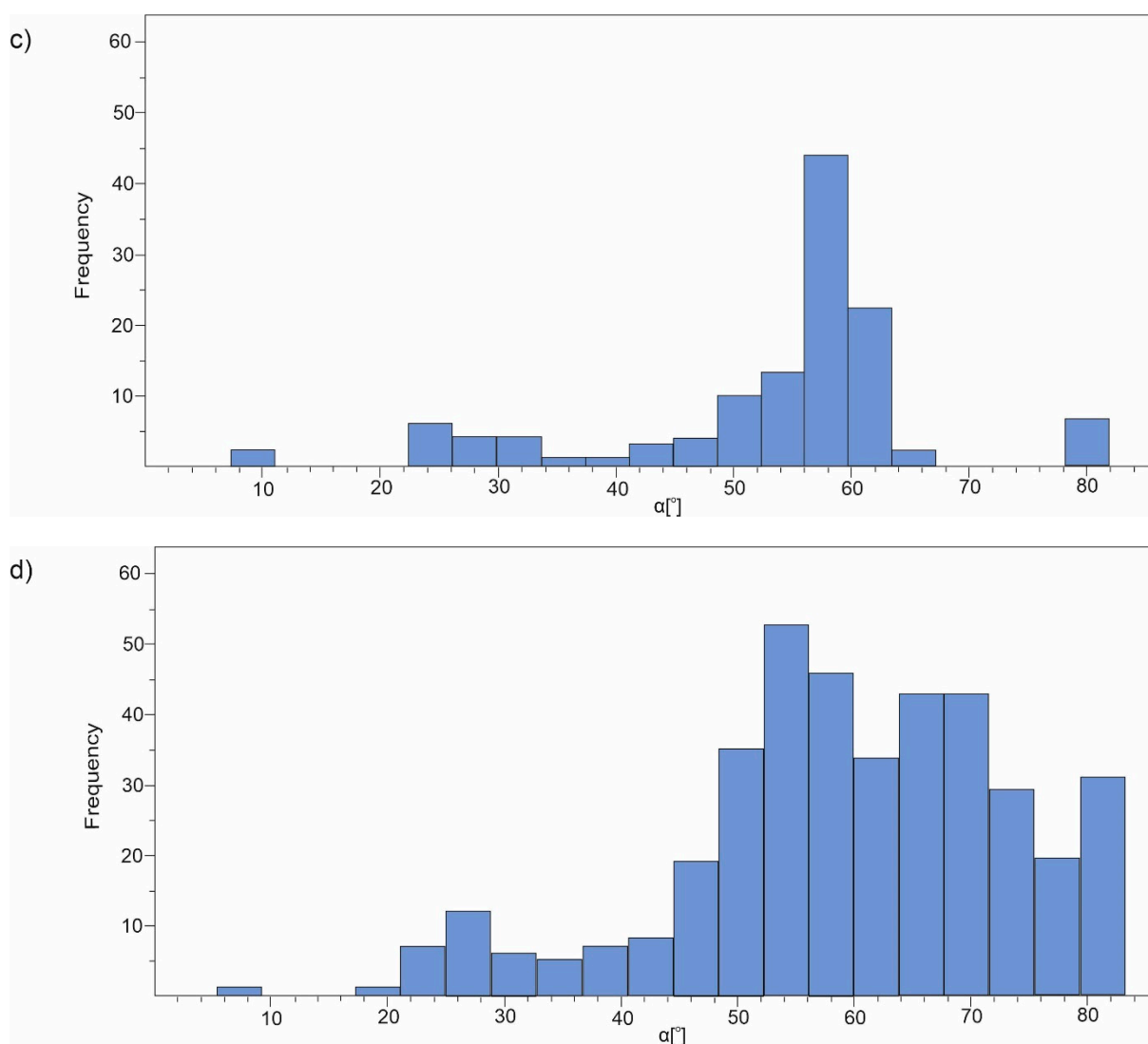
Figure 1. Histogram for the α angle of 5*H*-dibenzo[b,f]azepine (**a**), 5*H*-dibenzo[a,d][7]annulene (**b**), 10,11-dihydro-5*H*-dibenzo[b,f]azepine (**c**) and 10,11-dihydro-5*H*-dibenzo[a,d][7]annulene (**d**).

Similar correlations exist for 5*H*-dibenzo[a,d][7]annulene. The correlation between the distance of C10 and C11 to the A plane is as follows: $y = 0.9408x + 0.0291$, $R^2 = 0.9067$; the distance of C10 and C5 as well as C11 and C5 are as follows: $y = 0.8678x - 0.0228$, $R^2 = 0.7506$ and $y = 0.8693x - 0.0258$, $R^2 = 0.7716$, respectively.

While for 5*H*-dibenzo[a,d][7]azepine and 5*H*-dibenzo[a,d][7]annulene the distances of the carbon atoms to the A plane are similar, replacing of the double bond with a single one in 10,11-dihydro-5*H*-dibenzo[b,f]azepine leads to a difference in both distances. The replacement of the double bond with a single in 10,11-dihydro-5*H*-dibenzo[b,f]azepine causes that the correlation between the distance of C10 and C11 to the A plane can be detected for compounds with substituents at C10 and C11 atoms, while it is very weak for other compounds (Figure 2a). Differentiation of the C10 and C11 distance to the A plane results in different correlation lines for the distances for the N and C atoms. Additionally, the correlation of the longer C distance splits into correlation for substituted C10(C11) and unsubstituted. Correlation for shorter C distance to the A plane is not a straight line. The correlations in Figure 2 express irregular changes of C10, C11 and C5 distance to the A plane. For 10,11-dihydro-5*H*-dibenzo[a,d][7]annulene analogous correlations are not seen.
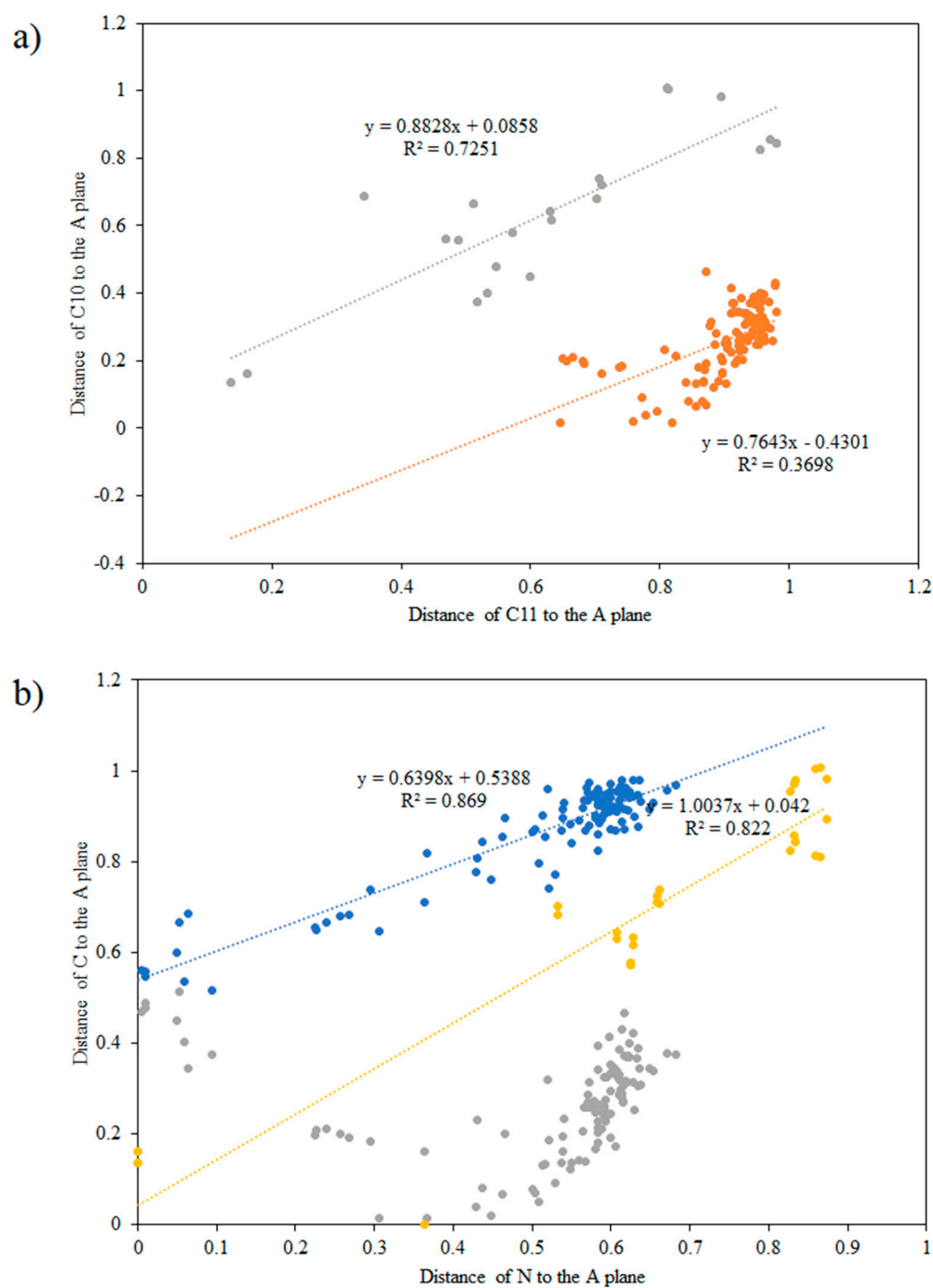
Figure 2. Correlation for 10,11-dihydro-5*H*-dibenzo[b,f][7]azepine. (**a**) Correlation of C10 and C11 distance to the A plane: gray—azepines with substituents in C10 and C11 positions, orange—azepines without substituents in C10 and C11 positions. (**b**) The distance of C10 and C11 to N5 of the A plane: blue and gray—azepines without substituents in C10 and C11 positions, yellow—azepines with substituents in C10 and C11 positions for 10,11-dihydro-5*H*-dibenzo[b,f][7]azepine.

To investigate the influence of substitution on the geometry of the 5*H*-dibenzo[b,f]azepine, 10,11-dihydro-5*H*-dibenzo[b,f]azepine, 5*H*-dibenzo[a,d][7]annulene and 10,11-dihydro-5*H*-dibenzo[a,d][7]annulene, the structures with CH_3, CH_2CH_3, $C(CH_3)_3$, CHO, COOH, NO_2, NH_2, OH and Cl substituents in the central ring at the 5-position have been optimized. The values of α angle for the optimized structures change from 22 to 57° (Table 3). An important parameter which, apart from the α angle, describes the non-planar structure of the molecule is the distance of the carbon and nitrogen atoms to the A plane. For this purpose, the α

angle for the optimized compounds has been correlated with the distance of the C5 and N5 to the A plane (Figure 3). As the distance of the C5 and N5 atoms from the A plane increases, the α angle also increases and therefore flatness of the middle ring decreases. The shortest distance is observed for the nitrogen atom in 10,11-dihydro-5*H*-dibenzo[b,f]azepine without a substituent, which is also connected with the lowest α angle.

a)

$y = 0.0135x - 0.0969$
$R^2 = 0.9615$

b)

$y = 0.0116x + 0.032$
$R^2 = 0.8928$

c)

$y = 0.0171x - 0.3687$
$R^2 = 0.9974$

d)

$y = 0.0104x + 0.0252$
$R^2 = 0.9118$
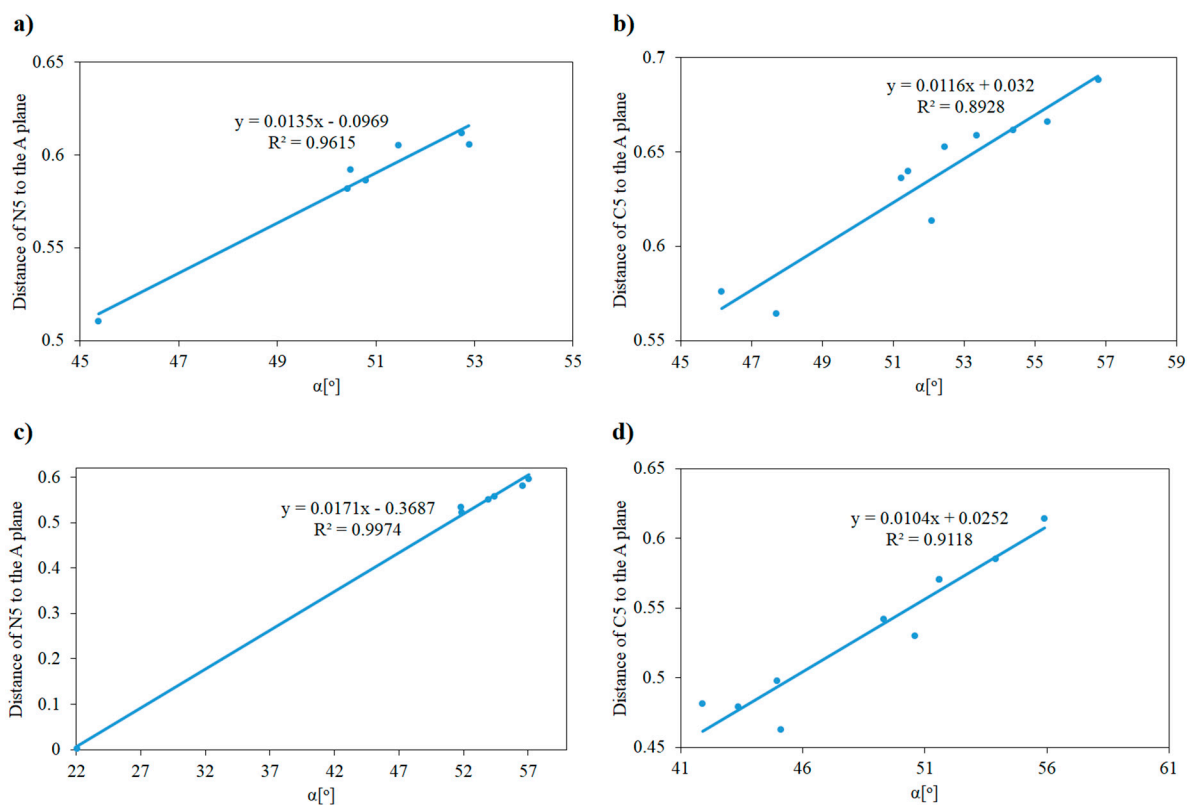
Figure 3. Correlation of the distance of the C5 or N5 atom from the A plane on the α angle on for: 5*H*-dibenzo[b,f]azepine (**a**), 5*H*-dibenzo[a,d][7]annulene (**b**), 10,11-dihydro-5*H*-dibenzo[b,f]azepine (**c**), 10,11-dihydro-5*H*-dibenzo[a,d][7]annulene (**d**).

Table 3. Geometry parameters for optimized structures.

a substituent in the 5-position	5*H*-dibenzo[b,f]azepine					5*H*-dibenzo[a,d][7]annulene				
	α	C10C11 bond length	distances of the atoms from the A plane			α	C10C11 bond length	distances of the atoms from the A plane		
			C10	C11	N5			C10	C11	C5
unsubstituted structure	45.37	1.345	0.442	0.442	0.511	56.79	1.351	0.527	0.527	0.688
CH$_3$	50.49	1.349	0.449	0.449	0.592	51.23	1.349	0.439	0.439	0.636
CH$_2$CH$_3$	51.46	1.349	0.452	0.456	0.605	51.41	1.349	0.440	0.436	0.640
C(CH$_3$)$_3$	52.89	1.349	0.498	0.498	0.606	46.15	1.346	0.380	0.380	0.576
CHO	50.80	1.348	0.480	0.483	0.587	54.38	1.350	0.493	0.500	0.662
COOH	52.73	1.350	0.489	0.504	0.612	55.35	1.350	0.512	0.514	0.666
NO$_2$	50.42	1.351	0.476	0.476	0.582	52.08	1.350	0.494	0.494	0.614
NH$_2$						52.45	1.350	0.450	0.447	0.653
OH						53.35	1.352	0.466	0.466	0.659
Cl						47.70	1.348	0.440	0.440	0.564

Table 3. *Cont.*

a substituent in the 5-position	10,11-dihydro-5H-dibenzo[b,f]azepine					10,11-dihydro-5H-dibenzo[a,d][7]annulene				
	α	C10C11 bond length	distances of the atoms from the A plane			α	C10C11 bond length	distances of the atoms from the A plane		
			C10	C11	N5			C10	C11	C5
unsubstituted structure	22.02	1.544	0.464	0.470	0.003	55.90	1.538	0.891	0.213	0.614
CH_3	51.82	1.534	0.885	0.143	0.523	43.34	1.534	0.759	0.046	0.480
CH_2CH_3	51.79	1.536	0.856	0.151	0.534	51.59	1.536	0.838	0.125	0.571
$C(CH_3)_3$	56.55	1.536	0.232	0.911	0.582	41.90	1.529	0.698	0.053	0.481
CHO	54.37	1.537	0.211	0.901	0.558	49.30	1.535	0.082	0.828	0.542
COOH	57.06	1.539	0.911	0.271	0.597	53.88	1.536	0.180	0.876	0.585
NO_2	53.94	1.539	0.897	0.227	0.551	50.59	1.535	0.858	0.155	0.530
NH_2						44.95	1.535	0.774	0.022	0.498
OH						51.59	1.536	0.838	0.125	0.571
Cl						45.09	1.534	0.812	0.047	0.463

The distance of C10 and C11 to the A plane formed by the carbon atoms of the central ring common to aromatic rings has also been examined. The distances of C10 and C11 to the A plane are similar for both 5H-dibenzo[b,f]azepine and 5H-dibenzo[a,d][7]annulene derivatives. The analogous linear correlations exist for 5H-dibenzo[b,f]azepine $y = 1.0838x - 0.0361$, $R^2 = 0.9538$, while for 5H-dibenzo[a,d][7]annulene $y = 1.0255x - 0.0116$, $R^2 = 0.9964$ (Figure 4). The C10 and C11 distances to the A plane for 10,11-dihydro-5H-dibenzo[b,f]azepine and 10,11-dihydro-5H-dibenzo[a,d]annulene do not correlate with the α angle.
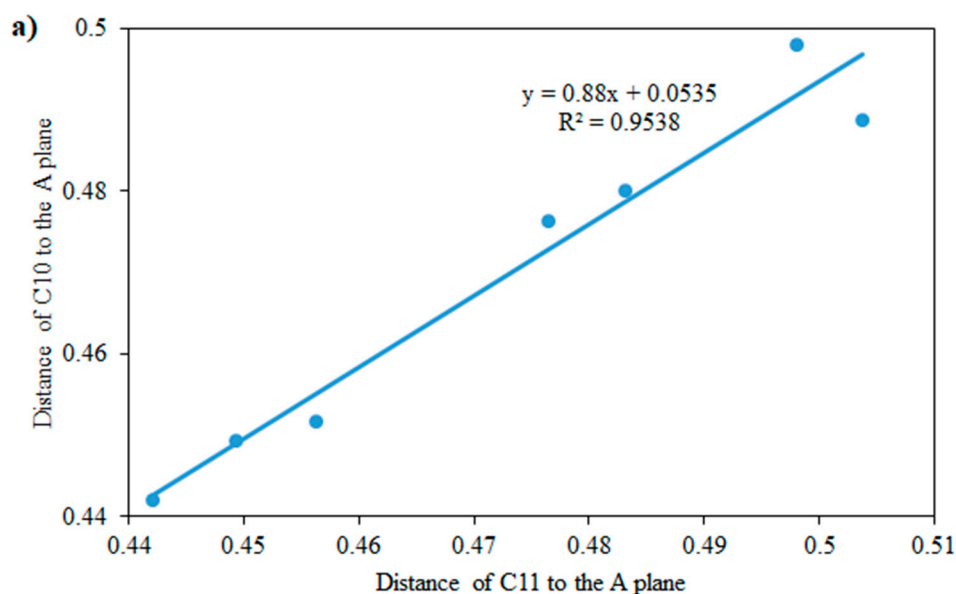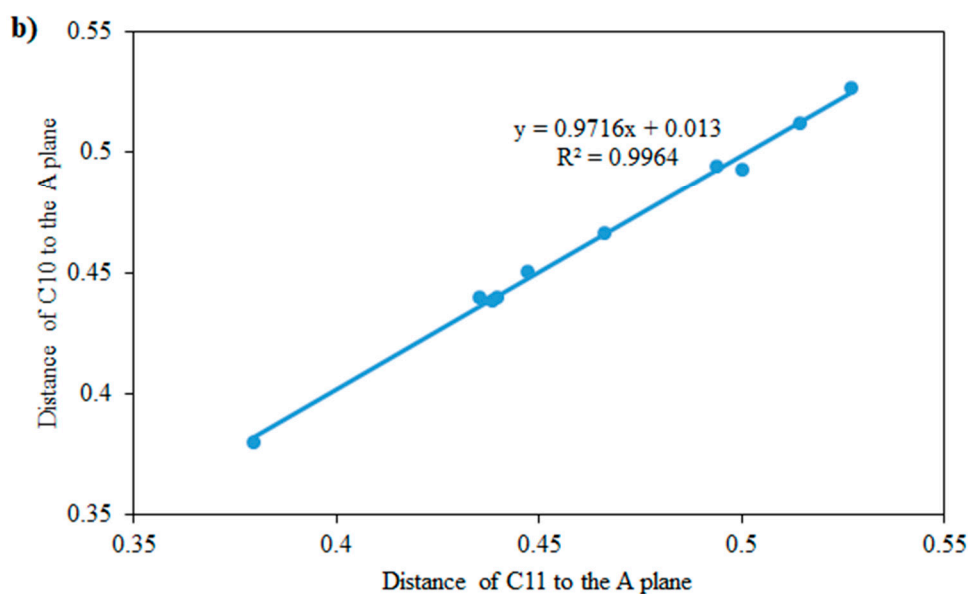

Figure 4. *Cont.*

Figure 4. Correlation of C10 and C11 distance to the A plane for 5*H*-dibenzo[b,f]azepine (**a**), 5*H*-dibenzo[a,d][7]annulenne (**b**).

Despite sensitivity of the α angle to substitution of the investigated compounds, the C10C11 bond length changes slightly. The length of the C10C11 double bond in 5*H*-dibenzo[b,f]azepine and 5*H*-dibenzo[a,d][7]annulene changes from 1.345 Å to 1.352 Å. Larger differences from 1.529 Å to 1.544 Å are observed for the single C10C11 bond in 10,11-dihydro-5*H*-dibenzo[b,f]azepine and 10,11-dihydro-5*H*-dibenzo[a,d][7]annulene. In most cases the presence of nitrogen at the 5-position does not affect the length of the C10C11.

All analyzed changes in geometry indicate that the central ring in the investigated compounds is very flexible and may change the geometry from typical for completely aliphatic rings to almost flat. Changes in the geometry of the central ring result from its substitution. It can be also possible that the geometry changes can be caused by the environment of the molecule.

In order to study the influence of the environment, optimization of substituted structures of 5*H*-dibenzo[b,f]azepine, 10,11-dihydro-5*H*-dibenzo[b,f]azepine, 5*H*-dibenzo[a,d][7]annulene and 10,11-dihydro-5*H*-dibenzo[a,d][7]annulene has been carried out in solvents with different electric permittivity. The influence of the solvent on the α angle and the C10-C11 bond length has not been observed.

The structures of 5*H*-dibenz[b,f]azepine-5-carboxamide (carbamazepines) taken from the crystallographic database have been collected in Table 4. It is worth noting that carbamazepine has five polymorphs relating to the conformation of the middle ring, which is the reason for the differences in geometry [45]. The data in Table 4 have been compared with the optimized structure. The length of the C10C11 bond for the optimized molecule (1.350 Å) is very close to the median length of the same bond in the crystal structures. Similar results have been obtained for the distances of the C10 and C11 atoms from the A plane and for the optimized structure it is 0.491 and 0.506, respectively. For polymorphs it ranges between 0.347 and 0.650 for C10 and 0.395–0.570 for C11. Despite the fact that carbamazepine has a double C10C11 bond, the distances of C10 and C11 atoms from the A plane are different, which means that they do not lie in the same plane.

Table 4. Geometry parameters for carbamazepine structures from CSD crystal database.

Refcode.	Bond Length C10-C11	Distance C10 to the A Plane	Distance C11 to the A Plane	R-factor	T	Space Group
CBMZPN01 [37]	1.330	0.543	0.514	3.5	rt	P21/c
CBMZPN02 [38]	1.325	0.515	0.556	8.4	rt	P21/n
CBMZPN03 [39]	1.3456	0.549	0.540	6.9	rt	R-3
CBMZPN10 [40]	1.331	0.520	0.546	3.9	rt	P21/n
CBMZPN11 [41]	1.337	0.528	0.536	5.06	158	P-1
CBMZPN12 [42]	1.340	0.492	0.469	3.57	158	C2/c
CBMZPN13 [43]	1.376	0.547	0.531	17.96	160	P-1
CBMZPN14 [44]	1.336	0.543	0.518	4.04	rt	P21/n
CBMZPN16 [45]	1.347	0.505	0.571	4.5	123	Pbca
CBMZPN17 [46]	1.350	0.542	0.509	4	rt	P21/n
CBMZPN18 [46]	1.352	0.543	0.510	1.08	100	P21/n
CBMZPN19 [46]	1.352	0.543	0.510		0	P21/n
CBMZPN20 [47]	1.333	0.539	0.527	3.95	rt	P21
CBMZPN21 [48]	1.353	0.545	0.509	6.79	100	P21/n
CBMZPN22 [48]	1.351	0.543	0.510	4.07	100	P21/n
CBMZPN23 [48]	1.352	0.545	0.512	2.4	100	P21/n
CBMZPN27 [49]	1.344	0.511	0.543	4.26	183	P21/n
CBMZPN28 [50]	1.243	0.650	0.514	25.45	rt	P21/n
CBMZPN29 [50]	1.344	0.430	0.490	40.54	rt	P21/n
CBMZPN30 [50]	1.260	0.451	0.452	36.9	rt	P21/n
CBMZPN31 [51]	1.396	0.483	0.545	19.21	rt	P21/n
CBMZPN32 [52]	1.338	0.347	0.395	43.85	rt	P21/n

3.2. Aromaticity of the Central Ring of Investigated Compounds

Aromaticity is a phenomenon of the conjugated cyclic system of double bonds that shows delocalization of the π electrons. Such a system significantly modifies the chemical properties of the substances [53,54]. To determine the aromaticity of the rings of a chemical compound the Hückel's rule is used. According to this rule, aromaticity is a property of conjugated, planar, cyclic compounds with 4n + 2 π-electrons where n is a natural number. Taking into account this rule, we have the following: for 5*H*-dibenzo[b,f]azepine the number of π electrons is 16 = 14 from 7(C=C) bonds + 2 from N lone pair; for 5*H*-dibenzo[a,d][7]annulene: 14 = 7 from (C=C) bonds; for 10,11-dihydro-5*H*-dibenzo[b,f]azepine: 14 = 12 from 6(C=C) bonds + 2 from N lone pair; for 10,11-dihydro-5*H*-dibenzo[a,d][7]annulene: 12 = from 6(C=C) bonds. According to the Hückel's rule, aromatic compounds are: 5*H*-dibenzo[a,d][7]annulene and 10,11-dihydro-5*H*-dibenzo[b,f]azepine so the central ring for some of the investigated compounds must be almost flat if the term of planarity can be fulfilled. Because of the presence of the double bond in the central ring as well as the bonds common with the aromatic ring, conjugation of double bonds can be discussed. For 5*H*-dibenzo[b,f]azepine the lone pairs of the nitrogen atom may contribute to an increase in the aromaticity of the middle ring.

To describe and quantify aromaticity, many parameters resulting from geometry and physicochemical properties can be used [55–60]. The simplest and the most convenient to use, especially for large series of tested compounds, is the HOMA parameter basing on the bond length in the ring. For the benzene aromatic ring the HOMA index is equal to 1; for cyclohexane it is zero, for antiaromatic ring it is negative [61]. For compounds with heteroatoms in central ring, HOMED parameter is used, for which procedure, from a mathematical point of view, is the same as for HOMA, and CN parameter is included [35].

$$\text{HOMED} = 1 - \alpha/\text{n} \sum_{i=1}^{n} \left(R_{\text{opt}} - R_{\text{ij}}\right)^2 \tag{1}$$

R_{opt}—the optimized CC bond length of a perfectly aromatic system and equals 1.394 Å and the optimized CN bond length equals 1.334 Å

R_{ij}—determined bond length

α—standardization constant: 5*H*-dibenzo[b,f]azepine for CN bond 84.52 and for CC bond 80.90, 5*H*-dibenzo[a,d][7]annulene for CC bond 80.90, 10,11-dihydro-5*H*-dibenzo[b,f]azepine for CN bond 73.20 and for CC bond 69.55, 10,11-dihydro-5*H*-dibenzo[a,d][7]annulene for CC bond 69.55

n—number of bonds

Figure 5 shows histograms of the HOMED values for the middle ring of 5*H*-dibenzo[b,f]azepine, 10,11-dihydro-5*H*-dibenzo[b,f]azepine, 5*H*-dibenzo[a,d][7]annulene, 10,11-dihydro-5*H*-dibenzo[a,d][7]annulene taken from the database. According to the HOMED value for the central ring of 5*H*-dibenzo[b,f]azepine and 5*H*-dibenzo[a,d][7]annulene the ring is aromatic. The middle ring of 10,11-dihydro-5*H*-dibenzo[b,f]azepine and 10,11-dihydro-5*H*-dibenzo[a,d][7]annulene is less aromatic and the most frequent HOMED value is higher for 10,11-dihydro-5*H*-dibenzo[b,f]azepine than for 10,11-dihydro-5*H*-dibenzo[a,d][7]annulene.
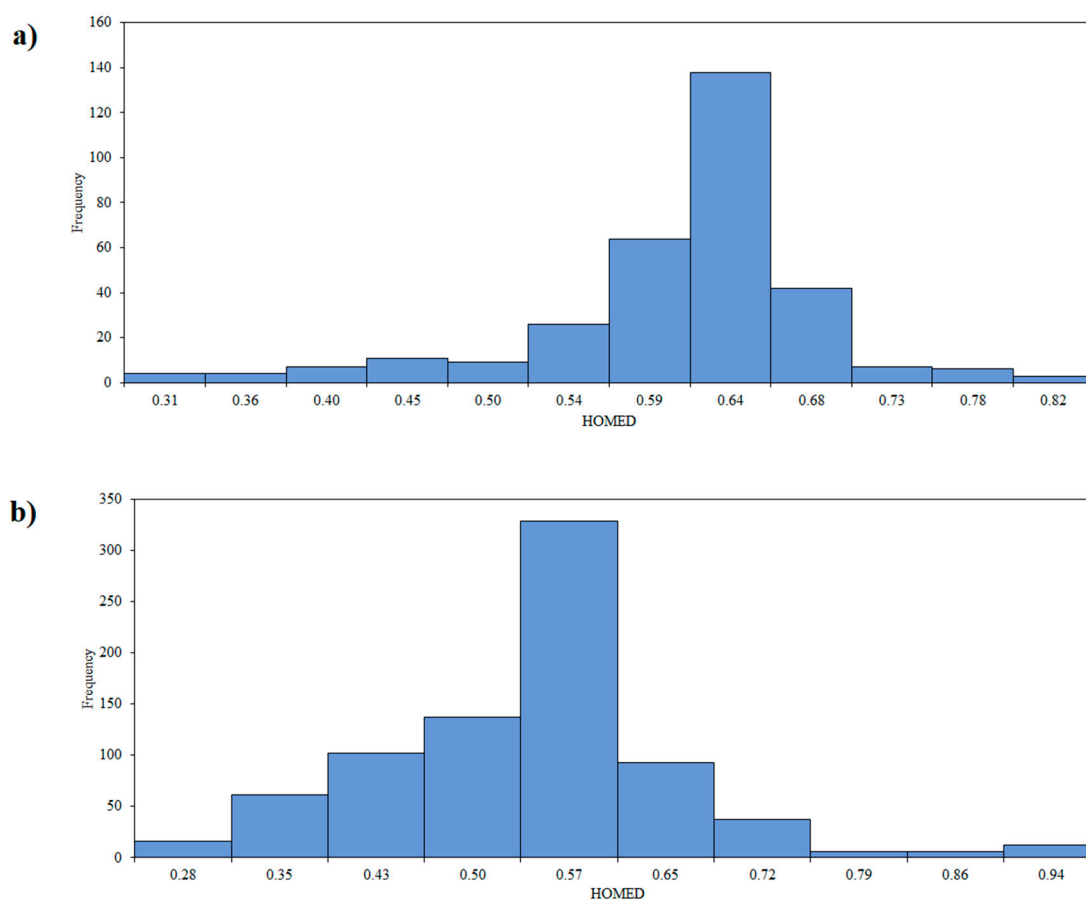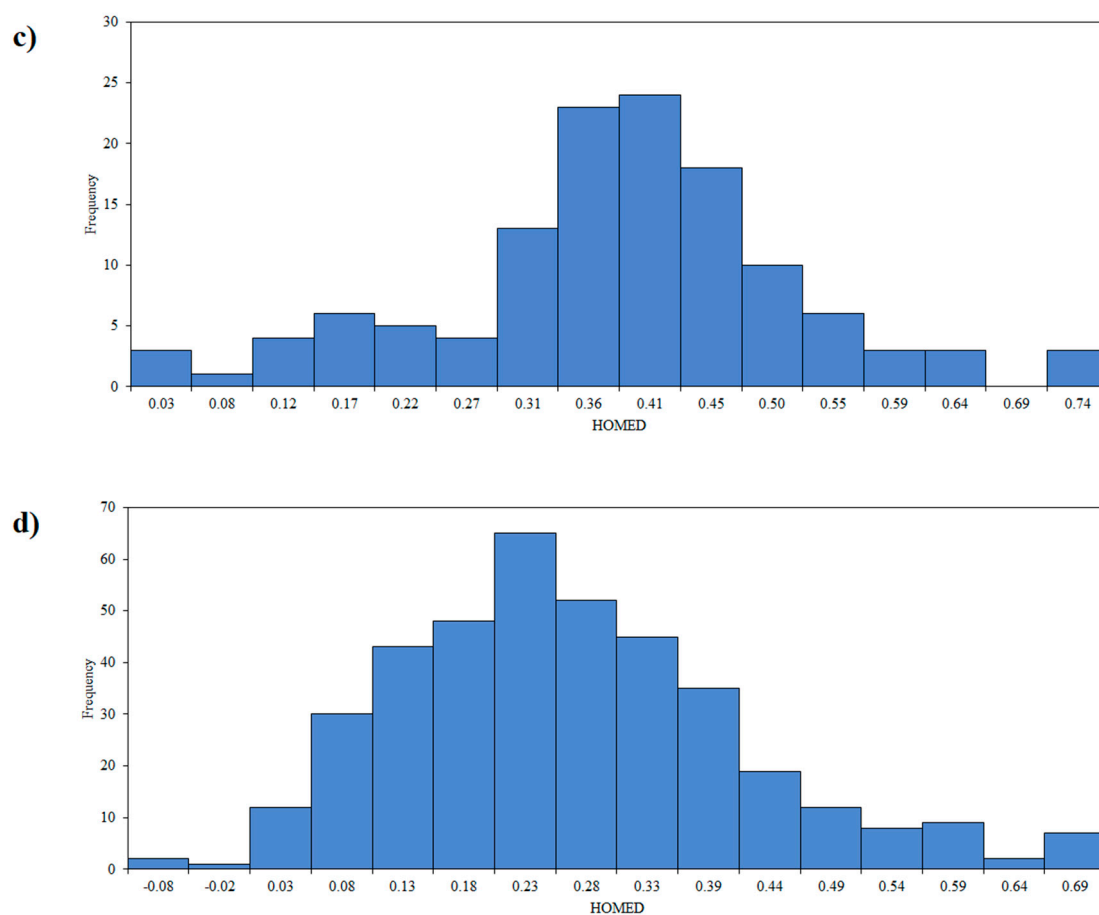

Figure 5. *Cont.*

Figure 5. Histogram for the HOMED value for the middle ring of 5*H*-dibenzo[b,f]azepine (**a**), 5*H*-dibenzo[a,d][7]annulene (**b**) 10,11-dihydro-5*H*-dibenzo[b,f]azepine (**c**) and 10,11-dihydro-5*H*-dibenzo[a,d][7]annulene (**d**). Compound structures are taken from CSD crystal database.

Comparison of the HOMED values for the derivatives of the investigated compounds listed in the CSD crystallographic database shows how much the aromaticity of the central ring depends on the substitution on the side rings and on the substituents in the central ring. While the HOMED value for the middle ring calculated for the optimized unsubstituted compound is 0.6876, substitution in both the middle ring and the side rings can lead to significant aromaticity changes. The highest HOMED value for the central ring of YIJPEM [62] is 0.8217, so this ring can be considered aromatic. The aromaticity of the central ring disappears in the case of HEMRIB [63] for which the HOMED value is −0.2506. In Figure 6 are presented the 5*H*-dibenzo[b,f]azepine derivatives with the highest and the lowest HOMED values for the middle ring.
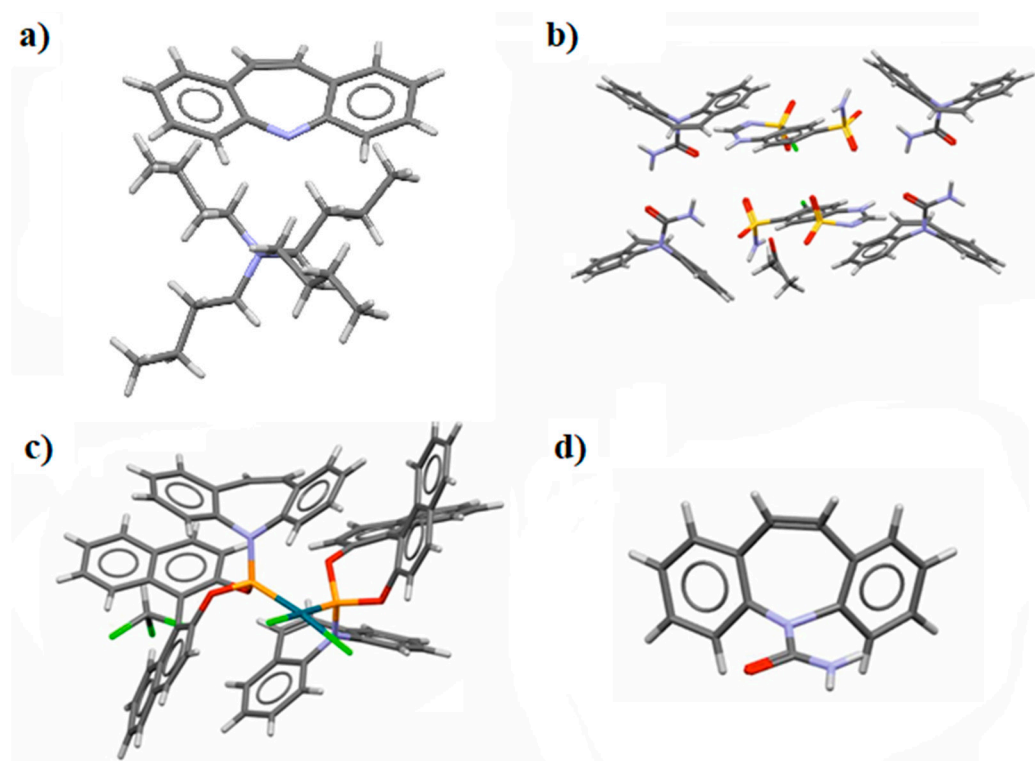
Figure 6. 5*H*-dibenzo[b,f]azepine derivatives with the highest and the lowest HOMED values for the middle ring: YIJPEM [62] (0.8217) (**a**), VEJZUI [64] (0.7934) (**b**), YIFCUM [65] (−0.1731) (**c**), HEMRIB [63] (−0.2506) (**d**). In parentheses are given the HOMED values for the middle ring.

The examples of 5*H*-dibenzo[b,f]azepine derivatives in Figure 6 with different HOMED values for the middle ring illustrate how the aromaticity of the central ring can be easily modified by the substituent and the environment of the molecule. This is especially true when comparing VEJZUI and HEMRIB. Despite the same substituent at the nitrogen atom, the middle ring can be aromatic or anti-aromatic depending on the surroundings of the molecule caused by crystal packing.

3.3. Delocalization of Electrons

The changes in aromaticity described by the HOMED parameter are closely related to the changes in the delocalization of the electron density which determines reactivity of the molecule and many other physical and chemical properties. A method to visualize the electron delocalization used in this work is ACID (anisotropy of the current-induced density) [31]. Delocalization of π electrons of the aromatic ring and the double bond is significant when comparing to delocalization of the single bond electrons, and this method allows indication of the bond character [66]. The ACID surfaces for the optimized structures of the investigated compounds are presented in Figure 7.
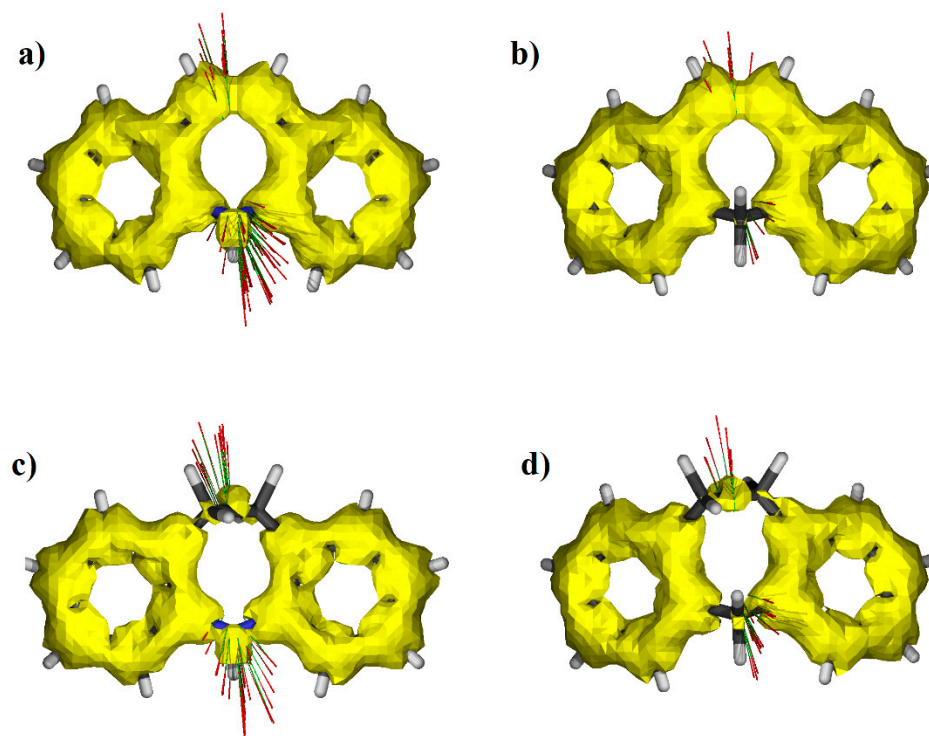
Figure 7. ACID surfaces for the optimized 5*H*-dibenzo[b,f]azepine (0.6876) (**a**), 5*H*-dibenzo[a,d][7]annulene (0.5448) (**b**), 10,11-dihydro-5*H*-dibenzo[b,f]azepine (0.4295) (**c**), 10,11-dihydro-5*H*-dibenzo[a,d][7]annulene (0.1863) (**d**). In parentheses are given the HOMED values for the middle ring.

For the optimized compounds with double bond in the central ring, delocalization of the electrons is significant. The lone pair of the nitrogen in 5*H*-dibenzo[b,f]azepine participates in the mobility of the electrons of the central ring, so it has partially aromatic character expressed by the HOMED value of 0.6876. If nitrogen has been replaced by carbon, the lack of the lone electron pair prevents electron delocalization in 5*H*-dibenzo[a,d][7]annulene.

In Figure 8 are presented ACID surfaces for selected 5*H*-dibenzo[b,f]azepine derivatives. Because the HOMED values for the central ring can be higher than for the unsubstituted compound, delocalization of the electrons in the central ring can be similar to the aromatic side rings. For the antiaromatic central ring cumulated with two aromatic rings and with one double bond, antiaromaticity is expressed with breaking the continuity of electron delocalization at the aliphatic C-C bonds.
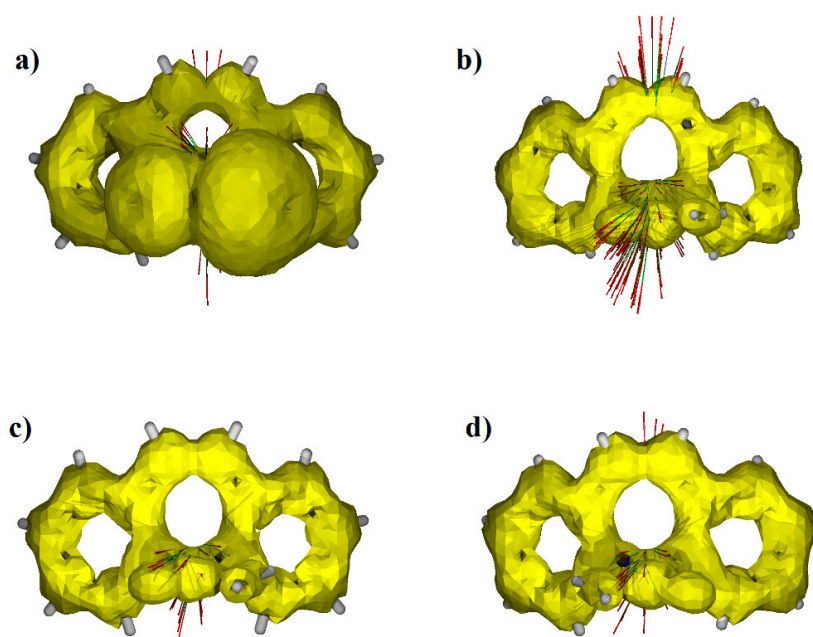
Figure 8. ACID surfaces for selected 5*H*-dibenzo[b,f]azepine derivatives with different aromaticity of the middle ring. The HOMED value for VUBCAW [67] is 0.7816 (**a**), for CBMZPN32 [52] −0.0896 (**b**), for TAZRAO01 [68] 0.6732 (**c**) and for HEMRIB [63] −0.2506 (**d**).

Replacing of the double bond in the middle ring with a single one caused the central ring to express less aromaticity. Substitution of the compound can cause the HOMED value for the middle ring to be higher than for a typical unsubstituted ring (Figure 9). Relatively high HOMED value and electron delocalization is connected with the presence of the lone pairs on the nitrogen atom and the aromatic bonds common for the central and the side ring.
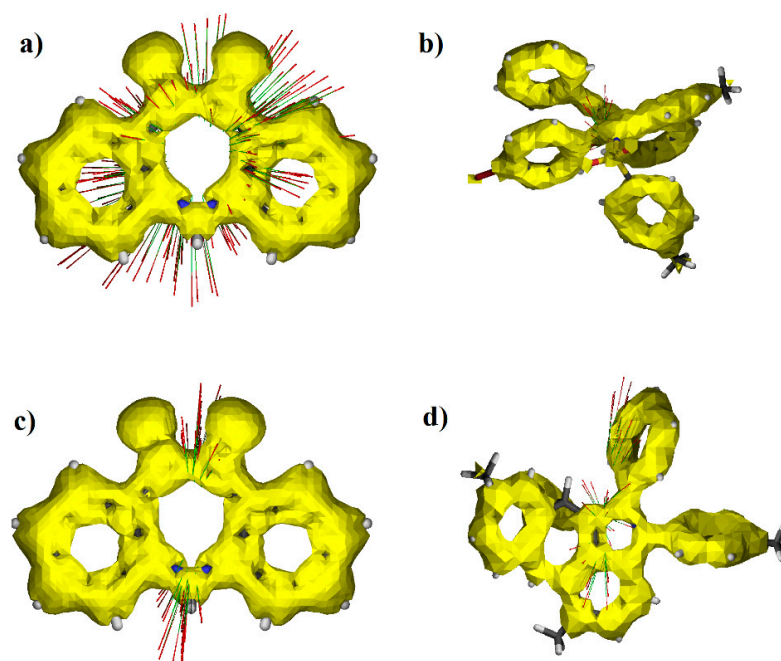

Figure 9. ACID surfaces for selected 10,11-dihydro-5*H*-dibenzo[b,f]azepine derivatives with different aromaticity of the central ring: GEXMAA01 [69] (0.7355) (**a**), RONRAQ [70] (0.7088) (**b**), GEXMAA [71] (0.6981) (**c**), TEVKUC [72] (0.6269) (**d**). In parentheses are given the HOMED values for the middle ring.

Replacing of the nitrogen atom in the middle ring with a carbon atom reduces aromaticity and related electron delocalization comparing to the azepine. Nevertheless, appropriate substitution can change the nature of the central ring and the ring is not typically aliphatic (Figure 10). In order for the central ring to become typically aliphatic, it is necessary to replace the nitrogen with a carbon and replacing the double bond with a single bond.
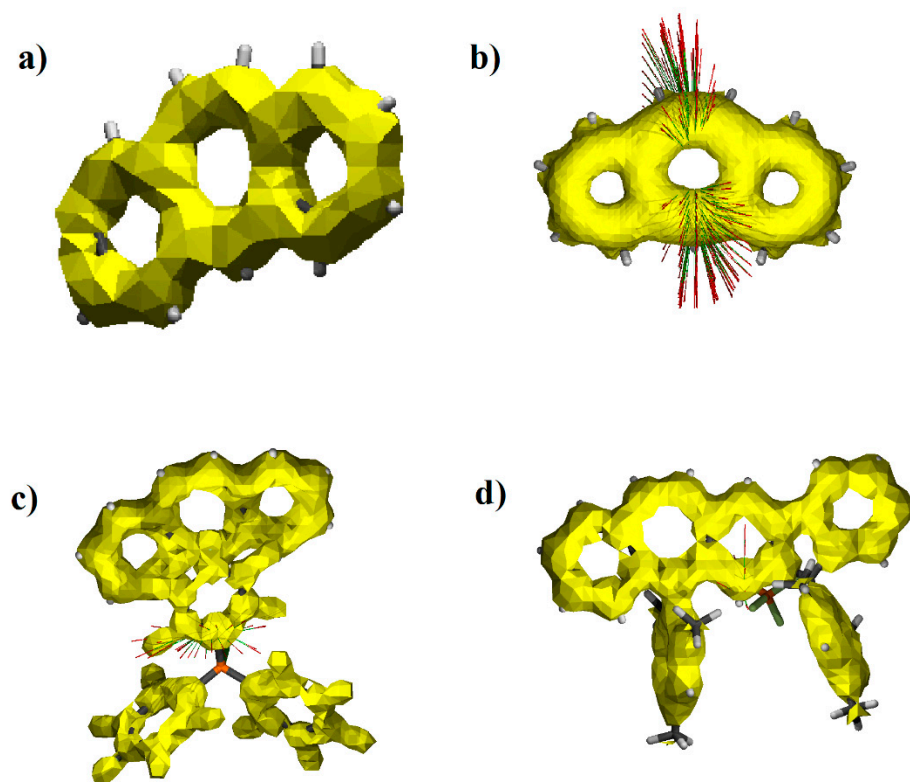

Figure 10. ACID surfaces for selected 5*H*-dibenzo[a,d][7]annulene derivatives with different aromaticity of the central ring: XOHXIC [73] (0.9363) (**a**), XOHXOI [73] (0.9201) (**b**), XOHXEY [73] (0.9169) (**c**), RULROI [74] (0.8818) (**d**). In parentheses are given the HOMED values for the middle ring.

3.4. NBO Analysis

Investigation of the chemical bond, especially the bonds in aromatic molecules, has a very long tradition. A particular chemical bond can be illustrated by molecular orbitals. To construct the molecular orbital representing the chemical bond, the natural atomic orbitals are transformed to natural atomic hybrid and finally to natural localized molecular orbitals (NLMO) which are close to molecular orbitals [75]. Natural localized molecular orbitals (NLMO) are traditionally used in chemistry to present the distribution of electron density in bonds linking atoms as well as in the lone pairs [76]. Detailed analysis of NLMO delivers information on participation of the atoms included in the bond, bond polarization, orbital occupancy and delocalization [77].

To explain the source of the partially aromatic character of the central rings of 5*H*-dibenzo[b,f]azepine and 5*H*-dibenzo[a,d][7]annulene the NLMO orbitals of this ring have been analyzed. In Figure 11 are shown the orbitals representing the double bond, the lone pair of the nitrogen atom and the aromatic bond common with the side ring. For a typical chemical bond, the localization is close to 100% and the occupancy is close to 2. One of the double bonds of 5*H*-dibenzo[b,f]azepine is localized and fully occupied (99.3329%, 1.9867). Occupancy of the second bond is 1.8823 when for the single bond it should be close to 2. Localization is 94.0865%, which is far off the normal localization of about 100%. The atoms next to the double bond also contribute to this bond, and their participation in the orbital is 1.3930%. It is characteristic that for 5*H*-dibenzo[a,d][7]annulene that localization,

occupancy and participation of the neighboring atoms in the NLMO of the double bond is 93.5957%, 1.8733 and 1.563%, respectively.
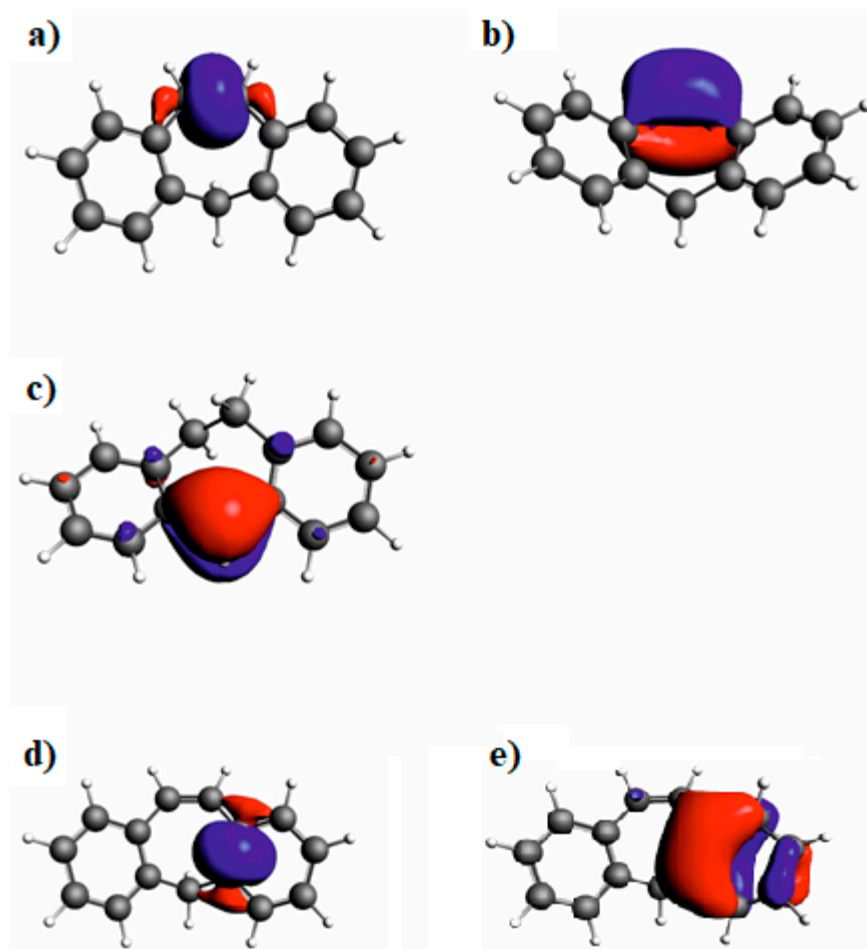

Figure 11. NLMO double bond molecular orbitals for optimized structure of 5*H*-dibenzo[a,d][7]annulene (**a**,**b**), lone pair on nitrogen atom orbitals for 10,11-dihydro-5*H*-dibenzo[b,f]azepine (**c**) and aromatic bond in 5*H*-dibenzo[a,d][7]annulene (**d**,**e**).

The free electron pair on the nitrogen atom is also delocalized. For 5*H*-dibenzo[b,f][7] azepina, its location is 89.3911%, occupancy is 1.7909 and the participation of neighboring atoms is 1.192 and 0.822%, respectively. Free pair delocalization is more pronounced for 10,11-dihydro-5*H*-dibenzo[b,f]azepine.

Another source of delocalized electrons in the central ring are aromatic bonds in common with the side rings. During the NBO analysis, the aromatic side bond has been divided into one localized and fully occupied orbital and another with a location of approximately 79% and an occupancy of approximately 1.6000. The source of the partially aromatic character of the central rings of the investigated compounds is the delocalization of the free electron pair on the nitrogen atom, the delocalization of the double bond and the participation of aromatic electrons coming from the side rings.

4. Conclusions

The geometrical parameters that best describe the nonplanarity of the central ring of the investigated compounds are the distances of the C10, C11, and N (C) atoms in the 5-position from the A plane formed by carbon atoms common to the plane of the central ring and aromatic rings.

Although the central ring in 5*H*-dibenzo[b,f]azepine and 5*H*-dibenzo[a,d][7]annulene is not a typical aromatic ring, both the HOMED values and ACID diagrams indicate aro-

maticity of this ring for 5*H*-dibenzo[b,f]azepine and a significant participation of aromaticity in the case of 5*H*-dibenzo[a,d][7]annulene. The source of the partially aromatic character of the central rings of the investigated compounds is the delocalization of the free electron pair on the nitrogen atom, the delocalization of the double bond and the participation of aromatic electrons coming from the side rings.

Author Contributions: All authors (M.S. and I.M.) contributed to the conceptualization, methodology and writing of the manuscript. All authors have read and agreed to the published version of the manuscript.

Data Availability Statement: Xyz or wfn files are available on request from the corresponding author.

Conflicts of Interest: The authors declare no conflict of interest. The funders had no role in the design of the study; in the collection, analyses, or interpretation of data; in the writing of the manuscript, or in the decision to publish the results.

Sample Availability: Samples of the molecular geometry are available from the authors.

References

1. Szymańska, M.; Majerz, I. Geometry and electron density of phenothazines. *J. Mol. Struct.* **2020**, *1200*, 127095. [CrossRef]
2. Prisinzano, T.E. Medicinal Chemistry: A Molecular and Biochemical Approach. *J. Med. Chem.* **2006**, *49*, 3428. [CrossRef]
3. Post, M.L.; Kennard, O.; Horn, A.S. The tricyclic antidepressants: Imipramine hydrochloride. The crystal and molecular structure of 5-(3-dimethylaminopropyl)-10,1l-dihydro-5*H*-dibenz[b,f]azepine hydrochloride. *Acta Cryst. Sect. B Struct. Sci.* **1975**, *31*, 1008–1013. [CrossRef]
4. Kaur, N.; Fang, Y.-C.; Lee, H.-Y.; Singh, A.; Nepali, K.; Lin, M.-H.; Yeh, T.-K.; Lai, M.-J.; Chan, L.; Tu, Y.-K.; et al. Protective effects of 10,11-dihydro-5*H*-dibenzo[b,f]azepine hydroxamates on vascular cognitive impairment. *Eur. J. Med. Chem.* **2020**, *187*, 111915. [CrossRef]
5. Vaghi, L.; Gaudino, E.; Cravotto, G.; Palmisano, G.; Penoni, A. A Structurally Diverse Heterocyclic Library by Decoration of Oxcarbazepine Scaffold. *Molecules* **2013**, *181*, 13705–13722. [CrossRef] [PubMed]
6. Kubota, K.; Kurebayashi, H.; Miyachi, H.; Tobe, M.; Onishi, M.; Isobe, Y. Synthesis and structure–activity relationship of tricyclic carboxylic acids as novel anti-histamines. *Bioorg. Med. Chem.* **2011**, *19*, 3005–3021. [CrossRef]
7. Walden, J.; Grunze, H.; Bingmann, D.; Liu, Z.; Düsing, R. Calcium antagonistic effects of carbamazepine as a mechanism of action in neuropsychiatric disorders: Studies in calcium dependent model epilepsies. *Eur. Neuropsychopharmacol.* **1992**, *2*, 455–462. [CrossRef]
8. Okada, M.; Hirano, T.; Mizuno, K.; Kawata, Y.; Wada, K.; Murakami, T.; Tasaki, H.; Kaneko, S. Effects of carbamazepine on hippocampal serotonergic system. *Epilepsy Res.* **1998**, *31*, 187–198. [CrossRef]
9. Blom, S. Trigeminal neuralgia: Its treatment with a new anticonvulsant drug (G-32883). *Lancet* **1962**, *279*, 839–840. [CrossRef]
10. Pierre, T.; Maron, M.; Rascle, C.; Cottencin, O.; Vaiva, G.; Goudemand, M. Carbamazepine in the treatment of neuroleptic malignant syndrome. *Biol. Psychiatry* **1998**, *43*, 303–305. [CrossRef]
11. Adam, R.W.; Al-Labban, H.M.Y.; Aljanaby, A.A.J.; Abbas, N.A. Synthesis, Characterization and Antibacterial Activity of Some New of Novel 1,2,3-Triazole-Chalcone Derivatives from N-Acetyl-5*H*-Dibenzo [b,f] Azepine-5-Carboxamide. *Nano Biomed. Eng.* **2019**, *11*, 99–110. [CrossRef]
12. Kumar, H.V.; Gnanendra, C.R.; Naik, N.; Gowda, C.D. In Vitro Antioxidant Activity of Dibenz[b,f]azepine and its Analogues. *E-J. Chem.* **2008**, *5*, 1123–1132. [CrossRef]
13. Kumar, H.V.; Ambati, R.R.; Sadineni, V.; Naik, N. Evaluation of In Vitro Antioxidant Activity of 5*H*-dibenz[b,f]azepine and Its Analogues. *J. Phys. Sci.* **2010**, *21*, 79–92.
14. Perri, R.D.; Maill, F.; Bramanti, P. The effects of amineptine on the mood and nocturnal sleep of depressed patients. *Prog. Neuropsychopharmacol. Biol. Psychiatry* **1987**, *11*, 65–70. [CrossRef]
15. Platzek, J. & Snatzke, G. Synthesis of potically active 10,11-dihydro-5*H*dibenzo[a,d]cycloheptenes. *Tetrahedron* **1987**, *43*, 4947–4968. [CrossRef]
16. Ting, P.C.; Lee, J.F.; Solomon, D.M.; Smith, S.R.; Terminelli, C.A.; Jakway, J.P.; Zambas, D.N.; Lee, J.F.; Solomon, D.M.; Smith, S.R.; et al. Synthesis of dibenzo[a,d]cycloheptanes as cytokine biosynthesis inhibitors. *Bioorg. Med. Chem. Lett.* **1995**, *5*, 2749–2754. [CrossRef]

17. Căproiu, M.T.; Dumitrascu, F.; Shova, S.; Chirită, I.C.; Missir, A.V.; Cioroianu, D.-M. Synthesis of new 10,11-dihydrodibenzo[a,d] cycloheptene S-thiocarbamate derivatives via a benzylic Newman–Kwart rearrangement. *Tetrahedron Lett.* **2014**, *55*, 4011–4013. [CrossRef]

18. Villani, F.J.; Daniels, P.J.; Ellis, C.A.; Mann, T.A.; Wang, K.-C.; Wefer, E.A. Derivatives of 10,11-dihydro-5*H*-dibenzo(a,d)cycloheptene and related compounds. 6. Aminoalkyl derivatives of the aza isosteres. *J. Med. Chem.* **1972**, *15*, 750–754. [CrossRef]

19. Socea, L.I.; Barbuceanu, S.F.; Iscrulescu, L.; Socea, B.; Hrubaru, M.; Pahontu, E.M.; Diaconu, C.C.; Bratu, O.G.; Olaru, O.T. New N-acylhydrazones with Potential Cytotoxic Activity. *Rev. Chim.* **2018**, *69*, 3341–3344. [CrossRef]

20. Socea, L.I.; Visan, D.C.; Barbuceanu, S.F.; Apostol, T.V.; Bratu, O.G.; Socea, B. The Antioxidant Activity of Some Acylhydrazones with Dibenzo[a,d][7]annulene Moiety. *Rev. Chim.* **2018**, *69*, 795–797. [CrossRef]

21. Socea, L.-I.; Saramef, G.; Mihalcea, F.; Apostol, T.V.; Andreescu, C.; Draghici, C.; Socea, B. New 1,2,4-triazoles and 1,3,4-oxadiazoles Derivatives with a 5*H*-dibenzo[a,d] [7] Annulene Moieties with Potential Antimicrobial Activity. *Rev. Chim.* **2014**, *65*, 156–159.

22. Kopanski, C.; Turck, M.; Schultz, J. Effects of long-term treatment of rats with antidepressants on adrenergic-receptor sensitivity in cerebral cortex: Structure activity study. *Neurochem. Int.* **1983**, *5*, 649–659. [CrossRef]

23. van Rossum, J.M. The Relation Between Chemical Structure and Biological Activity. *J. Pharm. Pharmacol.* **1963**, *15*, 285–316. [CrossRef] [PubMed]

24. Allen, F.H. The Cambridge Structural Database: A Quarter of a Million Crystal Structures and Rising. *Acta Cryst. Sect. B Struct. Sci.* **2002**, *58*, 380–388. [CrossRef]

25. Frisch, M.J.; Trucks, G.W.; Schlegel, H.B.; Scuseria, G.E.; Robb, M.A.; Cheeseman, J.R.; Scalmani, G.; Barone, V.; Mennucci, B.; Petersson, G.A.; et al. *Gaussian Inc 16*; Revision, A.03; Gaussian, Inc.: Wallingford, CT, USA, 2016.

26. Becke, A.D. Density-Functional Thermochemistry. III. The Role of Exact Exchange. *J. Chem. Phys.* **1993**, *98*, 5648–5652. [CrossRef]

27. Lee, C.; Yang, W.; Parr, R.G. Development of the Colle-Salvetti correlation-energy formula into a functional of the electron density. *Phys. Rev. B* **1988**, *15*, 785–789. [CrossRef]

28. Grimme, S.; Antony, J.; Ehrlich, S.; Krieg, H. A Consistent and Accurate Ab Initio Parametrization of Density Functional Dispersion Correction (DFT-D) for the 94 Elements H-Pu. *J. Chem. Phys.* **2010**, *132*, 154104. [CrossRef]

29. Boudhar, K.; Debieche, M.; Serhane, A.; Zeghdaoui, A. Crystal structure, Raman spectroscopy study and quantum chemical DFT calculations of N-phenyl-3-para nitro phenyl isoxazolidine-5-carbonitrile. *J. Mol. Struct.* **2021**, *1246*, 1–9. [CrossRef]

30. Abkari, A.; Chaabane, I.; Guidara, K. DFT (B3LYP/LanL2DZ and B3LYP/6311G+(d,p)) comparative vibrational spectroscopic analysis of organic–inorganic compound bis(4-acetylanilinium) tetrachlorocuprate(II). *Phys. E Low-Dimens. Syst. Nanostructures* **2016**, *81*, 136–144. [CrossRef]

31. Herges, R.; Geuenich, D. Delocalization of Electrons in Molecules. *J. Phys. Chem. A* **2001**, *105*, 3214–3220. [CrossRef]

32. Te Velde, G.; Bickelhaupt, F.M.; Baerends, E.J.; Fonseca Guerra, C.; van Gisbergen, S.J.A.; Snijders, J.G.; Ziegler, T.J. Chemistry with ADF. *Comput. Chem.* **2001**, *22*, 931–967. [CrossRef]

33. Fonseca Guerra, C.; Snijders, J.G.; teVelde, G.; Baerends, E.J. Towards an order-N DFT method. *Theor. Chem. Acc.* **1998**, *99*, 391–403. [CrossRef]

34. *ADF2019.302, SCM, Theoretical Chemistry*; Vrije Universiteit: Amsterdam, The Netherlands.

35. Raczyńska, E.D.; Hallman, M.; Kolczyńska, K.; Stępniewski, T.M. On the Harmonic Oscillator Model of Electron Delocalization (HOMED) Index and its Application to Heteroatomic π-Electron Systems. *Symmetry* **2010**, *2*, 1485–1509. [CrossRef]

36. Raczyńska, E.D.; Kosińska, W.; Ośmiałowski, B.; Gawinecki, R. Tautomeric Equilibria in Relation to Pi-Electron Delocalization. *Chem. Rev.* **2005**, *105*, 3561–3612. [CrossRef] [PubMed]

37. Reboul, J.P.; Cristau, B.; Soyfer, J.C.; Astier, J.P. 5*H*-Dibenz[b,f]azépinecarboxamide-5 (Carbamazépine). *Acta Crystallogr. Sect. B* **1981**, *37*, 1844–1848. [CrossRef]

38. Lisgarten, J.N.; Palmer, R.A.; Saldanha, J.W. Crystal and molecular structure of 5-carbamyl-5*H*-dibenzo[b,f] azepine. *J. Crystallogr. Spectrosc. Res.* **1989**, *19*, 641–649. [CrossRef]

39. Lowes, M.M.J.; Caira, M.R.; Lötter, A.P.; Van Der Watt, J.G. Physicochemical Properties and X-ray Structural Studies of the Trigonal Polymorph of Carbamazepine. *J. Pharm. Sci.* **1987**, *76*, 744–752. [CrossRef]

40. Himes, V.L.; Mighell, A.D.; De Camp, W.H. Structure of carbamazepine: 5*H*-dibenz[*b,f*]azepine-5-carboxamide. *Acta Crystallogr. Sect.* **1981**, *37*, 2242–2245. [CrossRef]

41. Grzesiak, A.L.; Lang, M.; Kim, K.; Matzger, A.J. Comparison of the Four Anhydrous Polymorphs of Carbamazepine and the Crystal Structure of Form I. *J. Pharm. Sci.* **2003**, *92*, 2260–2271. [CrossRef]

42. Lang, M.; Kampf, J.W.; Matzger, A.J. Form IV of Carbamazepine. *J. Pharm. Sci.* **2002**, *91*, 1186–1190. [CrossRef]

43. Fernandes, P.; Shankland, K.; Florence, A.J.; Shankland, N.; Johnston, A. Solving Molecular Crystal Structures from X-ray Powder Diffraction Data: The Challenges Posed by γ-Carbamazepine and Chlorothiazide N,N,-Dimethylformamide (1/2) Solvate. *J. Pharm. Sci.* **2007**, *96*, 1192–1202. [CrossRef] [PubMed]

44. Eccles, K.S.; Stokes, S.P.; Daly, C.A.; Barry, N.M.; McSweeney, S.P.; O'Neill, D.J.; Kelly, D.M.; Jennings, W.B.; Ní Dhubhghaill, O.M.; Moynihan, H.A.; et al. Evaluation of the Bruker SMART X2S: Crystallography for the nonspecialist? *J. Appl. Crystallogr.* **2011**, *44*, 213–215. [CrossRef] [PubMed]

45. Arlin, J.-B.; Price, L.S.; Price, S.L.; Florence, A.J. A strategy for producing predicted polymorphs: Catemeric carbamazepine form V. *Chem. Commun.* **2011**, *47*, 7074. [CrossRef]

46. El Hassan, N.; Ikni, A.; Gillet, J.-M.; Spasojevic-de Biré, A.; Ghermani, N.E. Electron Properties of Carbamazepine Drug in Form III. *Cryst. Growth Des.* **2013**, *13*, 2887–2896. [CrossRef]

47. Horstman, E.M.; Goyal, S.; Pawate, A.; Lee, G.; Zhang, G.G.Z.; Gong, Y.; Kenis, P.J.A. Crystallization Optimization of Pharmaceutical Solid Forms with X-ray Compatible Microfluidic Platforms. *Cryst. Growth Des.* **2015**, *15*, 1201–1209. [CrossRef]

48. Sovago, I.; Gutmann, M.J.; Senn, H.M.; Thomas, L.H.; Wilson, C.C.; Farrugia, L.J. Electron density, disorder and polymorphism: High-resolution diffraction studies of the highly polymorphic neuralgic drug carbamazepine. *Acta Crystallogr. Sect. B* **2016**, *72*, 39–50. [CrossRef] [PubMed]

49. Nievergelt, P.P.; Spingler, B. Growing single crystals of small molecules by thermal recrystallization, a viable option even for minute amounts of material? *CrystEngComm* **2017**, *19*, 142–147. [CrossRef]

50. Van Genderen, E.; Clabbers, M.T.B.; Das, P.P.; Stewart, A.; Nederlof, I.; Barentsen, K.C.; Portillo, Q.; Pannu, N.S.; Nicolopoulos, S.; Gruene, T.; et al. Ab initio structure determination of nanocrystals of organic pharmaceutical compounds by electron diffraction at room temperature using a Timepix quantum area direct electron detector. *Acta Crystallogr. Sect. A* **2016**, *72*, 236–242. [CrossRef] [PubMed]

51. Jones, C.G.; Martynowycz, M.W.; Hattne, J.; Tyler, J.; Fulton, T.J.; Stoltz, B.M.; Rodriguez, J.A.; Nelson, H.M.; Gonen, T. The CryoEM Method MicroED as a Powerful Tool for Small Molecule Structure Determination. *ACS Cent. Sci.* **2018**, *4*, 1587–1592. [CrossRef]

52. Kolb, U.; Krysiak, Y.; Plana-Ruiz, S. Automated electron diffraction tomography—Development and applications. *Acta Crystallogr. Sect. B* **2019**, *75*, 463–474. [CrossRef] [PubMed]

53. Anthony, J.E. Functionalized Acenes and Heteroacenes for Organic Electronics. *Chem. Rev.* **2006**, *106*, 5028–5048. [CrossRef] [PubMed]

54. Müller, M.; Ahrens, L.; Brosius, V.; Freudenberg, J.; Bunz, U.H.F. Unusual Stabilization of Larger Acenes and Heteroacenes. *J. Mater. Chem.* **2019**, *7*, 14011–14034. [CrossRef]

55. Schleyer, P.; von Rague Schleyer, P.; Maerker, C.; Dransfeld, A.; Jiao, H.; van Eikema Hommes, N.J.R. Nucleus-Independent Chemical Shifts: A Simple and Efficient Aromaticity Probe. *J. Am. Chem. Soc.* **1996**, *118*, 6317–6318. [CrossRef] [PubMed]

56. Schleyer, P.; von Rague Schleyer, P.; Manoharan, M.; Wang, Z.-X.; Kiran, B.; Jiao, H.; Puchta, R.; van Eikema Hommes, N.J.R. Dissected Nucleus-Independent Chemical Shift Analysis of π-Aromaticity and Antiaromaticity. *Org. Lett.* **2001**, *3*, 2465–2468. [CrossRef] [PubMed]

57. Cyrański, M.K. Energetic Aspects of Cyclic Pi-Electron Delocalization: Evaluation of the Methods of Estimating Aromatic Stabilization Energies. *Chem. Rev.* **2005**, *105*, 3773–3811. [CrossRef]

58. Matito, E.; Duran, M.; Solà, M. The aromatic fluctuation index (FLU): A new aromaticity index based on electron delocalization. *J. Chem. Phys.* **2005**, *122*, 14109. [CrossRef] [PubMed]

59. Poater, J.; Fradera, X.; Duran, M.; Solà, M. The Delocalization Index as an Electronic Aromaticity Criterion: Application to a Series of Planar Polycyclic Aromatic Hydrocarbons. *Chem. –A Eur. J.* **2003**, *9*, 400–406. [CrossRef] [PubMed]

60. Dominikowska, J.; Palusiak, M. EL: The new aromaticity measure based on one-electron density function. *Struct. Chem.* **2012**, *23*, 1173–1183. [CrossRef]

61. Krygowski, T.M. Crystallographic Studies of Inter- and Intramolecular Interactions Reflected in Aromatic Character of π-Electron Systems. *J. Chem. Inf. Comput. Sci.* **1993**, *24*. [CrossRef]

62. Reetz, M.T.; Hütte, S.; Goddard, R.; Minet, U. Tetrabutylammonium salts of carbazole and dibenzoazepine: Synthesis, crystal structures and use in anionic polymerization. *J. Chem. Soc. Chem. Commun.* **1995**, *2*, 275–277. [CrossRef]

63. Florence, A.J.; Leech, C.K.; Shankland, N.; Shankland, K.; Johnston, A. Control and prediction of packing motifs: A rare occurrence of carbamazepine in a catemeric configuration. *CrystEngComm* **2006**, *8*, 746–747. [CrossRef]

64. Aljohani, M.; Pallipurath, A.R.; McArdle, P.; Erxleben, A. A Comprehensive Cocrystal Screening Study of Chlorothiazide. *Cryst. Growth Des.* **2017**, *17*, 5223–5232. [CrossRef]

65. Briceño, A.; Dorta, R. cis-Dichloridobis{[(S)-N-(3,5-dioxa-4-phosphacyclohepta [2,1-a;3,4-a′]dinaphthalen-4-yl]dibenz[b,f]azepin-κP}palladium(II) deuterochloroform disolvate. *Acta Crystallogr. Sect. E* **2007**, *63*, m1718–m1719. [CrossRef]

66. Leitner, T.D.; Gmeinder, Y.; Röhricht, F.; Herges, R.; Mena-Osteritz, E.; Bäuerle, P. Twisted Thienylene–Phenylene Structures: Through-Space Orbital Coupling in Toroidal and Catenated Topologies. *Eur. J. Org. Chem.* **2020**, *3*, 285–294. [CrossRef]

67. Reck, G.; Thiel, W. Crystal structures of the adducts carbamazepine-ammonium chloride and carbamazepine-ammonium bromide and their transformation to carbamazepine dihydrate. *Pharmazie* **1991**, *46*, 509–512.

68. Nicolaï, B.; Fournier, B.; Dahaoui, S.; Gillet, J.-M.; Ghermani, N.-E. Crystal and Electron Properties of Carbamazepine-Aspirin Co-crystal. *Cryst. Growth Des.* **2019**, *19*, 1308–1321. [CrossRef]

69. Faudone, S.N.; Paschoal, A.R.; Carvalho, P.S.; Ellena, J.; Martins, F.T.; Cuffini, S.L.; Ayala, A.P.; Sperandeo, N.R. X-ray diffraction, vibrational and thermal study of dibenzazepinodione, a pharmacopeial impurity of oxcarbazepine. *J. Mol. Struct.* **2019**, *1182*, 204–212. [CrossRef]

70. Wang, W.; Yang, M.; Han, D.; He, Q.; Fan, R. Tandem Palladium Catalysis for Rapid Construction of 3,4-Fused Tricyclic Indoles. *Adv. Synth. Catal.* **2020**, *362*, 1281–1285. [CrossRef]

71. Loya, J.D.; Li, S.J.; Unruh, D.K.; Hutchins, K.M. Mechanochemistry as a Tool for Crystallizing Inaccessible Solids from Viscous Liquid Components. *Cryst. Growth Des.* **2022**, *22*, 285–292. [CrossRef]

72. Zhang, L.; Li, Z.; Fan, R. 1,2- and 1,4-Additions of 2-Alkynylcyclohexadienimines with Aromatic Amines To Access 4-Amino-N-arylindoles and -azepinoindoles. *Org. Lett.* **2012**, *14*, 6076–6079. [CrossRef] [PubMed]

73. Cordoneanu, A.; Drewitt, M.J.; Bavarian, N.; Baird, M.C. Synthesis and characterization of weakly coordinating anion salts of a new, stable carbocationic reagent, the dibenzosuberenyl (dibenzotropylium) ion. *New J. Chem* **2008**, *32*, 1890–1898. [CrossRef]

74. Fu, X.; Han, H.; Zhang, D.; Yu, H.; He, Q.; Zhao, D. Polycyclic aromatic hydrocarbon diradical with pH-responsive magnetic properties. *Chem. Sci.* **2020**, *11*, 5565–5571. [CrossRef]

75. Reed, A.E.; Weinhold, F. Natural localized molecular orbitals. *J. Chem. Phys.* **1985**, *83*, 1736–1740. [CrossRef]

76. Weinhold, F.; Landis, C.R. Natural bond orbitals and extensions of localized bonding concepts. *Chem. Educ. Res. Pract.* **2001**, *2*, 91–104. [CrossRef]

77. Löwdin, P.-O. Quantum Theory of Many-Particle Systems. I. Physical Interpretations by Means of Density Matrices, Natural Spin-Orbitals, and Convergence Problems in the Method of Configurational Interaction. *Phys. Rev.* **1955**, *97*, 1474–1489. [CrossRef]

Article

Prototropy, Intramolecular Interactions, Electron Delocalization, and Physicochemical Properties of 1,8-dihydroxy-9-anthrone—DFT-D3 Study of Substituent Effects

Małgorzata Szymańska * and Irena Majerz *

Faculty of Pharmacy, Wroclaw Medical University, Borowska 211a, 50-556 Wroclaw, Poland
* Correspondence: m.szymanska@umw.edu.pl (M.S.); irena.majerz@umw.edu.pl (I.M.)

Abstract: 1,8-dihydroxy-9-anthrone are tricyclic compounds with a ketone group in the middle ring and two hydroxyl groups substituted in the side-aromatic rings what results in formation of two intramolecular hydrogen bonds in which the oxygen atom from the ketone group is the proton acceptor. 1,8-dihydroxy-9-anthrones in which intramolecular proton transfer between C10 and CO in the middle ring occurs, can exist in a tautomeric keto-enol equilibrium. For anthralin, the most important representative of this group, this equilibrium has been studied previously, but it has not been studied for its derivatives. Substituents in the middle ring change the geometry of 1,8-dihydroxy-9-anthrones so they are also expected to affect the keto-enol equilibrium. It is also important to study the effect of intramolecular hydrogen bonds on the structure of both tautomeric forms. It was found that the nature of the substituent in the middle ring could affect the antioxidant properties of the investigated compound.

Keywords: 1,8-dihydroxy-9-anthrones; keto-enol equilibrium; QTAIM; aromaticity

1. Introduction

In the previous work [1], we studied the influence of substituent on the structure of anthrones and anthraquinones-tricyclic compounds with a wide importance in biological processes. The change of the angle between the anthrone aromatic rings is associated with the change in electron density at the ring critical point of the central ring.

An important group of anthrone derivatives are 1,8-dihydroxy-9-anthrones with substituents in the 1 and 8 position (Scheme 1). Anthralin, the popular drug from the 1,8-dihydroxy-9-anthrones group, has two hydroxyl groups at position 1 and 8 on either side of the ketone group located at position 9 (Scheme 1) and is used primarily in the treatment of psoriasis [2]. In the ketone form, it is stabilized by hydrogen bonds which are formed between the OH groups and the ketone oxygen [3]. For this reason, according to Hellier et al. [4], anthraline exists in its entirety in the ketone form [4]. The release of the hydrogen atom from the C10 position initiates the formation of free radicals, and although it may have an effect on skin irritation, it can be important in the mechanism of action of the drug [3,5]. Anthralin reduction power can be directly modified by changes in the structure [6]. For this reason, scientists are looking for new analogues substituted at the C10 position, which will prove to be more effective and, additionally, will not have side effects [5,7].

Intramolecular interactions of polycyclic compounds affect their structure [8–10]. The structure of a compound is related to the pharmacological activity; therefore, it is important to understand the effects of substituents, intramolecular hydrogen bonds, and keto-enol equilibrium on the structures of 1,8-dihydroxy-9-anthrone derivatives.

Two side rings of the 1,8-dihydroxy-9-anthrones derivatives are aromatic. The central ring in the lowest-energy ketone structure contains one CH_2 group, which influences the aliphatic character of the ring. However, the remaining fragment of the central ring further

delocalized as a result of π-π cross conjugation [11] and affects the cross delocalization of the other rings. The sensitivity of the middle ring to substitution can shift the character of the middle ring toward aromaticity, which can be affected by its non-planarity [1]. The presence of a ketone group in the middle ring and two adjacent OH groups in the side aromatic rings at the 1 and 8 positions causes the hydrogen atoms to form intramolecular hydrogen bonds. Migration of the proton between these ketone and hydroxyl group results in formation of tautomers [12–15]. Compounds, in which the intramolecular proton transfer takes place, are important in medicine and pharmacy and designing new drugs [16–19].
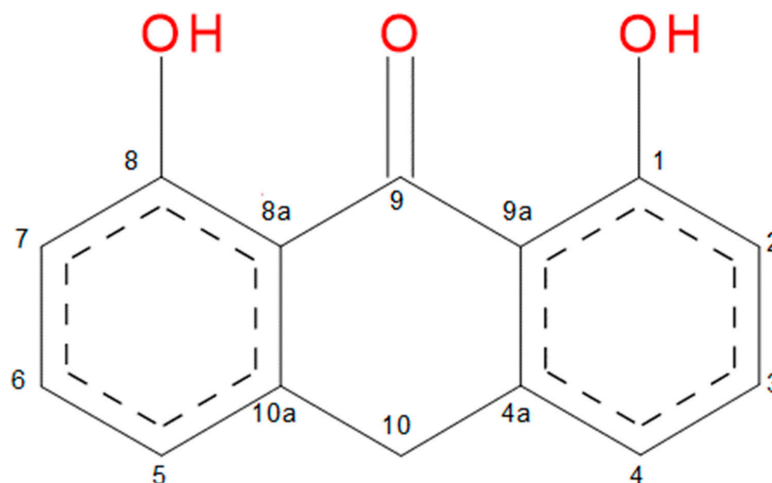
Scheme 1. Molecular structure and atom numbering of 1,8-dihydroxy-9-anthrones.

Keto-enol equilibrium can exist in 1,8-dihydroxy-9-anthrones through to a single proton transfer from C10 to CO in the middle ring (Scheme 2). According to Marrero-Carballo et al. [15], for proton transfer to occur the central ring must be twisted into a boat-like conformation. This equilibrium is influenced by the solvents in which the substance is dissolved [13,20,21], the substituents [21–24], and the temperature [21]. Baba and Takemura [13] studied the keto-enol equilibrium between anthrone and anthranol-1 in isooctane using the spectrophotometric method. After dropping the anthrone in isooctane, no changes in the spectrum were observed even after two days. The reaction was much faster in the presence of a small amount of triethylamine, which is basic in nature [13]. Using computational methods, Marrero-Carballo et al. [15] compared the activation energy of intramolecular proton transfer in the chrysophanol molecule with the proton transfer to the pyridine molecule. They found that, in the case of intramolecular proton transfer in the anthrone molecule, the activation energy is much greater than in the case of proton transfer to the pyridine molecule. The higher activation energy is related to the deformation of the central ring in the anthrone molecule [15].
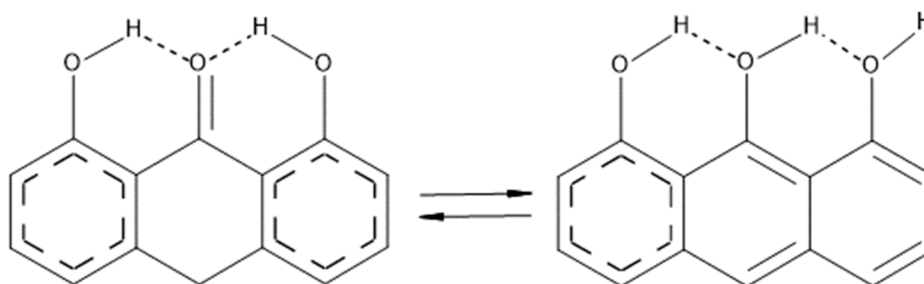
Scheme 2. The keto-enol equilibrium in 1,8-dihydroxy-9-anthrone.

Laurella et al. [21] studied the effects of substituents on the keto-enol balance of β-ketoamides. They found that electron-withdrawing properties of chlorine atom causes an equilibrium shift towards the enol form, while methoxy groups that donate the electrons

increases the content of the keto form. Additionally, they noticed that the equilibrium was also influenced by the position of the substituent, which is related to intramolecular hydrogen bonds in the molecule [21].

It is important to study the antioxidant properties of the analyzed compounds. Antioxidants have the ability to neutralize the harmful effects of free radicals. One of the methods of predicting the antioxidant properties is the determination of the enthalpy of the OH bond dissociation (BDE) and so the nature of the substituents in the ring affects the BDE value [25]. In the enol form, dissociation of the O-H bond at C9 is probable, which may have a positive effect on antioxidant properties. According to Lucarini et al. [26], electron-positive substituents decrease the BDE of O-H, while electron withdrawing substituents increase the BDE of O-H value relatively to unsubstituted phenol [26].

This work is a continuation of our previous [1] work in which we studied the influence of substituents on the structure of anthrones and anthraquinones and an analysis of 50 optimized compounds was performed. The substituents used in that work were differed in size, electron donating and electron accepting properties: NO_2, CHO, COOH, CH_3, CH_2CH_3, NH_2, OH, Cl, $C(CH_3)_3$. In this work, each structure with a specific substituent has been optimized in the ketone form and in the enol form and the energy difference between them has been calculated. The lowest energy has been obtained for the keto structure with two hydrogen bonds and has been used as the reference energy. The electron density of the middle ring is sensitive to substitution as mentioned in the previous work [1,27] so also in this work it is used as a measure of substituent influence and aromaticity of the central ring. The process of intramolecular proton transfer is responsible for acid-base regulation in the cell or for enzymatic reactions, so it is important to study the effect of substituents on this reaction [12,15]. Moreover, the intramolecular hydrogen bonds have an influence on the geometry investigated compounds. If the substituents and hydrogen bonds affect the structure, then it is important to study their effect on the keto-enol equilibrium, which is the aim of the research undertaken.

Computational Details

Optimization of the 1,8-dihydroxy-9-anthrone derivatives was performed with a Gaussian 16 package [28] at DFT-D3 B3LYP/6-311++G** level [29,30]. Grimme dispersion [31] was included to reproduce correctly the hydrogen bond in the investigated molecules. Vibrational frequencies were calculated to confirm that the optimized molecule reached the minimum of energy. QTAIM parameters were calculated with the AIMALL program [32] using the wave function for the optimized molecule.

2. Results

2.1. 1,8-Dihydroxy-9-anthrone Tautomers

To investigate the tautomeric preference, the Gibbs energy of different isomers in ketone form for four different substituents NH_2, NO_2, OH, and H has been compared (Table 1). There are six possible different tautomeric structures of the ketone form (Scheme 3). For NH_2, NO_2, H, and OH substituted structures, five isomers with different energies have been obtained. In all cases, the K3 isomer converges to the K6 isomer, which is confirmed by the C9-O (1.261 Å), C9-C9a (1.462 Å), 4a-9a (1.412 Å), and 8a-10a (1.412 Å) bond lengths equal and respectively identical as these bond length for the K6 tautomer. The lowest value of the Gibbs energy for the K6 isomer has been obtained. Isomers with relative Gibbs energies higher than 10 kcal/mol can be neglected in the isomeric mixture owing to their exceptionally low percentage contents (<5 ppm). The smallest differences in Gibbs energy of 10 kcal/mol is obtained between isomers of NH_2 and OH substituted structures. In all cases, the α angle is the greatest for the lowest energy structures. The HOMA values in the side rings of the preferred isomeric forms are always close to 1.

Table 1. G at 298 K, α and HOMA parameter for optimized isomers.

X	Isomer	ΔG [kcal/mol]	α	HOMA (A)	HOMA (B)	HOMA (C)
	E	13.8	0.23	0.6188	0.6666	0.5957
	K1	9.1	0.03	0.7927	0.6583	−0.7815
	K2	10.7	0.01	0.7769	0.7006	−0.8107
H	K3	0.0	6.73	0.9053	−0.7159	0.9053
	K4	12.4	0.01	0.8550	0.4044	−0.5983
	K5	10.2	0.01	0.8602	0.3176	−0.5043
	K6	0.0	6.72	0.9053	−0.7159	0.9053
	E	10.3	3.51	0.6190	0.6178	0.5807
	K1	4.9	3.04	0.7994	0.5773	−0.7667
	K2	5.6	2.79	0.7766	0.6521	−0.7804
NH$_2$	K3	0.0	12.01	0.9095	−0.9130	0.9098
	K4	7.3	3.04	0.8480	0.3583	−0.5692
	K5	6.1	4.29	0.8600	0.2443	−0.5002
	K6	0.0	12.02	0.9019	−1.0218	0.9019
	E	16.8	0.88	0.6223	0.6518	0.6053
	K1	13.0	0.73	0.7967	0.6358	−0.7255
	K2	12.9	2.53	0.7760	0.6861	−0.7420
NO$_2$	K3	0.0	14.93	0.9176	−0.6255	0.9176
	K4	14.0	3.21	0.8446	0.4079	−0.4888
	K5	13.8	0.80	0.8556	0.3158	−0.4320
	K6	0.0	14.97	0.9176	−0.6255	0.9176
	E	10.8	2.71	0.6159	0.6807	0.6067
	K1	6.4	1.95	0.8110	0.6111	−0.7856
	K2	7.6	0.89	0.7945	0.6725	−0.8222
OH	K3	0.0	13.81	0.9074	−0.9632	0.9074
	K4	9.3	0.81	0.8660	0.3664	−0.6312
	K5	7.5	1.53	0.8723	0.2799	−0.5133
	K6	0.0	13.83	0.9074	−0.9632	0.9074

2.2. Crystal Structures

It can be expected that the tautomerism of dihydroxyantrone will be reflected in the structures of compounds deposited in the CSD database [33]. Since the structure of the model compounds is known [34], the analysis of the bond lengths in the 1,8-dihydroxy-9-anthrone derivatives in the crystalline state should allow to indicate which tautomer is realized in the crystal of individual derivatives. Table S1 summarizes the C-C bond lengths for the 1,8-dihydroxy-9-anthrone derivatives present in the CSD database. The table also includes CO bond lengths, HOC angles, and torsion angles allowing for the indication of proton deviation from the plane defined by the system of intramolecular hydrogen bonds typical of 1,8-dihydroxy-9-anthrones. The geometrical parameters should indicate which tautomeric forms are realized in the crystalline state.
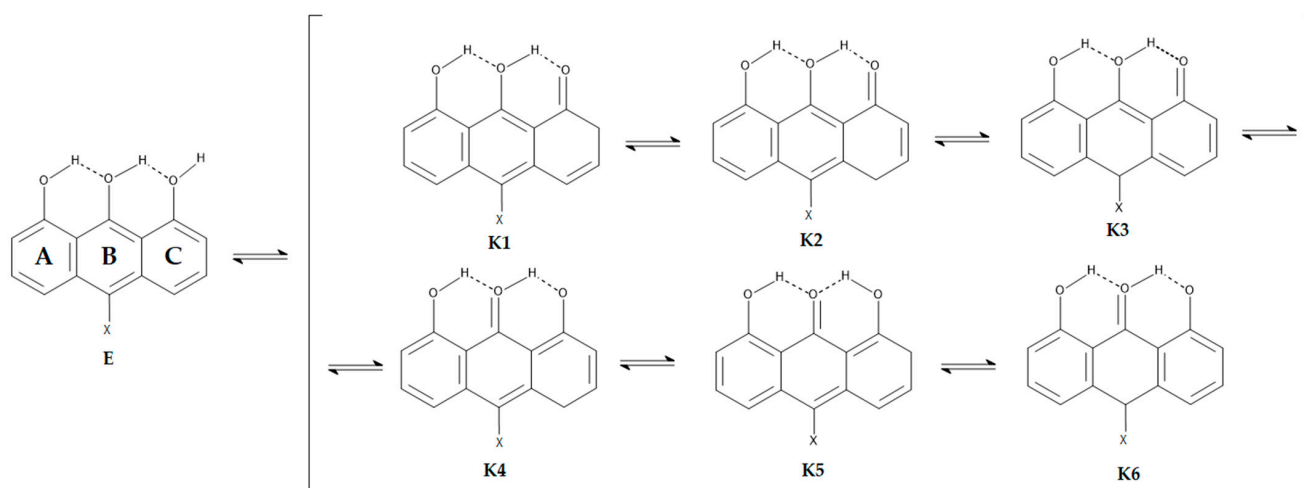
Scheme 3. Tautomeric equilibrium in 1,8-dihydroxy-9-anthrone.

　　　The analysis of the CO bond system allows for a preliminary indication of the tautomeric form present in the crystal structures. In the structures K1, K2, and K3, the double bond of CO occurs in the side ring. The comparison of CO bonds in Table S1 clearly shows that all solid state structures can be of the K4, K5, or K6 type, in which the CO double bond connects oxygen to the central ring. According to the model structures (Scheme 3), individual tautomeric forms should differ from each other in the arrangement of single and double bonds. The analysis of the CC bond lengths in the 1,8-dihydroxy-9-anthrone rings allows for the unequivocal elimination of the K5 tautomer, because all C3-C4 bonds are longer than those typical for benzene and are typical single bond. Since all the C2-C3 lengths in the analyzed compounds are shorter than the length typical for benzene (1.399) and the C1-C9a bond length is also shortened for a number of compounds, it can be considered that this structure is typical for solid-state 1,8-dihydroxy-9-anthrones. The analysis of C4a-C9a and C8a-C10a bond lengths indicates their shortening below the value typical for benzene in some dihydroxyantrone derivatives, which proves the possibility of the presence of the K6 tautomeric structure, characterized by the lowest energy. The linkage lengths of the dihydroxyanntron derivatives therefore indicate the possible presence of the K6 tautomer, with the K4 tautomer being more likely. However, the precision in determining the bond length should be taken into account. The comparison of the bond lengths in the central ring clearly shows that the K6 isomer dominates in the 1,8-dihydroxy-9-anthrone crystals. The shortest bonds, similar in length to benzene, are the bonds 4a-9a and 8a-10a.

　　　It is a noteworthy fact that, in some structures, the protons of the hydroxyl groups remain unconnected with the carbonyl oxygen of the middle ring (BOLPEX [35], CARMYC11 [36], DHANQU03 [37], DHANQU04 [37], DHANQU08 [37], JUKREM [38], PIRFIH [39], QEGXUV [40], VURHEV [41]), as confirmed by the values of the torsion angles in Table S1. The deviation of the proton from the plane convenient for the formation of intramolecular hydrogen bonds is due to the participation of the oxygen atoms in other interactions resulting from intermolecular interactions in the crystal.

2.3. Geometry of the Investigated Compounds

　　　The α angles and relative energies for the optimized structures with different substituents are collected in Table 2. The lowest energy structure in the ketone form has been obtained for the K6 tautomer and remaining discussions in the study apply only to it. The Ea structure represents the enol form with one hydrogen bond and Eb with two hydrogen bonds. The Ka structure represents ketone form without hydrogen bonds, Kb with one hydrogen bond, and Kc with two hydrogen bonds. As in the previous works [1,27], the angle between the planes of the two side aromatic rings has been used as a measure of the substituent influence on the geometry of the ring system (Scheme 4. Depending on the

character of the substituent and its size as well as the presence of hydrogen bonds, the α angle changes from 0 to 52°. The H···O distance in the hydrogen bonds is close to 1.7 Å. Molecules in the ketone form, without hydrogen bonds, are characterized by the highest α angle. The angle decreases with the increasing number of the hydrogen bonds in the molecule. Deviations for this rule were observed for the structures of 9K6c, 9K6b and 5K6b, 5K6a. This is due to the different orientation of the substituent in the molecule. The α angle in the enol form is smaller than in the ketone form. The substituent always causes an increase of the α angle in the keto and enol form relatively to the unsubstituted molecule. The highest values of the α angle in keto form has been obtained for structure 4K6a and in enol form for the structure 4Ea. Both structures have a tertbutyl substituent so the increase of the α angle is connected with steric interaction of a bulky substituent.

Table 2. ΔG at 298 K, α and HOMA parameter for optimized structures of enol and ketone forms. Angle defined according to Scheme 1. For each substituent, the lowest energy has been obtained for the structure in the keto form with two hydrogen bonds.

X	Isomer	ΔG [kcal/mol]	α	HOMA (A)	HOMO (B)	HOMA (C)
H	1Ea	21.8	0.45	0.6129	0.6307	0.6091
	1Eb	13.8	0.23	0.6188	0.6666	0.5957
	1K6a	24.6	28.08	0.9567	−1.3219	0.9567
	1K6b	12.1	13.70	0.9300	−0.9360	0.9181
	1K6c	0.0	6.72	0.9053	−0.7159	0.9053
NH$_2$	2Ea	18.8	3.74	0.6088	0.5888	0.5984
	2Eb	10.3	3.51	0.6190	0.6178	0.5807
	2K6a	27.2	40.59	0.9629	−1.6549	0.9629
	2K6b	16.2	31.66	0.9385	−1.2796	0.9229
	2K6c	0.0	12.02	0.9019	−1.0218	0.9019
OH	3Ea	19.7	4.28	0.6036	0.6265	0.6220
	3Eb	10.8	2.71	0.6159	0.6622	0.6252
	3K6a	23.6	28.70	0.9583	−1.5692	0.9583
	3K6b	11.5	17.62	0.9329	−1.2003	0.9196
	3K6c	0.0	13.83	0.9074	−0.9632	0.9074
$t-$Bu	4Ea	24.5	22.57	0.5724	0.5100	0.5744
	4Eb	17.2	21.17	0.5649	0.5301	0.5467
	4K6a	21.0	52.00	0.9593	−2.1410	0.9595
	4K6b	10.9	46.08	0.9314	−1.7695	0.9175
	4K6c	0.0	41.59	0.8914	−1.5024	0.8914
Et	5Ea	23.7	3.72	0.5849	0.5661	0.5549
	5Eb	15.4	3.38	0.5854	0.6003	0.5647
	5K6a	27.9	26.53	0.9549	−1.6922	0.9549
	5K6b	18.8	36.69	0.9332	−1.4496	0.9248
	5K6c	0.0	20.80	0.9083	−0.8027	0.9098

Table 2. *Cont.*

X	Isomer	ΔG [kcal/mol]	α	HOMA (A)	HOMO (B)	HOMA (C)
	6Ea	23.2	0.96	0.6067	0.5682	0.5523
	6Eb	15.1	0.51	0.6066	0.5918	0.5384
Me	6K6a	27.5	38.32	0.9599	−1.6960	0.9599
	6K6b	16.1	28.47	0.9305	−1.3403	0.9194
	6K6c	0.0	15.00	0.9097	−0.8068	0.9097
	7Ea	22.8	0.68	0.5990	0.5854	0.5947
	7Eb	14.9	0.43	0.6077	0.6258	0.5854
Cl	7K6a	27.0	30.39	0.9585	−1.5386	0.9585
	7K6b	11.3	20.47	0.9409	−0.7715	0.9275
	7K6c	0.0	17.12	0.9156	−0.5278	0.9156
	8Ea	21.9	6.80	0.6396	0.5081	0.6384
	8Eb	15.0	4.97	0.6224	0.5379	0.6198
CHO	8K6a	23.4	27.59	0.9567	−1.3638	0.9567
	8K6b	11.4	16.99	0.9324	−1.0007	0.9207
	8K6c	0.0	12.14	0.9088	−0.7817	0.9088
	9Ea	19.0	1.87	0.6211	0.6045	0.6146
	9Eb	11.8	1.45	0.6161	0.6361	0.6585
COOH	9K6a	25.8	30.29	0.9600	−1.6422	0.9621
	9K6b	7.9	15.43	0.9315	−1.0756	0.9169
	9K6c	0.0	17.85	0.9209	−0.8243	0.9209
	10Ea	23.8	0.74	0.6304	0.6163	0.6264
	10Eb	16.8	0.88	0.6223	0.6518	0.6053
NO$_2$	10K6a	23.3	26.59	0.9620	−1.2132	0.9699
	10K6b	11.3	18.68	0.9451	−0.8550	0.9309
	10K6c	0.0	14.97	0.9176	−0.6255	0.9176
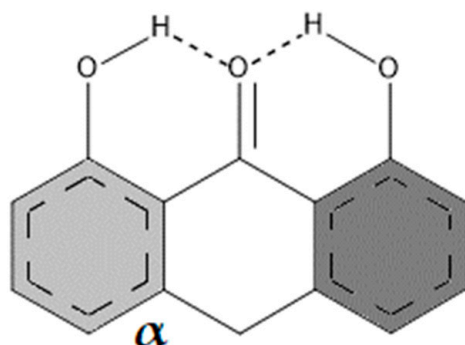
Scheme 4. Definition of the α angle for 1,8-dihydroxy-9-anthrones as the angle between the side rings planes.

Table 2 shows the energy differences between the keto and enol form. For each substituent, the lowest energy has been obtained for the structure in the keto form with two hydrogen bonds.

In order to better understand the influence of substituents and hydrogen bonds on the aromaticity of the ring, the HOMA index was determined [42]. For the benzene aromatic ring, the HOMA index is equal to 1; HOMA=0 for the hypothetical structure of 1,3,5-

cyclohexatriene with the reference C-C and C=C bonds of buta-1,3-diene [42]; and for the antiaromatic ring, it is negative.

$$HOMA = 1 - \frac{\alpha}{n} \sum (R_o - R_i)^2 \qquad (1)$$

R_o—the optimized CC bond length of a perfectly aromatic system equal to 1.388 Å.
R_i—determined bond length.
α—standardization constant of 257.7.
n—number of bonds.

The determined HOMA parameters for every ring of the investigated molecules are presented in Table 2. Additionally, as it was done in the previous work [1], to show the dependence of the particular geometry on the electron density, the value of the HOMA parameter of the middle ring has been correlated with the α angle. In the previous work [1], we determined the HOMA parameter for anthrones and anthraquinones with the same substituents in the middle ring. All compounds, irrespective of the nature of the substituent in the middle ring, which have OH groups in the side rings which do not form hydrogen bonds with the adjacent carbonyl group (enones), are characterized by the lowest value of the HOMA parameter for the middle ring. For the compounds investigated in this work the HOMA values for the middle ring are lower, if the OH groups in the aromatic side rings are not present. The presence of one or two hydrogen bonds in ketone form shifts the HOMA value of the middle ring towards higher aromaticity. The highest values of HOMA have been observed for all structures in the enol form with two hydrogen bonds. The electron density of the middle ring is related to the α angle and both parameters can be correlated (Figure 1). In Figure 1, the E and K6 structures have been used according to Scheme 3. As the HOMA shifts towards higher aromaticity, the α angle decreases and hence the molecule flattens out. Similar conclusions were obtained in the previous work [1]. The highest values of the alpha angle for the enol form were obtained for structures with a bulky tert-butyl substituent.
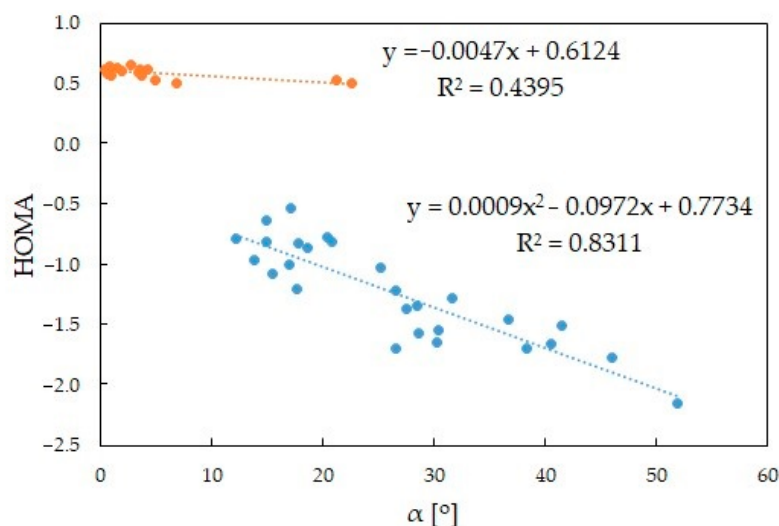
Figure 1. Correlations between the HOMA parameter for the central ring and α angle: yellow—enols, blue—ketones.

According to Ośmiałowski et al. [34], aromaticity and high π-electron delocalization in the whole system in the enol form plays an important role and determines the tautomeric preference of monohydroxyarenes. Nevertheless, high electron delocalization and stability in individual rings of the condensed systems also affect tautomeric equilibrium in the gas phase. The high HOMA in the side rings of the compounds affects the shift of the tautomeric equilibrium toward the ketone form.

2.4. Electron Density and Ellipticity at Bond Critical Point

The ellipticity of the electron density at the bond critical point (BCP) gives information about the nature of the C-C bond. A correlation between ellipticity and bond length for C8a-C9 and C9a-C9 has been found (Figure 2). The ellipticity and the length of the C-C bond in the middle ring is influenced by the form of the molecule is in and the number of the hydrogen bonds. No effect of the substituent on ellipticity and bond length has been noted. The highest ellipticity is observed for bonds in enol form. Suitable bond length of the C8a-C9 bond is in the range of 1.406–1.419 Å. The length of the C9a-C9 bond is in a slightly larger range of 1.405–1.424 Å. The smallest ellipticity and the highest C8a-C9 and C9a-C9 bond lengths are characteristic for the structures in the ketone form without intramolecular hydrogen bonds. The bond lengths of C8a-C9 and C9a-C9 have also been correlated with electron density at the BCP and the obtained correlation equations are: $y = -2.1207x + 2.0518$, $R^2 = 0.9986$; $y = -2.2251x + 2.0799$, $R^2 = 0.9971$.
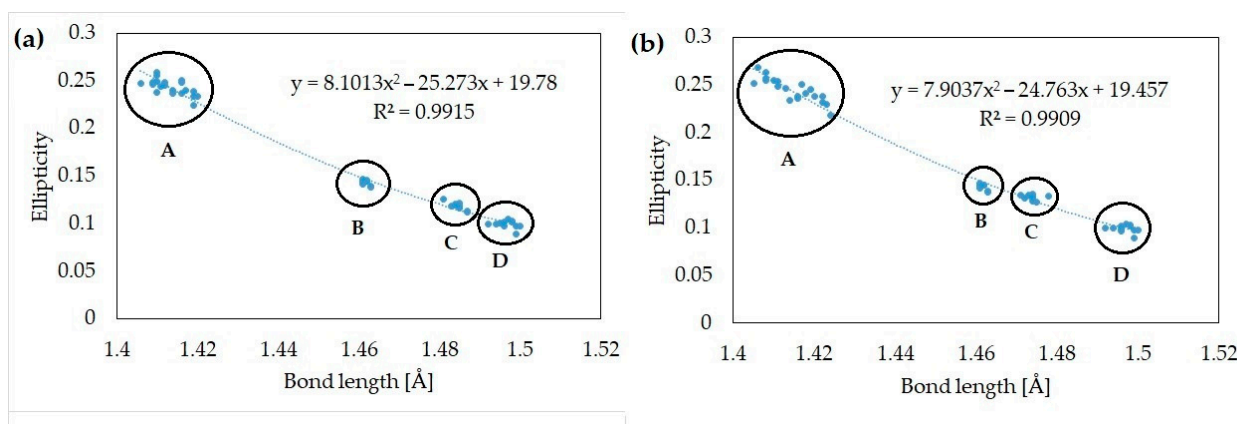
Figure 2. Correlations between ellipticity and bond length for (**a**)—C8a-C9 bond, (**b**)—C9a-C9 bond. Region A—enol, B—ketone form with two hydrogen bonds, C—ketone form with one hydrogen bond, D—ketone form without hydrogen bonds.

2.5. Selected Bands in the Theoretical IR Spectra of Dihydroanthrones

To study the effect of the substituent on the IR spectra, vibrational frequencies have been calculated for the favored structure in ketone form. In Table 3, the bands characteristic for C=O and OH groups are collected. For the NO_2 substituent, the strongest $\nu_{as}OH$ band is observed at 3399 cm^{-1}. This band repeats at a similar wavenumber for other substituents. Similar wavenumber repetition is observed for the vibration of νCO and δOH and the bands are located close to 1636 and 1670 cm^{-1}. For the structure with the NH_2 substituent, the vibration of νCO; δOH; δCH (C3, C4, C5, C6, C10) are observed at 1333 cm^{-1}, which is not observed for other substituents.

Table 3. Selected bands without a scaling factor for the optimized dihydroanthrones. Only the favored keto form (K6) with different substituents has been included.

Substituent	Wavenumber [cm^{-1}]	Int. [km/mol]	Description
NO_2	1381	109.2	νCO; δOH; δCH; νCN; νNO; νCC
	1399	189.7	νCO; δOH; δCH; νCN; νNO; νCC
	1519	230.8	νCO; δOH; δCH (side rings); νCC
	1636	144.5	νCO; δOH; δCH; νCC
	1670	261.2	νCO; δOH; δCH; νCC
	3399	520.1	$\nu_{as}OH$
	3427	50.2	$\nu_s OH$

Table 3. *Cont.*

Substituent	Wavenumber [cm^{-1}]	Int. [km/mol]	Description
t-Bu	1502	213.1	νCO; δOH; δCH; νCC (rings)
	1634	286.5	νCO; δOH; νCC (rings); δCH (rings)
	1662	193.3	νCO; δOH; νCC (rings); δCH (rings)
	3386	436.3	ν$_{as}$OH
	3415	67.5	ν$_s$OH
COOH	1394	144.3	νCO; δOH; δCH; νCC
	1518	213.9	νCO; δOH; δCH; νCC
	1635	186.8	νCO; δOH; δCH; νCC
	1669	236.9	νCO; δOH; δCH; νCC
	3389	561.5	ν$_{as}$OH
	3418	51.6	ν$_s$OH
CH$_3$	1389	96.2	νCO; δOH; δCH; νCC (rings)
	1515	236.5	νCO; δOH; δCH (rings); νCC (rings)
	1633	254.5	νCO; δOH; δCH (rings); νCC (rings)
	1668	192.3	νCO; δOH; δCH (rings); νCC (rings)
	3372	601.1	ν$_{as}$OH
	3403	45.1	ν$_s$OH
CHO	1514	209.6	νCO; δOH; δCH (side rings); νCC
	1629	279.4	νCO; δOH; δCH (side rings); νCC
	1667	224.9	νCO; δOH; δCH (side rings); νCC
	3381	574.2	ν$_{as}$OH
	3411	46.4	ν$_s$OH
Cl	1395	118.7	νCO; δOH; δCH (C2, C7); νCC
	1517	237.3	νCO; δOH; δCH (side rings); νCC
	1634	171.1	νCO; δOH; δCH (C3, C4, C5, C6); νCC
	1669	231.5	νCO; δOH; δCH (side rings); νCC
	3381	504.5	ν$_{as}$OH
	3417	49.1	ν$_s$OH
Et	1391	109.6	νCO; δOH; δCH (C2, C7); νCC (rings)
	1514	223.9	νCO; δOH; δCH; νCO; νCC (rings)
	1633	264.5	νCO; δOH; δCH (C3, C4, C5, C6); νCC (rings)
	1666	193.6	νCO; δOH; δCH (C2, C4, C5, C7); νCC (rings)
	3377	559.1	ν$_{as}$OH
	3407	51.4	ν$_s$OH
OH	1391	129.5	νCO; δOH; δCH (C2, C7, C10); νCC (rings)
	1511	269.6	νCO; δOH; δCH (rings); νCC
	1633	205.3	νCO; δOH (side rings); δCH (C3, C4, C5, C6); νCC
	1668	200.7	νCO; δOH (side rings); δCH (C2, C4, C5, C7); νCC
	3377	586.9	ν$_{as}$OH
	3407	45.7	ν$_s$OH

Table 3. *Cont.*

Substituent	Wavenumber [cm^{-1}]	Int. [km/mol]	Description
NH$_2$	1333	101.7	νCO; δOH; δCH (C3, C4, C5, C6, C10); δNH; νCC
	1510	244.9	νCO; δOH; δCH; δNH; νCC; νCN
	1635	252.2	νCO; δOH; δCH; δNH; νCC
	1666	207.2	νCO; δOH; δCH; δNH; νCC
	3372		ν_{as}OH
	3402		ν_{s}OH
H	1387	106.5	νCO; δOH; δCH (C2, C7, C10); νCC
	1518	244.9	νCO; δOH; δCH; νCC
	1633	242.2	νCO; δOH; δCH; νCC
	1668	188.4	νCO; δOH; δCH (C2, C4, C5, C7); νCC
	3690	657.3	ν_{as}OH
	3401	40.7	ν_{s}OH

2.6. Dipole Moment, Average Local Ionization Energy, and Electrostatic Potential

The dipole moment of the molecule provides important information about its structure. Table 4 shows the dipole moments of enol and ketone form with two hydrogen bonds. The dipole moments are in the range of 0.78–2.84 D. The highest value is obtained for the 9Eb structure. The COOH group significantly increases the polarity of the molecules. However, with the increase of the non-polar carbon chain, the polarity of the molecules decreases which can be observed in the structure with a tertbutyl substituted. Only in some cases (-Cl, CHO, NO$_2$ substituents), the effect of the form of the compound on the dipole moment is observed. For the compounds with other substituents the values of the dipole moment in keto and enol form are very similar.

Table 4. Dipol Moment, Average Local Ionization Energy, Electrostatic Potential of enol and ketone form with two hydrogen bonds.
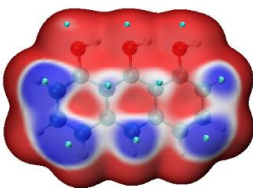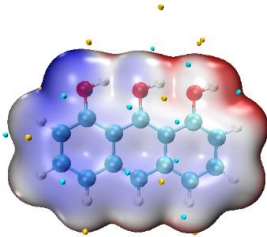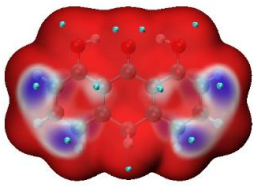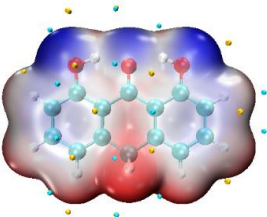
X	Isomer	Dipol Moment [D]	ALIE	ESP
H	1Eb	1.79		
	1K6c	1.76		

Table 4. *Cont.*
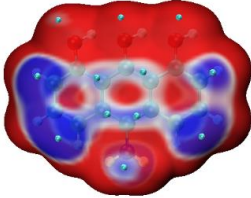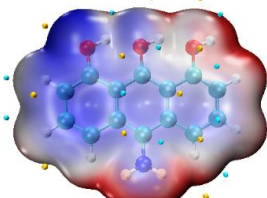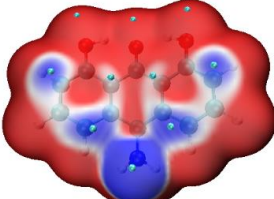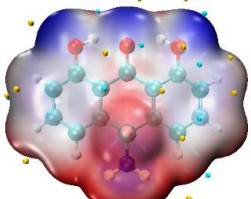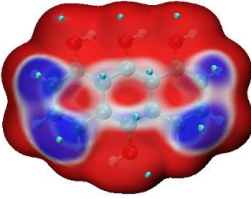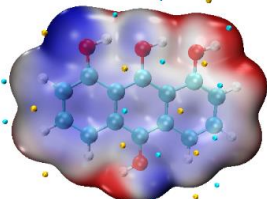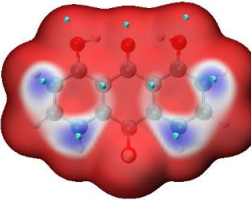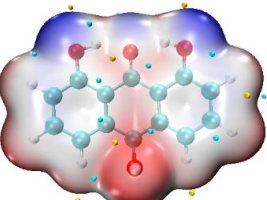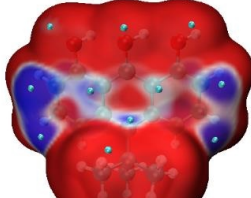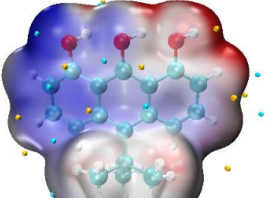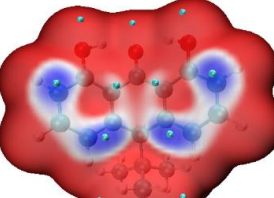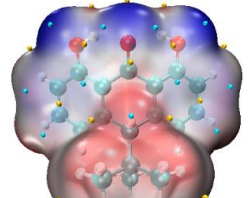
X	Isomer	Dipol Moment [D]	ALIE	ESP
NH$_2$	2Eb	1.80		
	2K6c	1.74		
OH	3Eb	1.33		
	3K6c	1.13		
t-Bu	3Eb	1.33		
	3K6c	1.13		

Table 4. *Cont.*
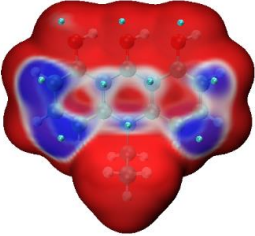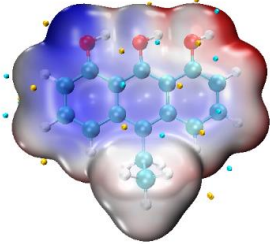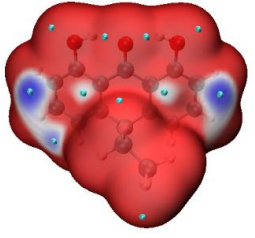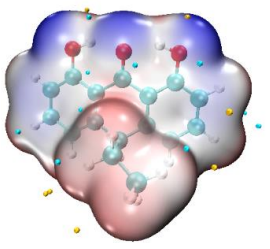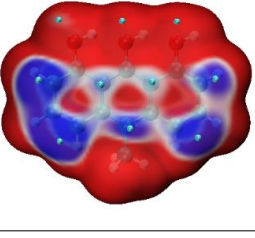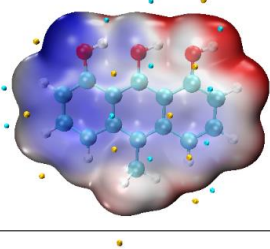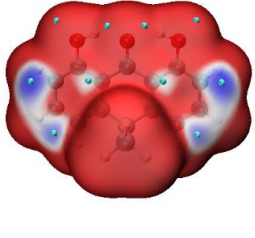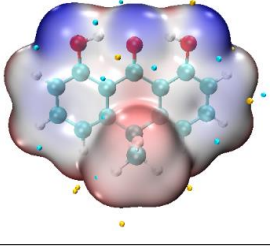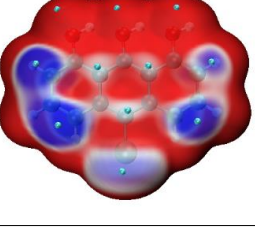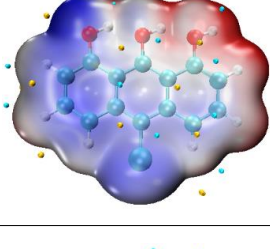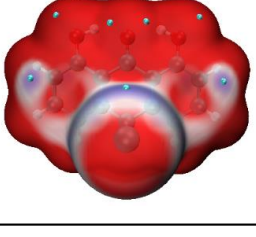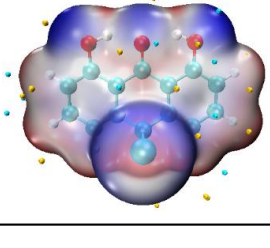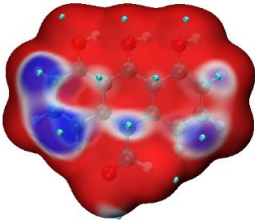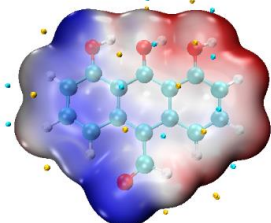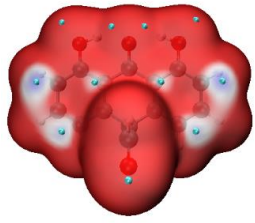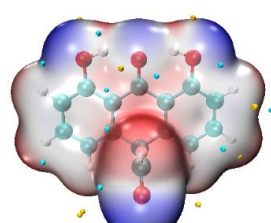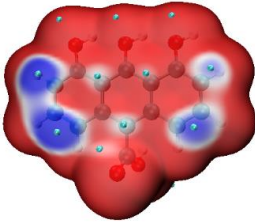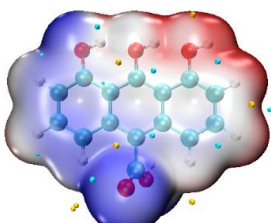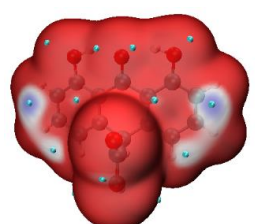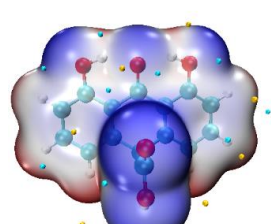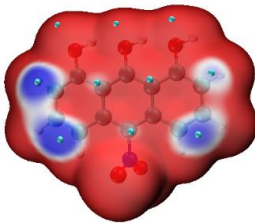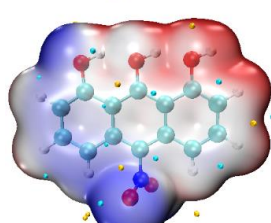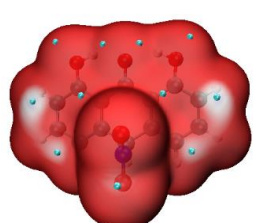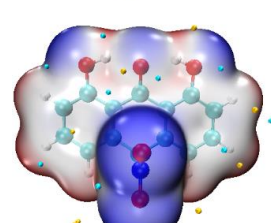
X	Isomer	Dipol Moment [D]	ALIE	ESP
Et	4Eb	1.73		
	4K6c	1.76		
Me	6Eb	1.76		
	6K6c	1.76		
Cl	7Eb	1.95		
	7K6c	1.41		

Table 4. *Cont.*

X	Isomer	Dipol Moment [D]	ALIE	ESP
CHO	8Eb	2.90		
	8K6c	0.78		
COOH	9Eb	2.84		
	9K6c	2.41		
NO$_2$	10Eb	2.66		
	10K6c	1.54		

Average local ionization energy (ALIE) is a function to reveal regions containing highly reactive electrons in chemical system. The surface used for presentation of the local ionization energy is plotted on $\rho = 0.0005$ a.u. isosurface. Light blue spheres correspond to ALIE minima on the isosurface, revealing favorable sites of electrophilic attack. Darker blue color reveals relatively low ALIE regions. In this region, the electrons have relatively high reactivity.

In the structure of the hydrogen-substituted enol form, electrophilic attack is possible on C10 and on carbon atoms in the side rings, which are not common with the middle ring. In the enol form, the C10 atom is not subject to electrophilic attack. The electron donor substituent in the 2Eb structure directs the electrophilic attack to the side ring atoms that are not in common with the middle ring. In the ketone form 2K6c, the electrophilic attack is directed at the NH_2 substituent. The OH substituent in the 3Eb structure revealed a favorable site of electrophilic attack on the carbon atoms of the side rings, which are not shared with the middle ring. In the enol structure, the site of electrophilic attack is the carbon atoms in the side rings that are not shared with the central ring. The site of electrophilic attack becomes less sensitive in the keto structure.

Electrostatic potential (ESP) is popular to visualize the electrostatic nature of molecules. It gives information about the chemical reactivity of a molecule indicating positively and negatively charged fragments of the molecule. For the structures in Table 4, the blue surface corresponds to minimal and red to maximal value of ESP.

For the enol form, the minimum of ESP is located at the oxygen atom not accepting the proton what is connected with the oxygen lone pairs. In the ketone forms, the minimum of ESP is distributed on the oxygen atoms in the side rings OH groups at the and at CO in the middle ring. In addition, the minimum of ESP is observed on COOH, NO_2, and Cl substituents and on the oxygen from CHO group. In the enol form, the maximum of ESP is accumulated on one of the hydrogen atoms in the OH group at the side ring.

2.7. Prototropy

Structures with OH and CHO substituents have labile protons, as they move around the molecule, can form a combination of different types of prototropic transformations [43]. Figure 3 shows all possible prototropic forms for OH-substituted 1,8-dihydroxy-9-anthrone. Five prototropic forms are obtained for the OH substituent and one for the CHO substituent (Figure 4). ΔE values, which are calculated relative to the isomer with the lowest energy, are placed under the structures. The highest energy for the OH substituent is obtained for the 3K5-C9a4aH structure, with a single bond between the C9a-C4a atoms. The most close in energy to the 3K6c structure is 3K6-C23H, which has a single bond between C2-C3 atoms. The only one prototropic transformation that has been obtained for the CHO substituent is very close energetically to the 8K6c structure (ΔE = 2.2 kcal/mol).

2.8. Antioxidant Activities

An important parameter for predicting antioxidant properties is the bond dissociation enthalpy (BDE) of the OH bond at C9 in enol form. The BDE of OH has been determined using the calculated total enthalpies (2). Additionally, BDE for C-H at C10 in keto form has been determined (3).

$$BDE(O - H) = H(enolO^{\cdot}) - H(H^{\cdot}) + H(enolOH) \qquad (2)$$

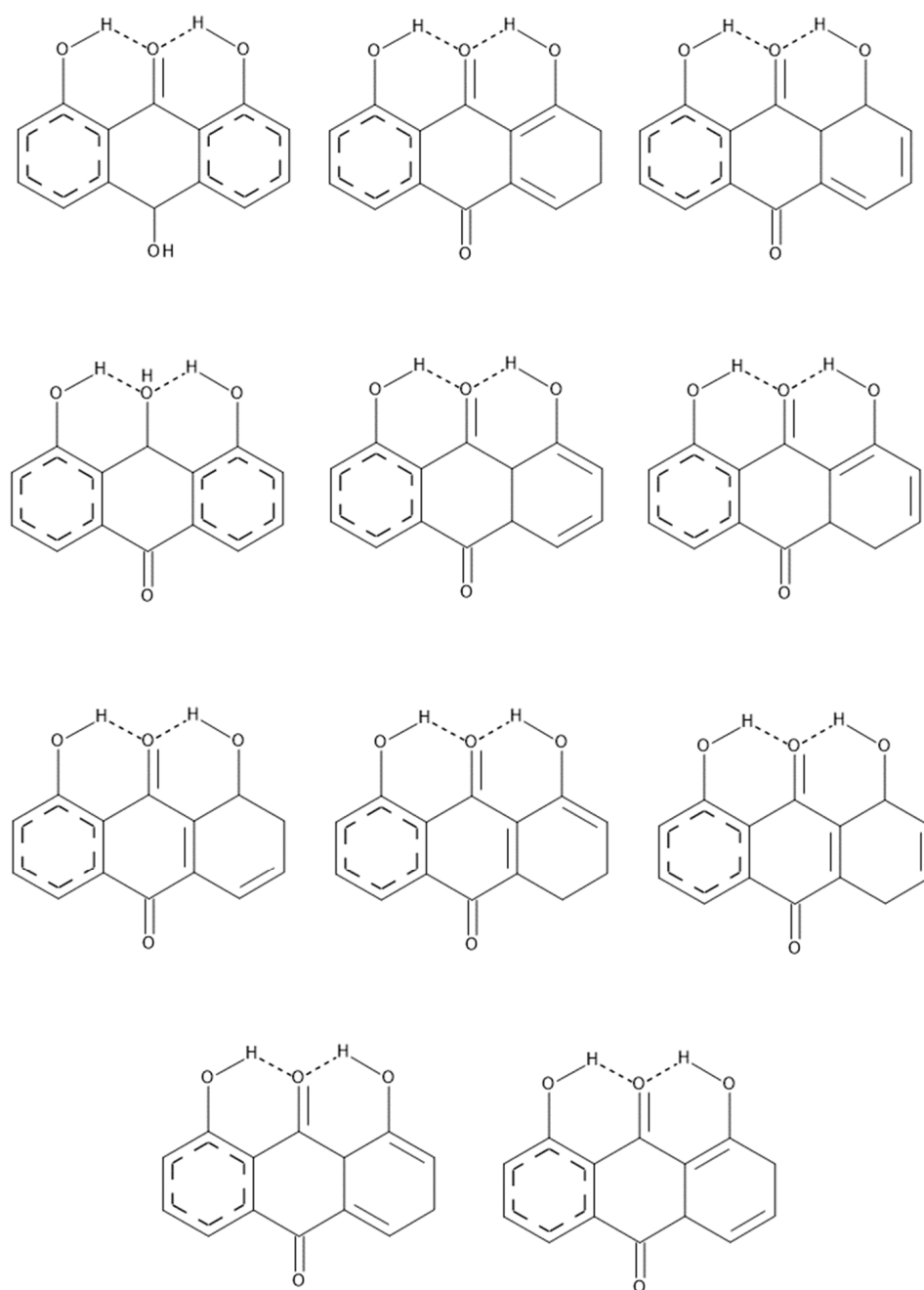$$\Delta H = BDE(C - H) - BDE(O - H) \qquad (3)$$

Figure 3. Possible prototropic forms for OH-substituted anthrone.

Investigation of the Substituents Effect on BDE (O-H) and BDE (C-H)

Table 5 shows the thermodynamic data for the tautomerization reaction. BDE values are given for C-H at C10 in keto form and O-H bond at C9 in the enol form. Structures with two and one intramolecular hydrogen bond have been considered. The low BDE(O-H) ensures easier detachment of hydrogen from the hydroxyl group. A low BDE(C-H) causes that the hydrogen attached to the C10 is easily removed by radicals [12]. A strongly electron-withdrawing substituent in the central ring like NO_2 causes a significant increase of BDE(O-H) and BDE(C-H) in a structure with two intramolecular hydrogen bonds comparing to the unsubstituted structure. In structure with NO_2 and one hydrogen bond slight increase of BDE(O-H) has been observed as well as a slight decrease of BDE(C-H) comparing to the unsubstituted structure. This means that the presence of the NO_2 substituent and two intramolecular hydrogen bonds makes more difficult detaching the hydrogen atom from the OH and CH group. The electron donating substituent (NH_2) causes a slight

decrease in the BDE(O-H) value relatively to the unsubstituted molecule in structures with two and one intramolecular hydrogen bond. Thus, it is easier to detach the hydrogen from the OH group at C9 in enol form relatively to the unsubstituted structure. However, according to Korth and Mulder, a low BDE(O-H) alone does not make a compound a good antioxidant [12]. The opposite situation has been observed for BDE(C-H). The NH_2 group caused a slight increase in the BDE(C-H) which means that it is more difficult to detach the hydrogen atom relatively to the unsubstituted structure. Similar BDE(O-H) results were obtained by Lucarini and Pedulli [26].

(a)

3K6c	3K6-C23H	3K6-C9H
0.0 kcal/mol	7.6 kcal/mol	16.7 kcal/mol

3K6-C4a4H	3K6-C9a1H	3K6-C9a4aH
24.7 kcal/mol	27.4 kcal/mol	30.3 kcal/mol

(b)

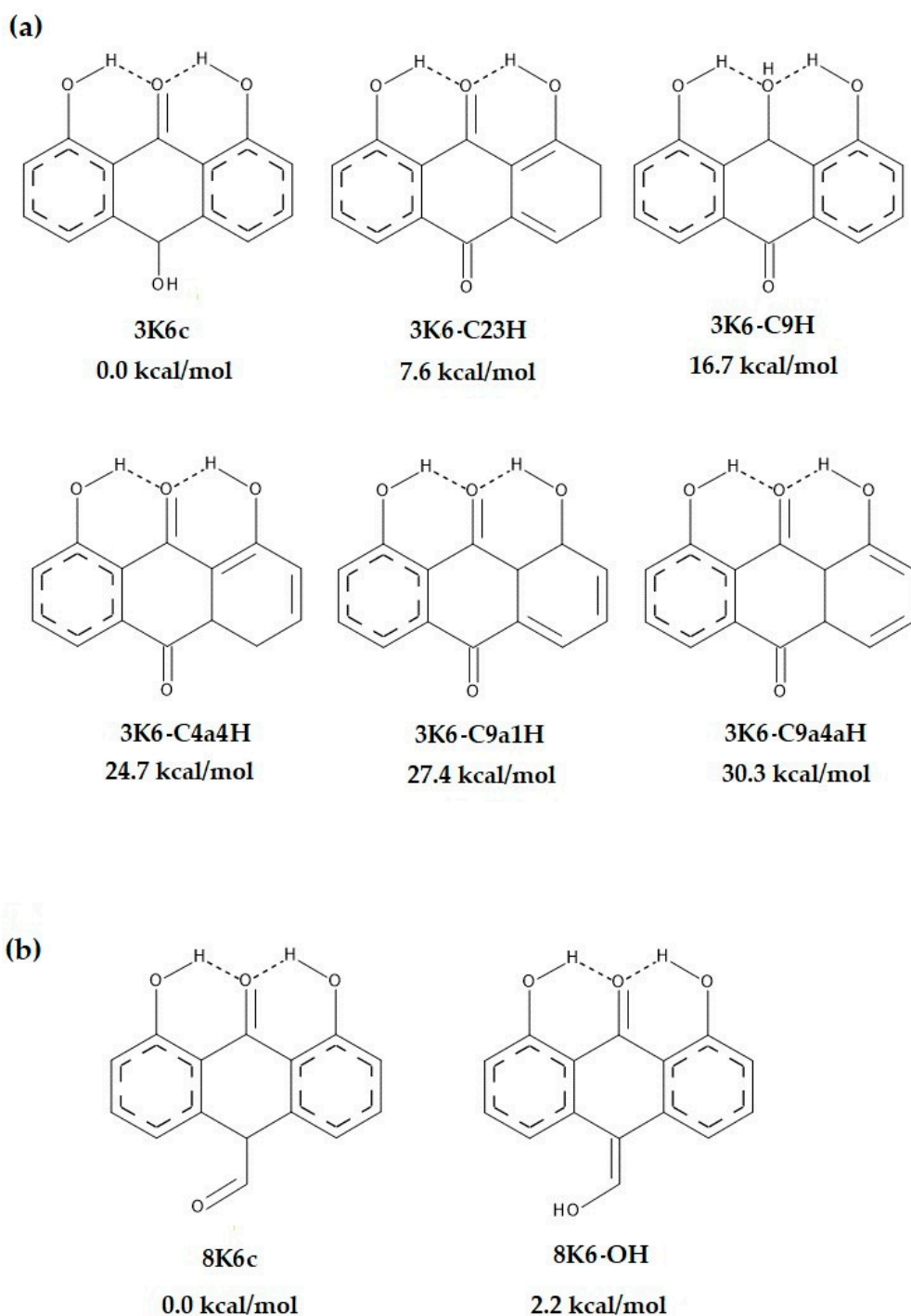| 8K6c	8K6-OH
0.0 kcal/mol	2.2 kcal/mol

Figure 4. Prototropic tautomers and ΔE at 298 K: (**a**)—OH substituent, (**b**)—CHO substituent.

Table 5. Enthalpy (ΔH) and Free Energy (ΔG) at 298 K for Tautomerization and the Bond Dissociation Enthalpy, BDE, in the enones (C-H) and in the enols (O-H). Structures without substituents are marked gray.

|	ΔH [kcal/mol]	ΔG [kcal/mol]	TΔS	BDE(C-H)	BDE(O-H)
10K6c ⇆ 10Eb	−17.3	−16.8	-7.82×10^4	79.0	96.3
K6c ⇆ 4Eb	−18.2	−17.2	-1.61×10^3	59.8	78.0
9K6c ⇆ 9Eb	−12.0	−11.8	-2.94×10^4	69.2	81.1
6K6c ⇆ 6Eb	−17.1	−15.1	-3.18×10^3	61.8	78.9
8K6c ⇆ 8Eb	−15.4	−15.0	-6.81×10^4	65.5	80.9
7K6c ⇆ 7Eb	−15.9	−14.9	-1.58×10^3	64.0	79.9
5K6c ⇆ 5Eb	−16.7	−15.4	-2.15×10^3	62.6	79.4
3K6c ⇆ 3Eb	−11.9	−10.8	-1.73×10^3	65.6	77.5
2K6c ⇆ 2Eb	−7.0	−5.6	-2.11×10^3	68.7	75.6
1K6c ⇆ 1Eb	−14.6	−13.8	-1.27×10^3	65.6	80.1
10K6b ⇆ 10Ea	−12.9	−12.5	-5.57×10^4	76.0	88.9
4K6b ⇆ 4Ea	−14.8	−13.6	-1.89×10^3	69.7	84.5
9K6b ⇆ 9Ea	−11.5	−11.2	-5.28×10^4	76.7	88.2
6K6b ⇆ 6Ea	−9.3	−7.1	-3.51×10^3	76.4	85.7
8K6b ⇆ 8Ea	−10.6	−10.4	-2.90×10^4	78.4	89.0
7K6b ⇆ 7Ea	−12.1	−11.4	-1.04×10^3	74.8	86.8
5K6b ⇆ 5Ea	−6.1	−4.9	-1.83×10^3	80.2	86.3
3K6b ⇆ 3Ea	−8.7	−8.1	-1.01×10^3	75.7	84.4
2K6b ⇆ 2Ea	−4.1	−2.7	-2.25×10^3	78.5	82.6
1K6b ⇆ 1Ea	−10.1	−9.8	-5.64×10^4	76.9	87.0

2.9. Hydrogen Bonds

Due to the presence of intramolecular hydrogen bonds, it is important to study their influence on the antioxidant potential and the tautomeric balance. In the conducted analysis, it is noticed that the BDE(O-H) and BDE(C-H) values are lower for the structures with two hydrogen bonds than with one hydrogen bond. Therefore, the presence of two hydrogen bonds increases the antioxidant properties of the compounds.

Hydrogen bonds have a significant impact on the enthalpy difference between ketone and enol structure. The free enthalpy difference between the ketone and enol form is greater for structures with two hydrogen bonds than for structures with one hydrogen bond. This means that two intramolecular hydrogen bonds have a greater effect on shifting the equilibrium towards the ketone form than the presence of one hydrogen bond.

To better illustrate the differences in energy associated with the presence of hydrogen bonds, Scheme 5 shows a cycle of changes in energy for 1,8-dihydroxy-9-anthrone. When, in ketone form, the hydrogens of the OH groups in the side aromatic rings are directed towards the center ring, hydrogen bonds are formed. The energy differences between 1K6a⇆1K6b, 1K6b⇆1K6c, and 1Ea⇆1Eb are the hydrogen bond energies. Higher intramolecular hydrogen bond energy is observed for structures in the ketone form with two intramolecular hydrogen bonds.

The energy of intramolecular hydrogen bonds is influenced by the substituents in the middle ring. For most compounds in the ketone form, the hydrogen bond energy is close to 12 kcal/mol. Form compounds in the enol form it is 8 kcal/mol. The exceptions are the compounds in the ketone form with COOH, CH_3, Cl, and CH_2CH_3 substituents, in which the energies of the hydrogen bond are within the range of 8–19 kcal/mol.
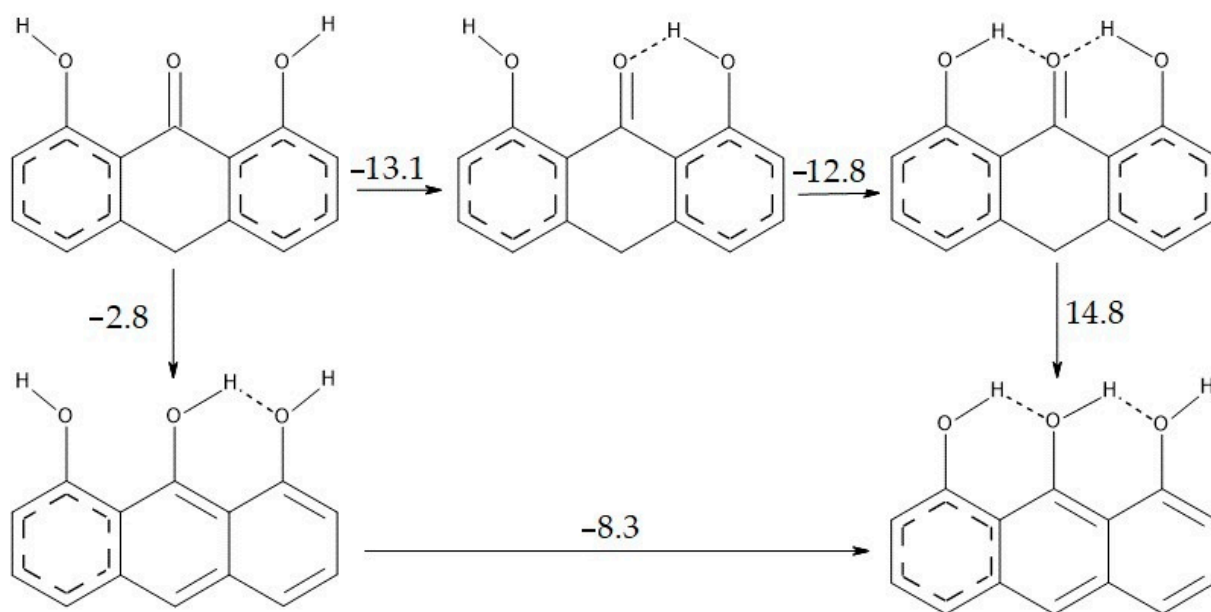
Scheme 5. Energy differences [kcal/mol] between the structures of the unsubstituted 1,8-dihydroxy-9-anthrone.

2.10. Influence of the Substituent on the Transition State

To better understand the proton transfer between the ketone and enol form, the most probably transition state has been optimized. According to Rubén Marrero-Carballo et al. [15], proton transfer in the ketone form occurs from the methyl group in the middle ring to the oxygen in the carbonyl group to form the enol form. In the current work, the same proton pathway has been used but the effect of three different substituents in the middle ring on the transition state geometry and energy has additionally been investigated. Substituents that accept electrons from the middle ring or donate them to the ring have been chosen.

All substituents have subtle effects on the transition state energies (Table 6). The differences in the transition state energies of the hydrogen atom-substituted structure and the NO_2 group-substituted structure are very similar. Despite the difference in the nature of the selected substituents, no direct interactions between the traveling proton and the substituents are observed.

Table 6. Energies at 298 K for optimized structures of the transition state, the reactants, and products for 1,8-dihydroxy-9-anthrone with different substituents.

	ΔE [kcal/mol]		
Substituent	**Reactant**	**Transition State**	**Product**
H	0	111.793	14.828
OH	0	105.881	12.503
NH_2	0	95.353	7.501
NO_2	0	111.648	17.800

For every transition state, the hydrogen bonds between the OH groups at the side rings and the CO group in the middle ring are broken. In the case of NH_2 and OH substituents, the hydrogens from the side OH groups are directed toward each other (Figure 5). Only in the case of the NO_2 substituent, both hydrogens from the OH groups face one direction. This is most likely due to the mesomeric effect of the NO_2 group. In addition, the angle of the CO bond to the plane of the central ring constructed with four carbon atoms in common with the side aromatic rings has been investigated. The smallest angle is for the structure with the NO_2 substituent, which pulls electrons out of the ring. On the other

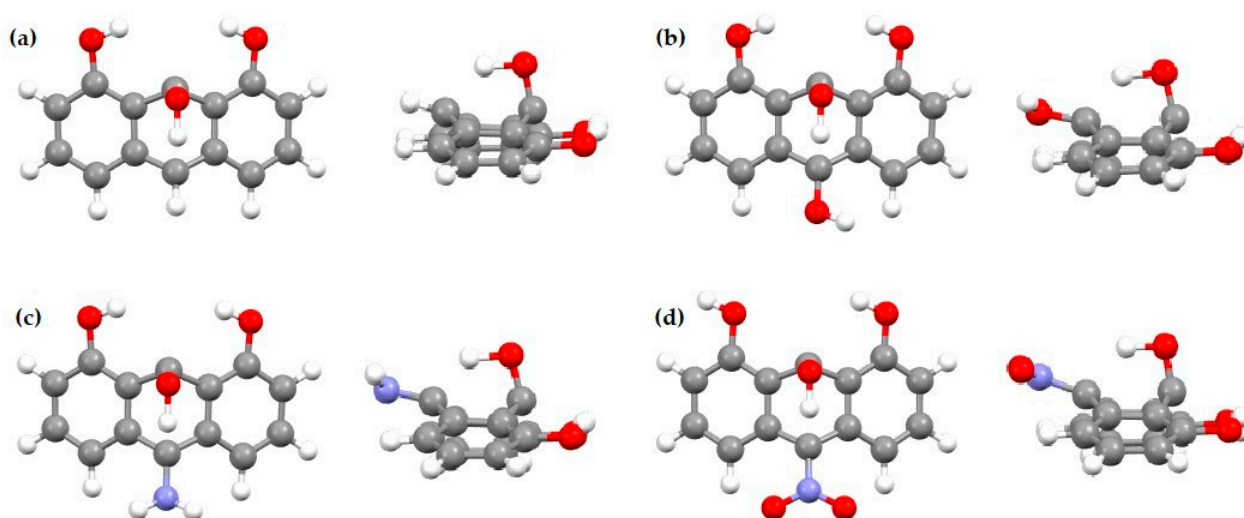hand, the highest angle has been obtained when the substituent is the NH_2 group, which is an electron donor.

Figure 5. Transition state for 1,8-dihydroxy-9-anthrone without substituent—(**a**), with OH substituent—(**b**), with NH_2—(**c**), and with NO_2—(**d**).

2.11. Transition State for the Keto-Enol Reaction with Pyridine

Another proton transfer pathway has been carried out with the help of a pyridine molecule as a carrier [15] for the keto-enol reaction of 1,8-dihydroxy-9-anthrone substituted with NO_2, OH, and H (Table 7). The lowest energy has been obtained for the initial state-pyridine with a substituted anthralin structure in the ketone form K + Pyr. In the first step, the proton from C10 is transferred to the nitrogen atom in the pyridine molecule. ΔG for the NO_2 substituent is 17.60 kcal/mol and for the OH substituent ΔG is equal to 17.34 kcal/mol. The lowest transition state energy TS1 of 8.37 kcal/mol has been obtained for the hydrogen atom substituted structure. The next step on the reaction progress is the formation of the INT1 ion. The nitrogen in the pyridine moves toward the oxygen in the middle ring of the substituted anthralin to form a hydrogen bond. This results in the formation of an ion pair (INT2). In order for the protonated pyridine to release a proton into oxygen yielding the enol form E + Pyr, a low free energy is needed. In the case of the NO_2 substituent, the ΔG is 13.93 kcal/mol, in the case of the OH group it is only 3.74 kcal/mol and for the H substituent-10.18 kcal/mol. For a better illustration of the reaction pathway involving pyridine, are provided figures showing each step of the reaction (Figure 6).

Table 7. Relative enthalpies, entropies, and Gibbs energies (kcal/mol) at 298 K for the stationary points involved in the pirydyne catalyzed tautomeric reaction of antralin with two different substituent (in gas phase).

Substituent	Compound	ΔG [kcal/mol]	ΔH [kcal/mol]	TΔS
NO_2	K + Pyr	0.00	0.00	0.00
	TS1	17.60	15.75	−1.85
	INT1	8.83	5.42	−3.41
	INT2	14.77	12.91	−1.86
	TS2	23.52	19.98	−3.54
	E + Pyr	9.59	11.08	1.49

Table 7. *Cont.*

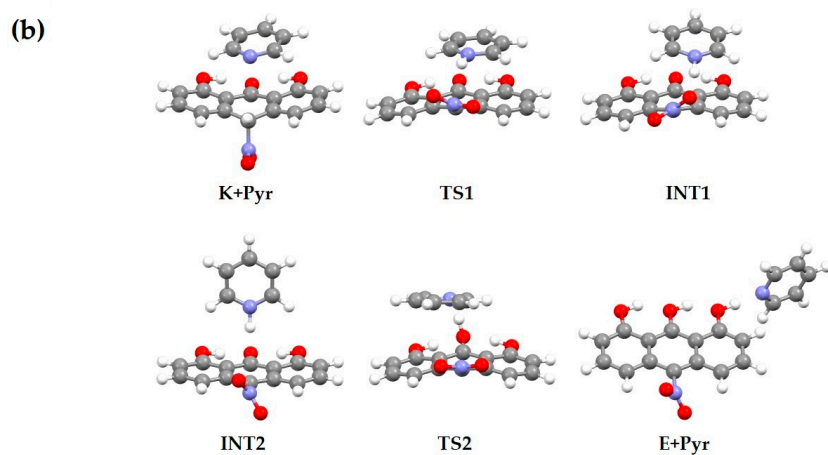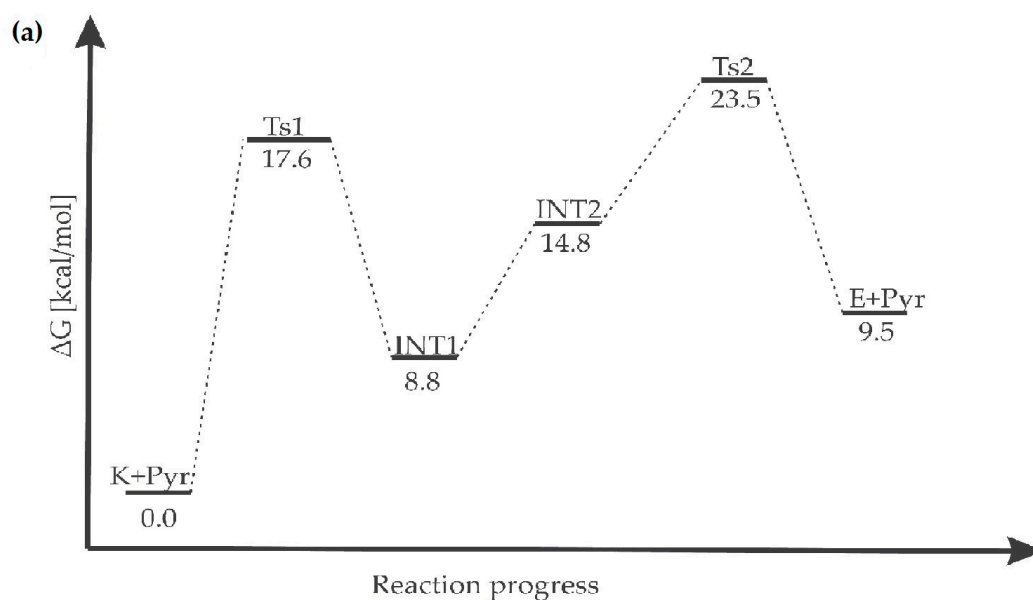| Substituent	Compound	ΔG [kcal/mol]	ΔH [kcal/mol]	TΔS
OH	K + Pyr	0.00	0.00	0.00
	TS1	17.34	15.48	−1.86
	INT1	14.38	11.73	−2.65
	INT2	5.59	5.02	−0.57
	TS2	6.93	6.07	−0.86
	E + Pyr	3.19	5.13	1.94
H	K + Pyr	0.00	0.00	0.00
	TS1	8.37	7.89	−0.48
	INT1	19.34	17.04	−2.30
	INT2	10.86	10.68	−0.18
	TS2	17.60	17.60	0.00
	E + Pyr	7.42	10.08	2.66

Figure 6. Steps of proton transfer reaction involving pyridine for 1,8-dihydroxy-9-anthrone with NO_2 substituent, (**a**)—Reaction progress ΔG [kcal/mol] at 298 K, (**b**)—optimized structures.

2.12. Theoretical Reaction Rate Constants

The rate constants in Table 8 illustrate how slow the conversion of the keto form to the enol form in 1,8-dihydroxy-9-anthrone molecules is. Comparison of the rate constants for the keto-enol reaction in substituted 1,8-dihydroxy-9-anthrones indicates that this reaction is not sensitive to substitution, except for the substitution of the NH_2 group, which accelerates the investigated reaction.

Table 8. Thermodynamic parameters for the keto-enol reaction of 1,8-dihydroxy-9-anthrone.

Substituent	$\Delta_r H^\circ$ (298 K) [kcal/mol]	$\Delta_r G^\circ$ (298 K) [kcal/mol]	k (298 K)
H	−14.58	−13.78	3.13×10^{-66}
NH_2	−6.96	−5.64	4.85×10^{-54}
NO_2	−17.32	−16.83	8.49×10^{-66}
OH	−11.92	−10.83	1.21×10^{-61}

The addition of pyridine changes the reaction mechanism, making it a two-stage process, with the second stage clearly faster. In the case of both stages of the reaction, the effect of the substituent on the reaction rate is visible (Table 9), which is particularly evident in the case of the second stage of the reaction of the OH-substituted 1,8-dihydroxy-9-anthrone.

Table 9. Thermodynamic parameters for the keto-enol reaction of 1,8-dihydroxy-9-anthrone with participation of pyridine.

Substituent	$\Delta r H_1$ (298 K) [kcal/mol]	$\Delta r G_1$ (298 K) [kcal/mol]	k_1 (298)	$\Delta r H_2$ (298 K) [kcal/mol]	$\Delta r G_2$ (298 K) [kcal/mol]	k_2 (298 K)
H	−17.04	−19.34	1.42×10^{-2}	0.59	3.44	7.09×10^{7}
NO_2	−5.43	−8.83	7.80×10^{-1}	1.83	5.19	2.38×10^{6}
OH	−11.73	−14.38	1.21×10^{0}	−0.11	2.41	3.66×10^{11}

3. Conclusions

The lowest energy structure is the K6 tautomer, which represents the ketone form.

The intramolecular hydrogen bond affects the geometry of 1,8-dihydroxy-9-anthrone. The changes of the α angle, which is the angle between the planes of the side rings, and so representing the general shape of 1,8-dihydroxy-9-anthrone, is sensitive to the OHO hydrogen bonds.

The electronodonor and electronoacceptor properties of the substituent in the middle ring as well as the presence of intramolecular hydrogen bonds affects the antioxidant properties of 1,8-dihydroxy-9-anthrone. The greatest decrease in BDE(O-H) has been obtained for the structure with the NH_2 substituent in the middle ring. Therefore, this compound can be expected to have the highest antioxidant properties.

The energy of the transition state in the keto-enol reaction in 1,8-dihydroxy-9-anthrone is unsensitive to the properties of the substituents in the central ring.

Taking into account the ΔH and the HOMA of the side aromatic rings, the preferred structure is the ketone form regardless the nature of the substituent in the middle ring of 1,8-dihydroxy-9-anthrone.

The keto-enol transformation in 1,8-dihydroxy-9-anthrone is significantly faster in the presence of pyridine.

References

1. Szymańska, M.; Majerz, I. Effect of Substitution of Hydrogen Atoms in the Molecules of Anthrone and Anthraquinone. *Molecules* **2021**, *26*, 502. [CrossRef]
2. Marsden, J.; Coburn, P.; Marks, J.; Shuster, S. Measurement of the response of psoriasis to short-term application of anthralin. *Br. J. Dermatol.* **1983**, *109*, 209–218. [CrossRef]
3. Ashton, R.E.; Andre, P.; Lowe, N.J.; Whitefield, M. Anthralin: Historical and current perspectives. *J. Am. Acad. Dermatol.* **1983**, *9*, 173–192. [CrossRef]
4. Hellier, F.F.; Whitefield, M. The treatment of psoriasis with triacetoxyanthracene. *Br. J. Dermatol.* **1967**, *79*, 491–496. [CrossRef]
5. Müller, K. Antipsoriatic and proinflammatory action of anthralin: Implications for the role of oxygen radicals. *Biochem. Pharmacol.* **1997**, *53*, 1215–1221. [CrossRef]
6. Pečar, S.; Schara, M.; Müller, K.; Wiegrebe, W. Reduction of nitroxides by anthralin and some of its derivatives. *Free Radic. Biol. Med.* **1995**, *18*, 459–465. [CrossRef]
7. Mueller, K.; Guerster, D.; Piwek, S.; Wiegrebe, W. Antipsoriatic anthrones with modulated redox properties. 1. Novel 10-substituted 1,8-dihydroxy-9(10H)-anthracenones as inhibitors of 5-lipoxygenase. *J. Med. Chem.* **1993**, *36*, 4099–4107. [CrossRef]
8. Szymanski, S.; Majerz, I. Aromaticity and Electron Density of Hypericin. *J. Nat. Prod.* **2019**, *82*, 2106–2115. [CrossRef]
9. Szymanski, S.; Majerz, I. In Silico Studies on Sennidines—Natural Dianthrones from Senna. *Biology* **2021**, *10*, 468. [CrossRef]
10. Szymański, S.; Majerz, I. Theoretical Studies on the Structure and Intramolecular Interactions of Fagopyrins—Natural Photosensitizers of *Fagopyrum*. *Molecules* **2022**, *27*, 3689. [CrossRef]
11. Limacher, P.A.; Lüthi, H.P. Cross-conjugation. *WIREs Comput. Mol. Sci.* **2011**, *1*, 477–486. [CrossRef]
12. Korth, H.-G.; Mulder, P. Anthrone and Related Hydroxyarenes: Tautomerization and Hydrogen Bonding. *J. Org. Chem.* **2013**, *78*, 7674–7682. [CrossRef]
13. Takemura, T.; Baba, H. Spectrophotometric investigations of the tautomeric reaction between anthrone and anthranol—II. *Tetrahedron* **1968**, *24*, 5311–5321. [CrossRef]
14. Fain, V.Y.; Zaitsev, B.E.; Ryabov, M.A. Tautomerism of anthraquinones: IV. 1-Hydroxy-9,10-anthraquinone and its substituted derivatives. *Russ. J. Org. Chem.* **2006**, *42*, 1469–1472. [CrossRef]
15. Marrero-Carballo, R.; Tun-Rosado, F.J.; Mena-Rejón, G.J.; Cáceres, D.; Barroso, J.; Murillo, F.; Merino, G.; Quijano-Quiñones, R.F. The base-catalyzed keto-enol tautomerism of chrysophanol anthrone. A DFT investigation of the base-catalyzed reaction. *Mol. Simul.* **2019**, *45*, 716–723. [CrossRef]
16. Radi, S.; Tighadouini, S.; Feron, O.; Riant, O.; Bouakka, M.; Benabbes, R.; Mabkhot, Y.N. Synthesis of Novel β-Keto-Enol Derivatives Tethered Pyrazole, Pyridine and Furan as New Potential Antifungal and Anti-Breast Cancer Agents. *Molecules* **2015**, *20*, 20186–20194. [CrossRef]
17. Gad, S.F.; El-Demerdash, S.H.; El-Mehasseb, I.M.; El-Nahas, A.M. Structure, stability and conversions of tautomers and rotamers of azulene-based uracil analogue. *J. Mol. Struct.* **2019**, *1182*, 271–282. [CrossRef]
18. Brovarets', O.O.; Hovorun, D.M. Prototropic tautomerism and basic molecular principles of hypoxanthine mutagenicity: An exhaustive quantum-chemical analysis. *J. Biomol. Struct. Dyn.* **2013**, *31*, 913–936. [CrossRef]
19. Samijlenko, S.P.; Yurenko, Y.P.; Stepanyugin, A.V.; Hovorun, D.M. Tautomeric Equilibrium of Uracil and Thymine in Model Protein−Nucleic Acid Contacts. Spectroscopic and Quantum Chemical Approach. *J. Phys. Chem. B* **2010**, *114*, 1454–1461. [CrossRef]
20. Ziółek, M.; Kubicki, J.; Maciejewski, A.; Naskrecki, R.; Grabowska, A. Enol-keto tautomerism of aromatic photochromic Schiff base N,N′-bis(salicylidene)-p-phenylenediamine: Ground state equilibrium and excited state deactivation studied by solvatochromic measurements on ultrafast time scale. *J. Chem. Phys.* **2006**, *124*, 124518. [CrossRef]

21. Laurella, S.L.; Sierra, M.G.; Furlong, J.J.P.; Allegretti, P.E. Substituent, Temperature and Solvent Effects on the Keto-Enol EQUILIBRIUM in β-Ketoamides: A Nuclear Magnetic Resonance Study. *Open J. Phys. Chem.* **2013**, *3*, 138–149. [CrossRef]

22. Wu, C.-C.; Lien, M.-H. Ab Initio Study on the Substituent Effect in the Transition State of Keto−Enol Tautomerism of Acetyl Derivatives. *J. Phys. Chem.* **1996**, *100*, 594–600. [CrossRef]

23. Antonov, L.; Fabian, W.M.F.; Nedeltcheva, D.; Kamounah, F.S. Tautomerism of 2-hydroxynaphthaldehyde Schiff bases. *J. Chem. Soc. Perkin Trans.* **2000**, *2*, 1173–1179. [CrossRef]

24. Taylor, P.J.; van der Zwan, G.; Antonov, L. Tautomerism: Introduction, History, and Recent Developments in Experimental and Theoretical Methods. *Tautomerism* **2013**, *2013*, 1–24. [CrossRef]

25. Nazarparvar, E.; Zahedi, M.; Klein, E. Density Functional Theory (B3LYP) Study of Substituent Effects on O–H Bond Dissociation Enthalpies of *trans*-Resveratrol Derivatives and the Role of Intramolecular Hydrogen Bonds. *J. Org. Chem.* **2012**, *77*, 10093–10104. [CrossRef]

26. Lucarini, M.; Pedulli, G.F. Free radical intermediates in the inhibition of the autoxidation reaction. *Chem. Soc. Rev.* **2010**, *39*, 2106–2119. [CrossRef]

27. Szymańska, M.; Majerz, I. Geometry and electron density of phenothiazines. *J. Mol. Struct.* **2020**, *1200*, 127095. [CrossRef]

28. Frisch, M.J.; Trucks, G.W.; Schlegel, H.B.; Scuseria, G.E.; Robb, M.A.; Cheeseman, J.R.; Scalmani, G.; Barone, V.; Petersson, G.A.; Nakatsuji, H.; et al. *Gaussian Inc. 16, Revision A.03*; Gaussian Inc.: Wallingford, CT, USA, 2016.

29. Becke, A.D. Density-functional thermochemistry. III. The role of exact exchange. *J. Chem. Phys.* **1993**, *98*, 5648–5652. [CrossRef]

30. Lee, C.; Yang, W.; Parr, R.G. Development of the Colle-Salvetti correlation-energy formula into a functional of the electron density. *Phys. Rev. B* **1988**, *37*, 785–789. [CrossRef]

31. Grimme, S.; Antony, J.; Ehrlich, S.; Krieg, H. A consistent and accurate ab initio parametrization of density functional dispersion correction (DFT-D) for the 94 elements H-Pu. *J. Chem. Phys.* **2010**, *132*, 154104–154119. [CrossRef]

32. Keith, T.A. *AIMALL (Version 19.10.12)*; TK Gristmill Software: Overland Park, KS, USA, 2019.

33. Allen, F.H. The Cambridge Structural Database: A quarter of a million crystal structures and rising. *Acta Crystallogr. Sect. B Struct. Sci.* **2002**, *58*, 380–388. [CrossRef]

34. Osmialowski, B.; Raczyńska, E.D.; Krygowski, T.M. Tautomeric Equilibria and Pi Electron Delocalization for Some MonohydroxyarenesQuantum Chemical Studies. *J. Org. Chem.* **2006**, *71*, 3727–3736. [CrossRef]

35. Brown, C.J.; Colclough, M.L. 1,8-Dinitro-4,5-dihydroxyanthraquinone, C14H6N2O8. *Acta Crystallogr. Sect. C Cryst. Struct. Commun.* **1983**, *39*, 300–302. [CrossRef]

36. Von Dreele, R.B.; Einck, J.J. The crystal and molecular structure of carminomycin I hydrochloride monohydrate. *Acta Crystallogr. Sect. B Struct. Crystallogr. Cryst. Chem.* **1977**, *33*, 3283–3288. [CrossRef]

37. Rohl, A.; Moret, M.; Kaminsky, W.; Claborn, K.; McKinnon, J.; Kahr, B. Hirshfeld Surfaces Identify Inadequacies in Computations of Intermolecular Interactions in Crystals: Pentamorphic 1,8-Dihydroxyanthraquinone. *Cryst. Growth Des.* **2008**, *8*, 4517–4525. [CrossRef]

38. Schmidt-Bäse, K.; Noltemeyer, M.; Egert, E.; Eigelt, E.; Zeeck, A. Structure of the anthracycline antibiotic aranciamycin. *Acta Crystallogr. Sect. C Cryst. Struct. Commun.* **1993**, *49*, 250–253. [CrossRef]

39. Armaghan, M.; Amini, M.M.; Ng, S.W.; Tiekink, E.R.T. Co-crystals of 1,8-dihydroxy-2,4,5,7-tetranitro-9,10-anthraquinone with dibenzothiophene and 4,6-dimethyldibenzothiophene. *Z. Kristallographie-Crystalline Mater.* **2013**, *228*, 598–606. [CrossRef]

40. Hernandez-Medel, M.D.R.; O Ramirez-Corzas, C.; Rivera-Dominguez, M.; Ramirez-Mendez, J.; Santillan, R.; Rojas-Lima, S. Diastereomeric C-glycosyloxanthrones from picramnia antidesma. *Phytochemistry* **1999**, *50*, 1379–1383. [CrossRef]

41. Aoyama, T.; Naganawa, H.; Muraoka, Y.; Nakamura, H.; Aoyagi, T.; Takeuchi, T.; Iitaka, Y. Benastatins A and B, new inhibitors of glutathione S-transferase, produced by Streptomyces sp. MI384-DF12. II. Structure determination of benastatins A and B. *J. Antibiot.* **1992**, *45*, 1391–1396. [CrossRef]

42. Krygowski, T.M. Crystallographic studies of inter- and intramolecular interactions reflected in aromatic character of .pi.-electron systems. *J. Chem. Inf. Comput. Sci.* **1993**, *33*, 70–78. [CrossRef]

43. Raczyńska, E.D.; Kosińska, W.; Ośmiałowski, B.; Gawinecki, R. Tautomeric Equilibria in Relation to Pi-Electron Delocalization. *Chem. Rev.* **2005**, *105*, 3561–3612. [CrossRef]